Coupled Effects of Mechanics, Geometry, and Chemistry on Bio-membrane Behavior

Thesis by

Ha Giang

In Partial Fulfillment of the Requirements

for the Degree of

Doctor of Philosophy

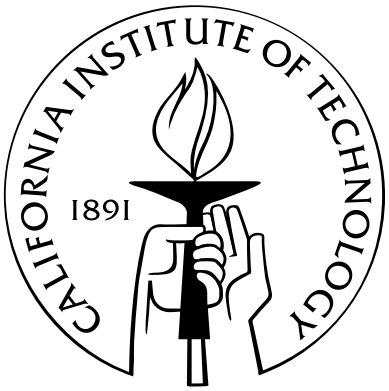

California Institute of Technology

Pasadena, California

2013

(Defended May 30, 2013)

Acknowledgements

I would like to express my sincere and deepest gratitude to my advisor Professor Kaushik Bhattacharya for his support, encouragement, and guidance over the past seven years. He has been such a great advisor that I can never say thank him enough.

I would also want to extend my thanks to my committee members, Professor Nadia Lapusta, Professor Rob Phillips, and Professor Guruswami Ravichandran for their advice, discussion, and support during my Ph.D. study.

I would like to thank all my group members, collaborators, and friends at Caltech. Particularly, thanks to Sefi Givli for a great collaboration experience, working with him was one of the key points to shape my research. Thanks to Jennifer and Christian Franck for helping me during my first two years here. Thanks to Cindy Wang and Srivatsan Hulikal for pleasant TA experiences. Thanks to Tristan Ursell, Maja Bialecka, and Heun Jin Lee for the vesicle recipe, equipment usages, and useful discussions. Thanks to Jacob Notbohm, Shuman Xia, and Petros Arakelian for helping me with experiment setups in Guggenheim. Thanks to Sohini Ray for her kindness and consolations during my hard time. Thanks to Leslie Rico and Cheryl Geer for their administrative work.

I would like to thank my family, particularly my parents, my brother, and my fiancé for their unconditional love, understandings, and encouragement.

Abstract

Lipid bilayer membranes are models for cell membranes–the structure that helps regulate cell function. Cell membranes are heterogeneous, and the coupling between composition and shape gives rise to complex behaviors that are important to regulation. This thesis seeks to systematically build and analyze complete models to understand the behavior of multi-component membranes.

We propose a model and use it to derive the equilibrium and stability conditions for a general class of closed multi-component biological membranes. Our analysis shows that the critical modes of these membranes have high frequencies, unlike single-component vesicles, and their stability depends on system size, unlike in systems undergoing spinodal decomposition in flat space. An important implication is that small perturbations may nucleate localized but very large deformations. We compare these results with experimental observations.

We also study open membranes to gain insight into long tubular membranes that arise for example in nerve cells. We derive a complete system of equations for open membranes by using the principle of virtual work. Our linear stability analysis predicts that the tubular membranes tend to have coiling shapes if the tension is small, cylindrical shapes if the tension is moderate, and beading shapes if the tension is large. This is consistent with experimental observations reported in the literature in nerve fibers. Further, we provide

numerical solutions to the fully nonlinear equilibrium equations in some problems, and show that the observed mode shapes are consistent with those suggested by linear stability. Our work also proves that beadings of nerve fibers can appear purely as a mechanical response of the membrane.

Contents

List of Figures

Chapter 1

Introduction

Lipid bilayer membranes are ubiquitous in living organisms [ABH+04, HMO+01]. They are the fundamental building blocks of cell walls, mitochondria, Golgi apparatus and numerous other important organelles. They protect by providing a barrier, they regulate flow of nutrients and waste, and they host many metabolic functions. Yet, they are exceedingly simple in their basic construction. They are made of amphiphilic molecules consisting of a hydrophilic (water-loving) head and hydrophobic (water-avoiding) tails as shown on the left of Fig. 1.1. When such molecules are put in water at concentration that is higher than a critical aggregation threshold, they assemble into bilayer membranes exposing their hydrophilic heads to the water and hiding their hydrophobic tails as shown in the center

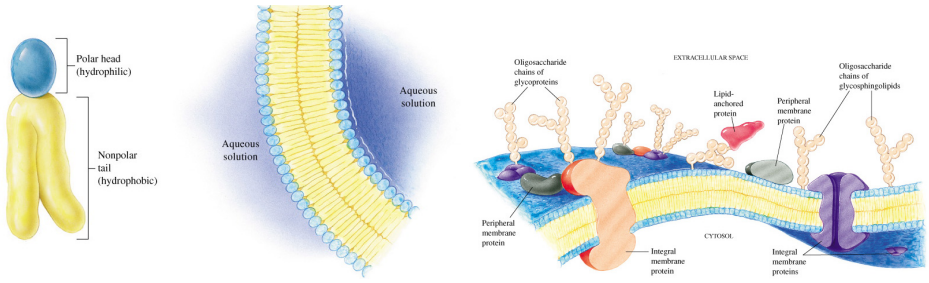

Figure 1.1: Introduction to lipid bilayer membranes. Left: A typical amphiphilic lipid with a hydrophilic head group and hydrophobic tails. Center: A lipid bilayer membrane. Right: A typical plasma membrane with membrane proteins and other functional groups. From Horton et al. [HMO+01]

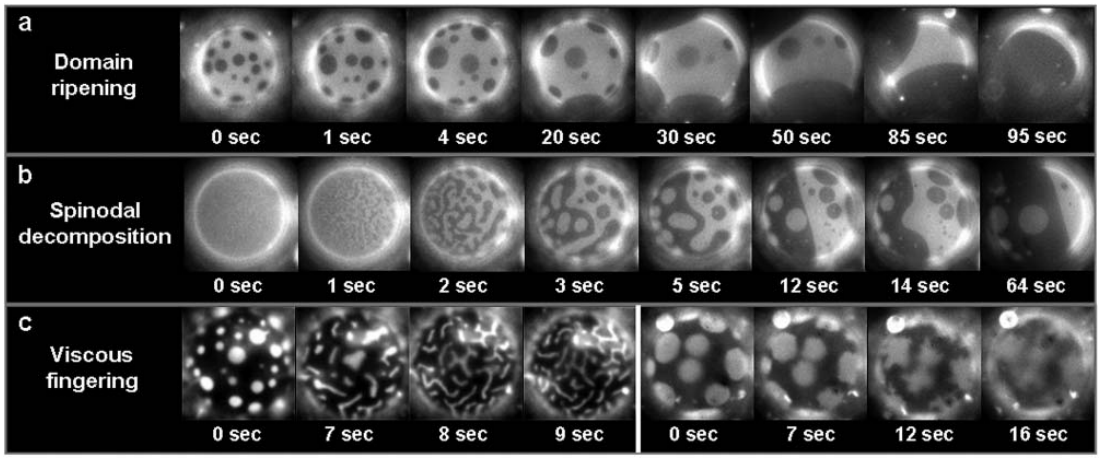

Figure 1.2: Various behaviors of liquid phases in a DOPC/DPPC/Cholesterol ternary mixture. Note that though there are three materials, one has only two phases because cholesterol is incorporated into the lipid. (a) Domain ripening where almost circular domains migrate, collide and fuse; (b) Spinodal decomposition with nucleation, diffusion mediated coarsening and; (c) Fingering instability on heating. (Reprinted from [VK03], Copyright (2013), with permission from Elsevier.)

of Fig. 1.1. These membranes are about 4–5 nm thick and have the average area per lipid molecules about 0.5 nm^2. Moreover, they are extremely floppy with bending modulus around 24 kT [Boa02] and have fluid-like behavior in the plane (they resist stretching but not shear).

In recent years, the membrane mechanical properties have received significant attention due to their role in mechano-sensitive channels, phase segregation, and cell adhesion. In living organisms, the lipid bilayer membrane is infiltrated with a variety of membrane proteins and other functional molecules as shown on the right of Fig. 1.1. An important class is the mechano-sensitive channels, which are proteins that respond to the stress in the membrane by opening and closing, and the thus regulating flow through the membrane. Further, the lipid membranes are not always homogeneous. One may have a membrane with more than one type of amphiphilic lipid molecule. Or, one may have molecules, such as cholesterol, dispersed through the bilayer membrane. Furthermore, there are a number

of bilayer phases—gels, liquid disordered and liquid ordered—depending on the in-plane arrangement of the molecule. Depending on the temperature, the pressure, and the nature of interactions between the lipids, the membrane can remain homogeneous or segregate into different phases, e.g. phase segregation observations shown in Fig. 1.2 [VK03]. Importantly, the different phases have different mechanical properties, and this influences their morphology and dynamics. Therefore, studying heterogeneous membranes plays an important role in understanding bio-membrane functions.

Since the pioneering work of Helfrich [Hel73] and Evans [Eva74], the lipid bilayer membranes have been studied extensively. Jenkins derived equilibrium laws for a version of the Helfrich model [Jen77b], and applied it to study shape transitions in red blood cells [Jen77a]. Siefert, Lipowsky, Taniguchi and their collaborators adapted the Helfrich energy to multi-phase membranes, and studied shape transformations [SBL91, Lip92, JL93, KAKT93, TKAK94, JL96, Tan96, DEK+97]. However, much of the existing work on multi-component membranes either rely on advanced numerical methods such as nonlinear finite elements and phase field methods [MK08, DLW04, LRV09, FK06, ES10], or use models with various simplifying assumptions such as axi-symmetry, small deformations, spherical caps landscape, and complete separation of the phases [BDWJ05, JL93, VG07, Bou99]. A complete theoretical examination of the different models, theories, regimes and their relationship is yet to be developed. This thesis is a contribution in this direction. We have developed a model that allows systematic studies of the membranes, and showed that the intricate coupling between the lipid composition and the membrane properties can lead to highly diverse functionalities of the membranes.

Specifically, a key feature of multicomponent vesicles is the coupling between the mechanics, the geometry and the chemistry. We explore this in both closed and open mem-

branes. The former are of interest as models of cell walls. They are also relatively easier to model because they are closed systems and have a well-defined potential energy functional. The latter are of interest in understanding isolated segments of long tubular membranes motivated, for example, by neurons. They are also harder to model, being open systems capable of exchanging molecules with the outside.

First, we study a general class of closed multi-component membranes in Chapter 2[1]. The equilibrium equations and stability conditions are presented and the stability of a uniform spherical vesicle is investigated. The analysis is based on a generalized Helfrich energy that accounts for geometry through the stretch and curvature, and the composition, as well as the interaction between geometry and composition. The use of non-classical differential operators and related integral theorems, in conjunction with appropriate composition and mass conserving variations, simplify the derivations. We show that instabilities of multi-component membranes are significantly different from those in single component membranes, as well as those in systems undergoing spinodal decomposition in flat spaces. This is due to the intricate coupling between composition and shape, as well as the non-uniform tension in the membrane. Specifically, critical modes have high frequencies, unlike single-component vesicles, and stability depends on system size, unlike in systems undergoing spinodal decomposition in flat space. An important implication is that small perturbations may nucleate localized but very large deformations. We also show that the predictions of our analysis are in qualitative agreement with experimental observations.

We then move on to study open systems in Chapters 3 and 4. Chapter 3 is devoted to single component systems while Chapter 4 to multicomponent system. Because open systems can exchange molecules with the outside, we use a principal of virtual work to

[1]This work was reported in [GGB12]

derive the equilibrium equation. We focus, in particular, on cylindrical membranes and their stability.

Our linear stability study of open membranes, reported in both Chapters 3 and 4, suggests that the tubular membranes tend to have coiling shapes if the tension is small, cylindrical shapes if the tension is moderate, and beading shapes if the tension is large. This prediction agrees well with experiment observations on stretching nerve cells, in that the bands of Fontana (coiling shapes) appear when the nerves are relaxed under small stretch, and beadings appear when the nerves are under large stretch. We also predict that the open multi-component membranes will be highly unstable and will have more instability modes due to the coupling between geometry and chemistry.

We also present in Chapter 3 detailed numerical solutions to the equilibrium equation in the axisymmetric setting for the single component open system. We note that the derivation of these equations require some care. In particular, one has to derive these equations in the general three-dimensional setting, and then restrict to the axisymmetric setting, rather than imposing axisymmetry at the start by restricting the energy to axisymmetric shapes. We find that our numerical solutions to the equilibrium equations are consistent with the predictions of the linear stability analysis – cylindrical shapes for moderate tension and beading for large. Beading is of interest in neurons. Our numerical solutions prove that beading of nerve fibers can occur by purely mechanical response, and one does not need neural abnormalities, such as metabolic perturbation, mechanical trauma, aging, or toxic agents, as is commonly assumed in the literature.

The thesis is organized as follow. In Chapter 2, we study a general class of closed multi-component membranes. In Chapter 3, we present a framework to study open single-component membranes. Then, we study the stability of open multi-component membranes

in Chapter 4. Lastly, we summarize the conclusions of this thesis and discuss potential future work in Chapter 5.

Chapter 2

Closed Multi-component Membranes

In this chapter, we systematically derive the equilibrium equations and linear stability conditions for a general class of multi-component biological membranes (BMs) motivated by the following facts: (i) stable configurations are the observable in most experiments; (ii) chemo-mechanical instabilities in cell membranes often relate to critical changes in bio-chemical processes, cell behavior, or fate. Examples are formation of focal adhesions, initiation of filopodia, and opening of ion channels; (iii) knowledge of the stability conditions can be used to measure, indirectly, mechanical and chemical properties of lipids, protein aggregates, and other functional components of the membrane.

We consider a closed biological membrane composed of two phases. These can represent two different lipid phases (e.g. liquid ordered and liquid disordered phases), two different types of lipid molecules, or mobile membrane proteins embedded in a lipid phase. Equilibrium equations and stability conditions are obtained by calculating the first and second variations of a generalized Helfrich energy functional. We assume that overall composition, i.e. total number of molecules of each phase, does not change in the course of the experiment. In calculating the variations of the energy functional, we take advantage of non-classical differential operators and related integral theorems developed by Yin and col-

laborators [YCN+05, Yin05a, Yin05b, YYN05, YYC07, YYW07]. Further, we introduce density and composition conserving variations, so that the use of Lagrange multipliers is avoided. In addition, we account for the spatial non-uniform stretching of the membrane. This feature, which is commonly ignored by assuming a constant membrane area, is especially important in multi-component membrane applications, and can have important implications in processes such as the activity of gated ion channels.

2.1 A Model of a Multi-component Vesicle

2.1.1 The Energy Functional

We consider a closed lipid membrane composed of two components, which we shall refer to as type I and type II. These can represent two different lipid phases (e.g. liquid ordered and liquid disordered phases), two different types of lipid molecules, or mobile membrane proteins embedded in a lipid phase. The current geometric configuration of the membrane is described by a closed surface S. Let H be the mean curvature, K the Gauss curvature of this surface and V_S the volume enclosed by S. We introduce a total density $\rho : S \to R^+$ that describes the total density (both components combined) at each point of the membrane, and a concentration $c : S \to [0, 1]$ that describes the ratio between the two components. It follows that at any given point on the membrane $c\rho$ and $(1 - c)\rho$ are the densities of component I and component II, respectively. Further, if M_I and M_{II} denote the total number of molecules of each component, we have

$$\int_S c\rho \, dS = M_I \quad \text{and} \quad \int_S \rho \, dS = M \qquad (M \equiv M_I + M_{II}). \tag{2.1}$$

Suppose that this membrane is subjected to an osmotic pressure difference P between

the fluid inside and outside the vesicle. Then, the total potential energy of the vesicle may be written as

$$\mathcal{F} = \int_S \phi(H, K, \rho, c)\, dS - P\, V_S \tag{2.2}$$

where the generalized free energy is given by

$$\phi(H, K, \rho, c) = k_\rho \left(\frac{\rho}{\rho_0} - 1\right)^2 + \frac{1}{2} k_H(c)\, (2H - H_0(c))^2 + k_K K + f(c) + \frac{1}{2} k_c |\nabla c|^2. \tag{2.3}$$

The first term depends on the density or, equivalently, the specific area, and describes the energy required to stretch the membrane. Therefore, we refer to k_ρ as the stretching modulus. Importantly, this term depends only on specific area, instead of on the entire metric tensor. This reflects the fact that the membrane is a fluid and cannot resist any shear in the plane. Various researchers use the fact that k_ρ is large, and replace this energy with a constraint of constant membrane area [SBL91, ZCH89]. While this is acceptable for single component BMs, it makes certain subtleties harder in multi-component situations as we shall see later.

The second term is the Helfrich energy, and depends on the mean curvature. k_H is the bending modulus and H_0 is the spontaneous curvature, and both depend on composition. If the two components have different molecular structure, any inhomogeneity induces a local spontaneous curvature. Therefore, spontaneous curvature is dictated by composition, resulting in a coupling between composition and shape. For example, membrane proteins can act on the membrane as wedges leading to areas of high curvature. Also, different types of lipids can have different molecular shapes. For example, in phosphatidylcholine, the head group and lipid backbone have similar cross-sectional areas, and therefore the molecule has a cylindrical shape. On the other hand, phosphatidylethanolamine molecules have a small

headgroup and are cone-shaped, while in lysophosphatidylcholine the hydrophobic part occupies a relatively smaller surface area and the molecule has the shape of an inverted cone [SvdSvM01]. The mixture of cylindrical lipids and conical lipids will have a spontaneous curvature that depends on the concentration of the conical lipids [DTB08]. In addition, the two phases can have different mechanical properties. This is accounted for by the dependency of k_H on composition [BHW03].

The third term is taken to be linear in the Gauss curvature, and consequently does not affect closed vesicles.

The fourth term, f, describes the interaction between the two phases. A simple model for f combines the aggregation enthalpy and the entropy of mixing [VG07]

$$f = k_B T \rho_0 \left(c \ln c + (1-c)\ln(1-c)\right) + \frac{1}{2} B \rho_0 c(1-c) \tag{2.4}$$

so that it is convex at high temperatures (miscible) but non-convex at low temperatures (immiscible). This above form is similar to relations used in other works [AKK92, Lei86], where fourth-order polynomials have been used in order to approximate a double-well energy landscape. It turns out that the critical temperature, $B/4k_B$, is typically close to room-temperature [VG07].

Finally, the last term penalizes rapid changes in composition as, for example, in phase boundaries.

2.1.2 Non-dimensionalization

We define the unit length R as the radius of the membrane if it takes a spherical shape with a uniform density $\rho = \rho_0$. Hence,

$$M = 4\pi R^2 \rho_0. \tag{2.5}$$

Accordingly, we introduce the following non-dimensional quantities

$$\widetilde{H} = HR,\ \widetilde{K} = KR^2,\ \widetilde{\nabla} = R\nabla,\ \widetilde{\rho} = \frac{\rho}{\rho_0},\ \widetilde{P} = \frac{P}{k_H^*}R^3, \tag{2.6}$$

and

$$\widetilde{k}_H = \frac{k_H}{k_H^*},\ \widetilde{k}_K = \frac{k_K}{k_H^*},\ \widetilde{k}_\rho = \frac{k_\rho}{k_H^*}R^2,\ \widetilde{k}_c = \frac{k_c}{k_H^*}, \tag{2.7}$$

where $k_H^* = k_H\,|_{c=0.5}$. Therefore, the non-dimensional energy functional reads

$$\widetilde{F} = \frac{F}{k_H^*} = \int_{\widetilde{S}} \widetilde{\phi}\, d\widetilde{S} - \widetilde{P}\widetilde{V}_S, \tag{2.8}$$

where

$$\begin{aligned} \widetilde{\phi}(\widetilde{H}, \widetilde{K}, \widetilde{\rho}, \widetilde{c}) = &\ \frac{R^2}{k_H^*}\phi \\ = &\ \widetilde{k}_\rho\,(\widetilde{\rho}-1)^2 + \frac{1}{2}\widetilde{k}_H\left(2\widetilde{H} - \widetilde{H}_0(c)\right)^2 \\ &+ \widetilde{k}_K\widetilde{K} + \widetilde{f}(c) + \frac{1}{2}\widetilde{k}_c|\widetilde{\nabla}c|^2. \end{aligned} \tag{2.9}$$

In what follows, all quantities are non-dimensional, and we disregard the ($\sim$) symbol for brevity.

2.2 Mathematical Preliminaries

2.2.1 Definitions and Identities

We have represented a biological membrane as a surface or a $2D$ manifold in a $3D$ Euclidian space. This surface is described by

$$\mathbf{x} = \mathbf{x}(u^i), \quad i = 1, 2,$$

where u^1, u^2 are real parameters. We introduce the following quantities:

$$\begin{aligned}
&\mathbf{g}_i = \mathbf{x}_{,i}, && g_{ij} = \mathbf{g}_i \cdot \mathbf{g}_j, \quad g = \det(g_{ij}),\\
&\mathbf{g}^i \cdot \mathbf{g_j} = \delta_{ij}, && g^{ij} = (g_{ij})^{-1},\\
&\mathbf{n} = g^{-1/2}(\mathbf{g_1} \times \mathbf{g_2}), && L_{ij} = \mathbf{g}_{i,j} \cdot \mathbf{n}, \quad L = \det(L_{ij}).
\end{aligned}$$

Here, $(.)_{,i}$ denotes partial derivative with respect to u^i, $\mathbf{g}_i$ and $\mathbf{g}^i$ are, respectively, the covariant and contravariant base vectors tangent to the surface, $\mathbf{n}$ is the unit normal to the surface, δ_{ij} is the Kronecker's delta, and g_{ij} and L_{ij} are the first and second fundamental forms of the surface. In addition, the mean and Gauss curvatures of the surface are

$$H = \frac{1}{2}(c_1 + c_2) = \frac{1}{2} g^{ij} L_{ij}, \quad K = c_1 c_2 = \frac{L}{g},$$

where c_1 and c_2 are the principle normal curvatures.

The surface gradient operator is defined as [Sto69]

$$\nabla = \mathbf{g}^i \frac{\partial}{\partial u^i}.$$

Accordingly, the gradient of a scalar function f is simply

$$\nabla f = \mathbf{g}^i \frac{\partial}{\partial u^i} = f_{,j}\mathbf{g}^j,$$

and the Laplace-Beltrami operator is

$$\Delta f = \nabla^2 f \equiv \nabla \cdot \nabla f = \frac{1}{\sqrt{g}} \left(\sqrt{g} f_{,i} g^{ij}\right)_{,j}.$$

We recall two integral identities:

$$\int_S \nabla f \, dS = -\int_S 2\,H\, f\, \mathbf{n}\, dS, \quad \int_S \nabla \cdot \mathbf{v}\, dS = -\int_S 2\,H\, \mathbf{v}\cdot\mathbf{n}\, dS. \tag{2.10}$$

In addition to the above conventional surface operators, we shall also use extensively the following non-conventional operators introduced by Yin and his collaborators[1] [NO95, Yin05b]:

$$\overline{\nabla} = K\overline{L}^{ij}\mathbf{g}_i \frac{\partial}{\partial u^j}, \quad L_{im}\overline{L}^{mj} = \delta_{ij}; \tag{2.11}$$

$$\overline{\nabla}^2 f \equiv \nabla \cdot \overline{\nabla} f = \overline{\nabla} \cdot \nabla f = \frac{1}{\sqrt{g}} \left(\sqrt{g} K \overline{L}^{ij} f_{,i}\right)_{,j}. \tag{2.12}$$

These operators satisfy a number of integral identities that will prove useful in our calculations. These are listed in Appendix A. They largely follow from the following identities which appear to be formal analogs of (2.10) with the Gauss curvature replacing by mean curvature.

$$\int_S \overline{\nabla} f \, dS = -\int_S 2\,K\, f\, \mathbf{n}\, dS, \quad \int_S \overline{\nabla} \cdot \mathbf{v}\, dS = -\int_S 2\,K\, \mathbf{v}\cdot\mathbf{n}\, dS. \tag{2.13}$$

[1] Yin refers to them as the second gradient and second divergence operators, but we do not use that terminology here.

2.2.2 Perturbations

We are interested in finding the equilibria and their stability by studying the first and second variation of the potential energy. This requires some care, as the perturbations in shape, density and composition can be coupled, and because of the constraints (2.1). Consider arbitrary perturbations of shape, density and composition:

$$\mathbf{x}' = \mathbf{x} + \delta\mathbf{x}, \quad \rho' = \rho + \delta\rho, \quad c' = c + \delta c, \tag{2.14}$$

where

$$\delta\mathbf{x} = \mathbf{n}\,(\epsilon\,\zeta_1 + \epsilon^2\zeta_2), \quad \delta\rho = \epsilon\,\zeta_3 + \epsilon^2\zeta_4, \quad \delta c = \epsilon\,\zeta_5 + \epsilon^2\zeta_6, \tag{2.15}$$

ζ_i are arbitrary functions, and ϵ is an arbitrarily small scalar. The fact that we are dealing with a closed smooth surface enables us to use normal perturbations without any loss of generality. To deal with the constraints (2.1), we introduce

$$G_1(\rho, S) = \int_S \rho\, dS \qquad \text{and} \qquad G_2(\rho, c, S) = \int_S \rho\, c\, dS. \tag{2.16}$$

Evaluating these for the perturbed quantity and expanding them in ϵ, we obtain

$$\begin{aligned}
G_1(\rho', S') =& G_1(\rho, S) + \epsilon \int_S \{\zeta_3 - 2H\rho\zeta_1\}\, dS \\
&+ \epsilon^2 \int_S \Big\{ K\rho\zeta_1^2 - 2H\zeta_1\zeta_3 + \zeta_4 - 2H\zeta_2\rho + \frac{1}{2}\rho\left|\nabla\zeta_1\right|^2 \Big\} dS \\
&+ \mathcal{O}(\epsilon^3), \\
G_2(\rho', c', S',) =& G_2(\rho, c, S) + \epsilon \int_S \big\{ c[\zeta_3 - 2H\rho\zeta_1] + \rho\zeta_5 \big\} dS \\
&+ \epsilon^2 \int_S \Big\{ c[K\rho\zeta_1^2 - 2H\zeta_1\zeta_3 + \frac{1}{2}\rho\left|\nabla\zeta_1\right|^2] + \zeta_5[\zeta_3 - 2H\rho\zeta_1] \\
&\qquad - 2cH\zeta_2\rho + c\zeta_4 + \zeta_6\rho \Big\} dS + \mathcal{O}(\epsilon^3).
\end{aligned} \tag{2.17}$$

In order for the constraints to satisfy up to the second order, we need

$$\begin{aligned}
&\int_S \{\zeta_3 - 2H\rho\zeta_1\}\, dS = 0, \\
&\int_S \Big\{ K\rho\zeta_1^2 - 2H\zeta_1\zeta_3 + \zeta_4 - 2H\zeta_2\rho + \frac{1}{2}\rho\left|\nabla\zeta_1\right|^2 \Big\} dS = 0, \\
&\int_S \big\{ c[\zeta_3 - 2H\rho\zeta_1] + \rho\zeta_5 \big\} dS = 0, \\
&\int_S \Big\{ c[K\rho\zeta_1^2 - 2H\zeta_1\zeta_3 + \frac{1}{2}\rho\left|\nabla\zeta_1\right|^2] \\
&\qquad + \zeta_5[\zeta_3 - 2H\rho\zeta_1] - 2cH\zeta_2\rho + c\zeta_4 + \zeta_6\rho \Big\} dS = 0.
\end{aligned} \tag{2.18}$$

It follows that there exist functions $\beta_1, \beta_2, \gamma_1, \gamma_2$ such that

$$\begin{aligned}
&\Delta\gamma_1 = \zeta_3 - 2H\rho\zeta_1, \\
&\Delta\gamma_2 = K\rho\zeta_1^2 - 2H\zeta_1\zeta_3 + \zeta_4 - 2H\zeta_2\rho + \frac{1}{2}\rho\left|\nabla\zeta_1\right|^2, \\
&\Delta\beta_1 = c[\zeta_3 - 2H\rho\zeta_1] + \rho\zeta_5, \\
&\Delta\beta_2 = c[K\rho\zeta_1^2 - 2H\zeta_1\zeta_3 + \frac{1}{2}\rho\left|\nabla\zeta_1\right|^2] + \zeta_5[\zeta_3 - 2H\rho\zeta_1] - 2cH\zeta_2\rho + c\zeta_4 + \zeta_6\rho.
\end{aligned} \tag{2.19}$$

Solving (2.19) for $\zeta_{i,\, i=\overline{3,6}}$ and substituting them into (2.15) we have

$$\begin{aligned}\delta\rho &= \epsilon\left\{2H\rho\zeta_1 + \Delta\gamma_1\right\} \\ &\quad + \epsilon^2\Big\{2H\rho\zeta_2 + \zeta_1^2[4H^2 - K]\rho - \frac{1}{2}\rho|\nabla\zeta_1|^2 + 2H\zeta_1\Delta\gamma_1 + \Delta\gamma_2\Big\}, \\ \delta c &= \epsilon\frac{\Delta\beta_1 - c\Delta\gamma_1}{\rho} + \epsilon^2\frac{\rho\Delta\beta_2 - \Delta\beta_1\Delta\gamma_1 + c(\Delta\gamma_1)^2 - c\rho\Delta\gamma_2}{\rho^2}.\end{aligned} \tag{2.20}$$

We have shown that any arbitrary perturbation that satisfies the constraint to second order is necessarily of the form (2.20). The converse is also true by verification. Note also, that $\zeta_i, \beta_i, \gamma_i, i = 1, 2$ are independent.

Finally, we note that in light of the specific form of (2.20), taking first and second variations with respect to ζ_2, β_2 and γ_2 does not yield any new information. Thus, we take the variation of the surface, density and composition to be

$$\begin{aligned}\delta\mathbf{x} &= \epsilon\psi_1\mathbf{n}, \\ \delta\rho &= \epsilon\left(2H\rho\psi_1 + \Delta\psi_2\right) \\ &\quad - \epsilon^2\left((K - 4H^2)\rho\psi_1^2 + \frac{1}{2}\rho|\nabla\psi_1|^2 - 2H\psi_1\Delta\psi_2\right), \\ \delta c &= \epsilon\frac{\Delta\psi_3 - c\Delta\psi_2}{\rho} - \epsilon^2\Delta\psi_2\frac{\Delta\psi_3 - c\Delta\psi_2}{\rho^2}.\end{aligned} \tag{2.21}$$

for arbitrary functions $\psi_i, i = 1, 2, 3$. Another way to approach the problem is to introduce Lagrange multipliers associated with the constraints (1). Details on the equivalence between the two approaches are provided in Appendix C.

2.3 Equilibrium Configurations

We now derive the equilibrium equations in accordance with Section 2.2.2. By definition,

$$\delta^{(1)}\mathcal{F} = \frac{d\mathcal{F}(\mathbf{x}+\delta\mathbf{x}, \rho+\delta\rho, c+\delta c)}{d\epsilon}\bigg|_{\epsilon=0}. \tag{2.22}$$

Plugging (2.21) into (2.22), applying integral theorems associated with the conventional and non-conventional gradient operators, and letting $\delta^{(1)}\mathcal{F} = 0$ for arbitrary ψ_i, we conclude, after some algebraic manipulations, with the following three equilibrium equations

$$\begin{aligned}\Delta(k_H(c)(2H - H_0(c))) + 4k_H(c)H(H^2 - K) + k_H(c)H_0(c)(2K - HH_0(c)) \\ - 2Hf(c) + k_c(H|\nabla c|^2 - \nabla c \cdot \widetilde{\nabla} c) + 2k_\rho H(\rho^2 - 1) - P = 0,\end{aligned} \tag{2.23a}$$

$$\begin{aligned}\Delta\Bigg(2k_\rho(\rho-1) + c\frac{k_H(c)H_0'(c)(2H - H_0(c)) - f'(c) + k_c\Delta c}{\rho} \\ - \frac{c\,k_H'(c)(2H - H_0(c))^2}{2\rho}\Bigg) = 0\end{aligned} \tag{2.23b}$$

$$\Delta\left(-\frac{k_H(c)H_0'(c)(2H - H_0(c)) - f'(c) + k_c\Delta c}{\rho} + \frac{k_H'(c)(2H - H_0(c))^2}{2\rho}\right) = 0, \tag{2.23c}$$

where $()'$ denote the derivative with respect to c.

Equation (2.23a) is associated with variations in the membrane shape, and generalizes the *shape equation* for single component membranes [ZCH89]. The first three terms, which include the coefficient k_H, describe the contribution of bending. There is no term involving k_K because the integral of the Gauss curvature is conserved on a closed surface according to the Gauss-Bonnet theorem. The fourth and fifth terms come from the free energy associated with composition. The final two terms are a generalization of the Young-Laplace equation, and we identify $2k_\rho(\rho^2 - 1)$ as the membrane tension.

Similarly, we denote the equations associated with the perturbations in ρ (2.23b) and in c (2.23c) the *density* and *composition equations*, respectively. We note that if $\Delta\varphi = 0$ over a closed surface, φ is a constant function:

$$\begin{aligned} \Delta\varphi = 0 \Rightarrow 0 = \int_S \varphi\Delta\varphi \, dS = -\int_S \nabla\varphi \cdot \nabla\varphi \, dS \\ \Rightarrow \nabla\varphi = 0 \Rightarrow \varphi = const. \end{aligned} \tag{2.24}$$

Therefore, we can combine the density and composition equations, and show that

$$2k_\rho(\rho^2 - 1) = (\rho + 1)(\alpha_2 + \alpha_1 c), \tag{2.25}$$

where α_1 and α_2 are constants. It follows that the membrane tension is not necessarily uniform in multi-component membranes. Further, the coefficient α_1 linking tension and composition is a generalized specific chemical potential. Interestingly, this potential depends both on membrane shape and composition. Finally, the composition equation, (2.23c) may be interpreted as a generalized Cahn-Hilliard equation. The presence of $H_0'(c)$ indicates that shape can drive non-trivial variations in composition even when $f(c)$ is convex ($f'(c)$ monotone).

2.4 Linear Stability

The three coupled equations (2.23) enable us to find equilibrium configurations. Nevertheless, an equilibrium configuration is not necessarily a stable one. We therefore proceed with analyzing the linear stability of the equilibrium solutions by investigating the second

variation of the energy functional

$$\delta^{(2)}\mathcal{F} = \frac{d^2 F(\mathbf{x}+\delta\mathbf{x}, \rho+\delta\rho, c+\delta c)}{d\epsilon^2}\bigg|_{\epsilon=0} \tag{2.26}$$

with respect to (2.21). By applying integral theorems associated with the conventional and non-conventional gradients, we are able to write the second variation in the following compact form:

$$\delta^{(2)}\mathcal{F} = \int_S \sum_{i,j=1}^{3} D_{ij}\psi_i\psi_j \, dS, \tag{2.27}$$

where D is a symmetric differential operator with the following components

$$
\begin{aligned}
D_{11}\psi_1\psi_1 =& k_H(c)(\Delta\psi_1)^2 - k_c(\nabla c\cdot\nabla\psi_1)^2 + 2k_H(c)(2H-H_0)(2\psi_1\nabla H \\
&- \overline{\nabla}\psi_1)\cdot\nabla\psi_1 + \{2k_\rho[K(1-\rho^2)+4H^2\rho^2] + 2k_c[|\nabla c|^2(2H^2-K) \\
&- H\nabla c\cdot\overline{\nabla}c] + K[k_H(c)(H_0^2-20H^2+4K)+2f] + 16k_H(c)H^4 \\
&+ 2PH\}\psi_1^2 + \{\frac{1}{2}k_H(c)H_0(H_0-8H) + \frac{1}{2}k_c|\nabla c|^2 + k_\rho(1-\rho^2) + f \\
&+ k_H(c)6H^2\}|\nabla\psi_1|^2 + 4k_H(c)\{4H^2 - HH_0 - K\}\psi_1\Delta\psi_1, \\
D_{12}\psi_1\psi_2 =& \frac{c\Delta\psi_2}{\rho}\Big\{2k_c\nabla c\cdot[\nabla(H\psi_1) - \overline{\nabla}\psi_1] + k_H(c)H_0^{'}\Delta\psi_1 + [2k_c(H\Delta c - \overline{\Delta}c) \\
&+ 2(Hf^{'} + k_H(c)(HH_0H_0^{'} - KH_0^{'})) + 4k_\rho H\frac{\rho^2}{c}]\psi_1 \\
&- k_H^{'}(c)(2H-H_0(c))[\Delta\psi_1 + HH_0(c)\psi_1 + 2(H^2-K)\psi_1]\Big\}, \\
D_{13}\psi_1\psi_3 =& \frac{\Delta\psi_3}{\rho}\Big\{2k_c\nabla c\cdot[\overline{\nabla}\psi_1 - \nabla(H\psi_1)] - k_H(c)H_0^{'}\Delta\psi_1 \\
&- 2[k_c(H\Delta c - \overline{\Delta}c) + Hf^{'}HH_0H_0^{'} - k_H(c)KH_0^{'}]\psi_1 \\
&+ k_H^{'}(c)(2H-H_0(c))[\Delta\psi_1 + HH_0(c)\psi_1 + 2(H^2-K)\psi_1]\Big\}, \\
D_{22}\psi_2\psi_2 =& \frac{c\Delta\psi_2}{\rho}\Big\{\frac{\Delta\psi_2}{\rho}[k_H(c)H_0^{'}(cH_0^{'} + 2H_0 - 4H) + 2f^{'} - 2k_c\Delta c \\
&+ 2k_\rho\frac{\rho^2}{c} + cQ + k_H^{'}(c)(2H - H_0(c) - 2cH_0^{'}(c))] - k_c\Delta\left(\frac{c\Delta\psi_2}{\rho}\right)\Big\}, \\
D_{23}\psi_2\psi_3 =& \Delta\psi_2\Big\{\frac{c}{\rho}k_c\Delta\left(\frac{\Delta\psi_3}{\rho}\right) - \frac{1}{\rho^2}[k_H(c)H_0^{'}(cH_0^{'} + H_0 - 2H) + f^{'} \\
&- k_c\Delta c + cQ + \frac{1}{2}k_H^{'}(c)(2H-H_0(c))(2H-H_0(c)-4cH_0^{'}(c))]\Delta\psi_3\Big\}, \\
D_{33}\psi_3\psi_3 =& \frac{\Delta\psi_3}{\rho}\Big\{\frac{\Delta\psi_3}{\rho}\left[Q + k_H(c)H_0^{'2} - 2k_H^{'}(c)H_0^{'}(c)(2H-H_0(c))\right] \\
&- k_c\Delta\left(\frac{\Delta\psi_3}{\rho}\right)\Big\},
\end{aligned}
\tag{2.28}
$$

and

$$
Q = f^{''}(c) - k_H(c)H_0^{''}(c)(2H-H_0(c)) + \frac{1}{2}k_H^{''}(c)(2H-H_0(c))^2. \tag{2.29}
$$

Notice from (2.28) that D_{11} generalizes to what one expects for single-component vesicles [ZCH89]. Also, the important interplay between composition and geometry is captured by the parameter Q, which is the unique combination through which the second derivatives of both f and H_0 appear. It shows that instabilities may be triggered by f, or by H_0 or by size.

The critical configurations are identified by the solution of the eigenvalue problem associated with (2.27). Furthermore, stability can be examined by studying the eigenvalues of the operator D. In general, achieving this is difficult even for the homogeneous membrane [ZCH89]. Nevertheless, equation (2.27) provides a powerful tool for numerical analysis of the stability of any equilibrium configuration.

2.5 The Uniform Spherical Membrane

2.5.1 The Uniform Spherical Membrane

Besides being an attractive mathematical problem, the stability of a uniform spherical membrane is of practical importance. Many experiments on multi-component vesicles have demonstrated a complex landscape of morphologies with a spherical (or quasi-spherical) membrane shape [BDWJ05, BHW03, DTB08, VK03]. Moreover, the starting point of these experiments is often spherical and uniform vesicles, which respond to an external stimulation, such as changes in temperature or in osmotic pressure, by altering their composition landscape and shape.

Let us use standard spherical coordinates, and denote the equilibrium state associated

with the uniform spherical membrane with an overbar. Thus,

$$\overline{H} = -\overline{R}^{-1}, \quad \overline{K} = \overline{H}^2, \tag{2.30}$$

where $\overline{R}$ is the radius of the sphere. Also, the Laplace-Beltrami operator is the usual Laplace operator on the sphere, i.e.

$$\nabla^2 y = \Delta y = \frac{1}{R^2 \sin\theta}\left((y_{,\theta}\sin\theta)_{,\theta} + \frac{1}{\sin\theta} y_{,\phi\phi}\right). \tag{2.31}$$

Further, the Laplace-Beltrami operator and the operator $\overline{\nabla}^2$ defined in (2.12) satisfy the simple relation

$$\overline{\nabla}^2 y = \overline{H}\nabla^2 y. \tag{2.32}$$

Since density and composition are uniform, the density and composition equations (2.23b, 2.23c) are satisfied identically, and the shape equation (2.23a) becomes

$$k_H H_0(\overline{c})(2\overline{H}^2 - \overline{H}H_0(\overline{c})) + 2k_\rho \overline{H}(\overline{\rho}^2 - 1) - 2\overline{H}f(\overline{c}) - P = 0. \tag{2.33}$$

Recall that the total number of molecules in the vesicle, M, is fixed. Thus,

$$\overline{\rho} = \overline{H}^2. \tag{2.34}$$

Therefore, a two-phase vesicle with an overall concentration $\overline{c} = M_I/M$ can have an equi-

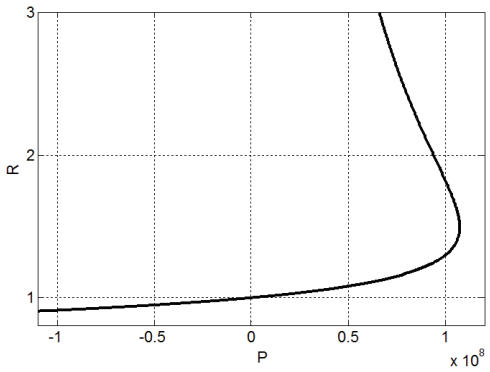

Figure 2.1: Pressure - radius relation for a uniform sphere.

librium configuration of uniform composition and spherical shape if

$$-2\overline{Hf} + k_H\overline{H}_0(2\overline{H} - \overline{HH}_0) + 2k_\rho\overline{H}(\overline{H}^4 - 1) - P = 0. \tag{2.35}$$

Above, $\overline{f}$ and $\overline{H}_0$ imply that these functions are evaluated at $\bar{c}$. Equation (2.35) provides an explicit expression for the relation between the pressure difference and the radius of the vesicle. We note that for a typical vesicle with a $100\,\mu$m diameter, the (non-dimensional) value of k_ρ is of the order 10^8. Further, pressure difference of 10 Pa corresponds to $P = 10^5$. Therefore, unless the pressure is much smaller than that, the contribution of the first two terms can be ignored. This radius-pressure relation is illustrated in Fig. 2.1. Further, we note that for relatively low pressures $1-\overline{H}^2 \ll 1$ (for example, with a pressure of 10 Pa, $1-\overline{H}^2 \approx 10^{-4}$). Therefore, from (2.34), the density of the membrane is almost unchanged. This agrees with the common assumption that the membrane has a constant area. Nevertheless, this assumption is questionable in cases where the (non-dimensional) pressure is relatively high and the membrane is strained by a few percents, as occurs in certain cells and bacteria [Boa02]. Importantly, the "constant area constraint" is usually imposed by introducing a constant (yet unknown) Lagrange multiplier [ES80, Sei97, ZCH89]. Therefore, the constant

area constraint implies that the membrane stretch is uniform. Obviously this is not the case in multi-component membranes where ρ can vary considerably (2.25). Accounting for the non-uniform stretch is important in studying phenomena such as mechano-sensation and ion-channels activity, where membrane stretching governs the mechanical response. Our formulation accounts for the non-uniform stretch in the membrane through ρ.

Next, we calculate the second variation of the energy functional for a uniform spherical membrane. To do that, we evaluate (2.27) and (2.28) using relation (2.30)-(2.32), (2.34) with $\rho = \overline{\rho} = const$ and $c = \overline{c} = const$. In addition, it is convenient to expand each of the functions ψ_i into a series of spherical harmonics [ZCH89, MLK02]

$$\psi_i = \sum_{l,m} A_i^{(l,m)} Y^{(l,m)}, \tag{2.36}$$

where $A_i^{(l,m)}$ are constants and $Y^{(l,m)}$ is the spherical harmonic of degree l and order m satisfying

$$\Delta Y^{(l,m)} = -\overline{H}^2 l(l+1) Y^{(l,m)}. \tag{2.37}$$

Because the membrane is closed, we have the periodic boundary conditions, as well as regularity conditions at both the north and south poles. It requires that l and m are integers that satisfy

$$l \geq 0 \quad \text{and} \quad |m| \leq l. \tag{2.38}$$

In addition, in order to ensure that ψ_i are real functions we impose the requirement

$$\left(A_i^{(l,m)}\right)^* = (-1)^m A_i^{(l,-m)}. \tag{2.39}$$

Above, the asterisk refers to complex conjugate, and the relation $\left(Y^{(lm)}\right)^* = (-1)^m Y^{(l,-m)}$

has been used. With the aid of the last four equations we conclude with

$$\delta^{(2)}\mathcal{F} = \sum_{l\geq 0}\sum_{|m|\leq l} G_{ij} A_i^{(l,m)} \left(A_j^{(l,m)}\right)^*, \tag{2.40}$$

where G_{ij} are the components of a 3×3 symmetric matrix $\mathbf{G}$ which depends on l but not on m:

$$\begin{aligned}
G_{11} =& \overline{H}^2\Big\{k_\rho[10\overline{H}^4 - 2 + l(l+1)(1-\overline{H}^4)] \\
&+ \frac{1}{2}(l+2)(l-1)[\overline{k}_H(2\overline{H}^2 l(l+1) + \overline{H}_0^2 - 4\overline{H}\overline{H}_0) + 2\overline{f}]\Big\}, \\
G_{12} =& \overline{H} l(l+1)\Big\{c\overline{k}_H[(\overline{H}l(l+1) + 2(\overline{H}-\overline{H}_0))\overline{H}_0^{'}] - 2c\overline{f}^{'} - 4k_\rho\overline{H}^4 \\
&+\overline{k}_H^{'}\overline{c}(2\overline{H}-\overline{H}_0)(\overline{H}_0 - \overline{H}l(l+1))\Big\}, \\
G_{13} =& -\overline{H}l(l+1)\Big\{\overline{k}_H\overline{H}_0^{'}[l(l+1)\overline{H} + 2(\overline{H}-\overline{H}_0)] - 2\overline{f}^{'} \\
&+\overline{k}_H^{'}(2\overline{H}-\overline{H}_0)(\overline{H}_0 - \overline{H}l(l+1))\Big\}, \\
G_{22} =& l^2(l+1)^2\Big\{2k_\rho\overline{H}^4 + k_c\overline{c}^2 l(l+1)\overline{H}^2 - \overline{c}[\overline{k}_H(4\overline{H} - 2\overline{H}_0 - \overline{c}\overline{H}_0^{'})\overline{H}_0^{'} \\
&- \overline{c}\overline{Q} - 2\overline{f}^{'} + \overline{k}_H^{'}\overline{c}(2\overline{H}-\overline{H}_0)(2\overline{H}-\overline{H}_0 - 2\overline{c}\overline{H}_0^{'})]\Big\}, \\
G_{23} =& l^2(l+1)^2\Big\{l(l+1)\overline{c}\overline{H}^2 k_c + \overline{k}_H(2\overline{H}-\overline{H}_0 - \overline{c}\overline{H}_0^{'})\overline{H}_0^{'} - \overline{c}\overline{Q} - \overline{f}^{'} \\
&-\frac{1}{2}\overline{k}_H^{'}(2\overline{H}-\overline{H}_0)(2\overline{H}-\overline{H}_0 - 4\overline{c}\overline{H}_0^{'})\Big\}, \\
G_{33} =& l^2(l+1)^2\Big\{l(l+1)\overline{H}^2 k_c + \overline{k}_H\overline{H}_0^{'2} + \overline{Q} - 2\overline{k}_H^{'}(2\overline{H}-\overline{H}_0)\overline{H}_0^{'}\Big\}.
\end{aligned} \tag{2.41}$$

The equilibrium configuration is stable if $\delta^2 F$ is positive for any $Q_i^{(l,m)}$. An equivalent representation of (2.40) is

$$\delta^2\mathcal{F} = \mathbf{A}\mathbf{J}\left(\mathbf{A}^*\right)^T, \tag{2.42}$$

where

$$\mathbf{A} = \left(\psi_1^{0,0}, \psi_2^{0,0}, \psi_3^{0,0}, \dots \psi_1^{l,-l}, \psi_2^{l,-l}, \psi_3^{l,-l}, \dots \psi_1^{l,l}, \psi_2^{l,l}, \psi_3^{l,l}\right) \tag{2.43}$$

and

$$\mathbf{J} = \begin{pmatrix} [G(l=0)] & & & & 0 \\ & \ddots & & & \\ & & [G(l)] & & \\ & & & \ddots & \\ & & & & [G(l)] \\ & 0 & & & & \ddots \end{pmatrix} \tag{2.44}$$

Therefore, critical configurations can be obtained by the requirement $\det(G) = 0$, and an equilibrium configuration is stable if all three eigenvalues of $\mathbf{G}(l)$ are positive for any $l \geq 0$.

2.5.2 Numerical Results

Equations (2.41) show how the stability of the uniform sphere is dictated by the mechanical properties of the membrane, k_H and k_ρ, the coupling between shape and composition, $H_0(c)$, and the nature of interaction between the two phases through $f(c)$ and k_c. While reports regarding measured values of k_H and k_ρ are consistent [Boa02, Sei97], the literature still lacks systematic measurements of the other quantities. These are harder to gauge, may significantly differ for different types of lipids or proteins, and are much more sensitive to temperature. For example, the interaction function $f(c)$ may change from single well to double well energy structure by varying the temperature by a few degrees. From (2.4) we can calculate f'' as

$$f''|_{c=0.5} = 4\frac{R^2\rho_0}{k_H}\kappa T_0\left(\frac{T}{T_0} - \frac{B}{4\kappa T_0}\right), \tag{2.45}$$

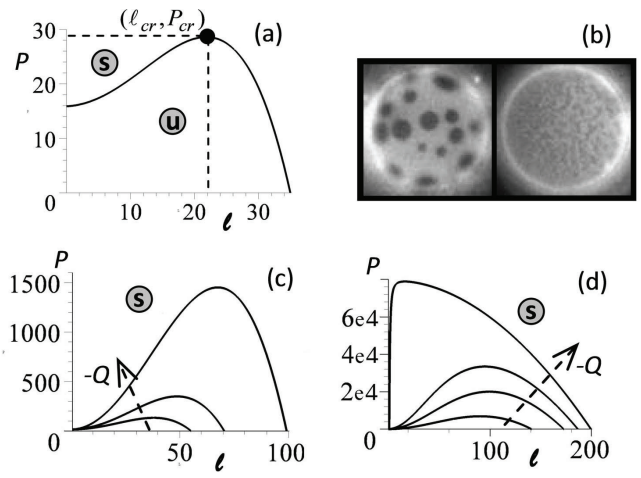

Figure 2.2: Projection of the stability phase diagram on the $P - l$ plane for different values of Q and $k_c = 0.01, H_0 = -10, H_0' = -20$. The solid line separates between stable and unstable regions, denoted here with "**s**" and "**u**", respectively. (a) $Q = -10$, (c) $Q = -30, -50, -100$, (d) $Q = -200, -300, -3500, -400$. (b) Immediately after temperature is lowered a characteristic length scale appears - experimental observations of [VK03] for two different setups. (Reprinted from [VK03], Copyright (2013), with permission from Elsevier.)

where T_0 is the room temperature. Recalling that $k_H \approx 10^{-19}$ J and $\rho \approx 10^4$ molecules per μm^2 (lateral area occupied by a single membrane proteins is roughly 10 nm), we conclude that a change of one kelvin corresponds to a change of ~ 100 in f''. Thus, for the same composition, $f''(c)$ changes sign (from convex to concave and vice-versa), which in turn can change the sign of the second variation. Therefore, we focus in the examples below on demonstrating how the stability of the uniform sphere is affected by $f''(c)$, k_c, and H_0'. Note that while changes in the first two quantities can be interpreted as changes in temperature, as discussed above, H_0' reflects the strength of the coupling between composition and shape.

In all examples below, we consider a 10 μm vesicle with $\bar{c} = 0.5$ ($M_I = M_{II}$). Thus, typical (dimensional) values of $k_H = 10^{-19}$ J and $k_\rho = 100\,\mathrm{mJ/m^2}$ correspond to non-dimensional values of $k_H = 1$ and $k_\rho = 10^8$. In addition, we assume that $f'\big|_{\bar{c}} = 0$, which means that $\bar{c}$ locates the bottom of the composition "energy well".

Fig. 2.2(a) illustrates a typical stability phase diagram projected on the $P - l$ plane showing stable regions (**G** positive definite) and unstable regions. A configuration is said to be stable if all modes, l, are stable. Note that a mode l describes variations in shape, composition, and density, where each of these variations is characterized by the same spherical mode l. Therefore, in what follows, we interchangeably interpret modes in terms of shape, composition, or both. We define the critical pressure P_{cr} as the lowest pressure for which the membrane is stable, and l_{cr} as the degree at P_{cr}. Fig. 2.2(c,d) repeat this for different values of Q. The first observation is that, in contrast to single component vesicles, multi-component vesicles can become unstable even at high positive pressures. Second, note that the critical pressure can change dramatically with Q. As noted earlier, a few degrees Celsius change in temperature can change Q by 100s. This means that the stability can depend sensitively on temperature. Consider for example a membrane with $P = 1400$ (equal to $0.14Pa$, which is typical and smaller than the pressure exerted by actin polymerization on the lamellipodium [VG07]). Such a membrane would be stable for $Q = -50$, but unstable for $Q = -100$.

A third interesting observation is that the critical modes have extremely high frequency ($l \sim 10 - 100$). This is in *marked contrast* with single-component vesicles where the critical mode is always 2 [ZCH89]. However, it is completely consistent with experimental observations [BHW03, VK03]. Fig. 2.2(b) reproduces the early stages of instability observed by Veatch and Keller [VK03] under two different experimental conditions. An important implication is that small perturbations may nucleate localized but very large deformations. The high frequency instability is consistent with (flat) spinodal decomposition. However, unlike (flat) spinodal decomposition, the critical temperature, pressure and mode depends on system size through our parameter Q.

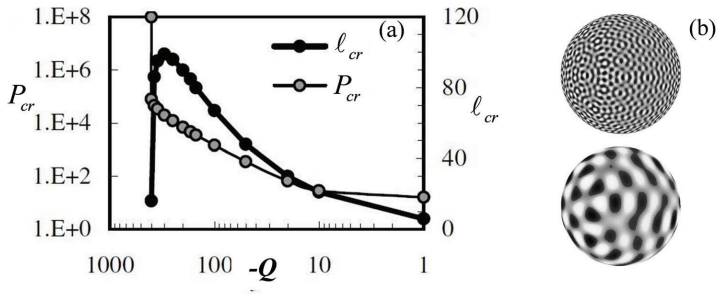

Figure 2.3: (a) Effect of temperature on critical pressure and critical mode. Change of 100 in Q corresponds to a few degrees Celsius. The P_{cr} curve separates between stable (above the curve) and unstable configurations.($k_c = 0.01, H_0 = -10, H_0' = -20$). (b) A characteristic length scale arises when a specific range of harmonics is involved. Series of spherical harmonics are illustrated in the bottom with l in the range of 14–16, and on the top with l in the range of 61–74.

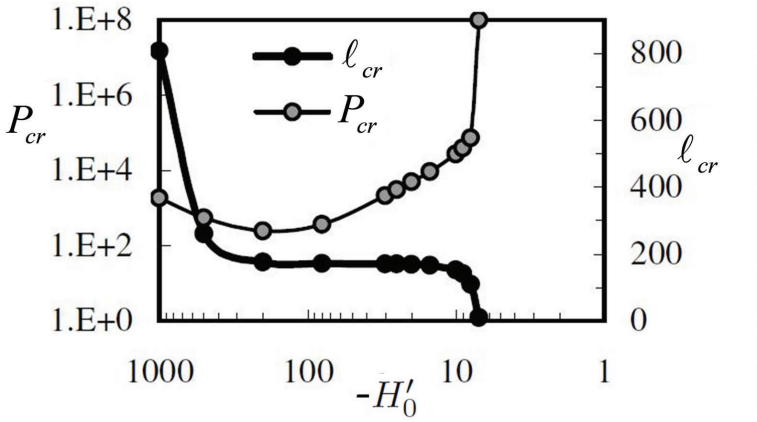

Figure 2.4: Effect of the coupling between composition and shape on critical pressure and critical mode. A negative curvature correspond to a convex shape.

Fig. 2.3 plots P_{cr} and l_{cr} as a function of Q. We note a critical value for Q below which the membrane is unstable for all pressures. We also note that P_{cr} decreases monotonically with increasing Q. However, the critical mode, l_{cr} is not monotonous. As Q decreases, the propensity for instability and consequently l_{cr} increases. However, increasing P_{cr} with decreasing Q increases the membrane tension. This, in turn, tries to reduce l_{cr}.

A second parameter that has a significant effect on the interplay between composition and geometry is H_0'. Fig. 2.4 shows how critical pressure and mode depend on this param-

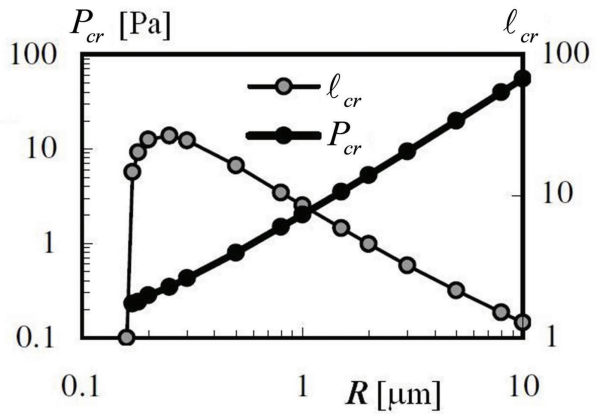

Figure 2.5: The influence of size (mass) of the vesicle on (non-dimensional) critical pressure and critical mode. Non-dimensional parameters are constant with values identical to Fig.2 with $Q = -100$ and $H_0'' = -2$ for a 10 μm vesicle.

eter. We observe that the critical pressure varies non-monotonically, but l_{cr} is monotonous. This is explained by the fact that higher values of H_0' correspond to higher spontaneous curvature of phase II, resulting in tendency of the system to have small regions in the membrane with high curvature. Interestingly, for moderate values of H_0', P_{cr} exhibits significant changes while l_{cr} is almost unaffected.

The effect of H_0', which reflects the strength of the composition-shape coupling, is demonstrated in Fig. 2.4. Here, unlike the effect of the phases interaction discussed above, the strength of the composition-shape coupling has a non-monotonous effect on the stability (P_{cr}) of the membrane. On the other hand, the effect on l_{cr} is monotonous. Interestingly, at moderate values of H_0', P_{cr} exhibits significant changes while l_{rc} is almost unaffected.

Fig. 2.5 illustrates how critical pressure and mode vary with vesicle size (mass) for the same experimental setup. This is in contrast to spinodal decomposition in flat space, which is independent of mass. Note that the critical pressure tends to zero for extremely small and large systems. The former is due to the stabilizing effect of the gradient term that dominates at small sizes, while the latter reflects the behavior of a flat membrane.

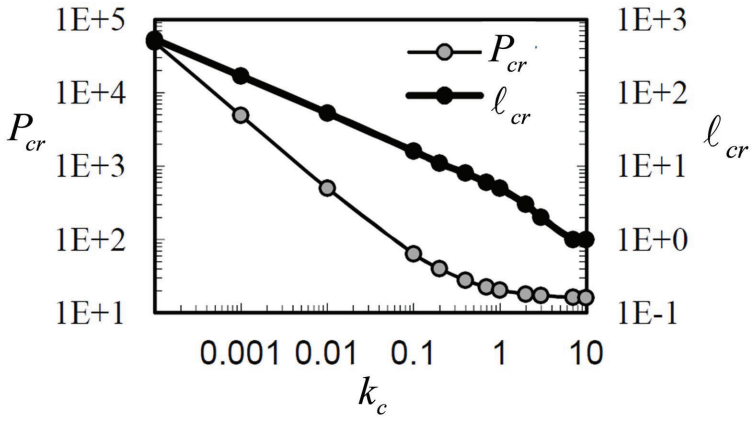

Figure 2.6: Critical pressure and critical mode as a function of k_c.

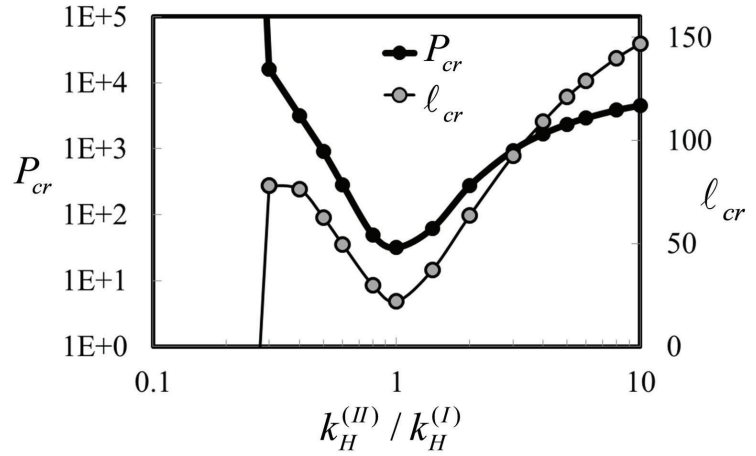

Figure 2.7: Influence of the disparity in the bending stiffness of the two components on the critical pressure and critical mode.

A higher k_c tends to make composition homogeneous. Thus, higher k_c stabilizes the membrane and excites modes with a smaller l. This is demonstrated in Fig. 2.6 where critical pressure and mode are calculated as a function of k_c. It is evident that the effect of k_c is monotonous, and a higher k_c both stabilizes the membrane and excites modes with a smaller l. The reason is that k_c penalizes for gradients in composition. Therefore, higher values of k_c tend to stabilize the uniform composition (and in turn membrane shape as well). Furthermore, since harmonics with the same amplitude and higher l correspond to higher composition gradients, high k_c tends to diminish excitation of modes with a high l.

Finally, we demonstrate how disparity in the bending stiffness of the two components influence the membrane stability. For specificity, we assume a linear relation between the bending stiffness and composition, i.e.

$$k_H(c) = c\, k_H^{(I)} + (1-c) k_H^{II}, \tag{2.46}$$

where $k_H^{(I)} = k_H\big|_{c=1}$, $k_H^{(II)} = k_H\big|_{c=0}$ are the bending stiffness of phase I and phase II, respectively. From (2.41), we see that the effect of the stiffness disparity stems from (non-dimensional) $k_H^{'}$. Using (2.46) and (2.7) we find that $k_H^{'} = 2\frac{r-1}{r+1}$, where $r = \frac{k_H^{(II)}}{k_H^{(I)}}$. Note that $|k_H^{'}|$ is bounded between zero and two. Fig. 2.7 demonstrates how the critical pressure and critical mode are affected by the ratio $k_H^{(II)}/k_H^{(I)}$, for $H_0^{'} = -30, Q = -10, k_c = 0.01$. The asymmetric behavior with respect to $k_H^{(II)}/k_H^{(I)} = 1$ is a consequence of the spontaneous curvature.

2.6 Conclusions

We have derived the general form of equilibrium equations and stability conditions for multi-component BMs. The energy functional generalizes Helfrich energy and accounts for the interaction between phases, the coupling between composition and shape, and the non-uniform spatial stretching of the membrane. The last two are specifically important in studying mechano-transduction, and coupling between membrane shape and bio-chemical events in the cell. The derivation is general and applicable to arbitrary membrane shapes, arbitrary characteristics of the interaction between the phases, and arbitrary form of the coupling between composition and shape. Calculations of the first and second variations of the energy functional include two important features that significantly simplify the derivations and make them more elegant. These are the use of the non-conventional differential operators and related integral theorems, and the introduction of appropriate composition and mass conserving variations to avoid Lagrange multipliers.

We have practiced the stability analysis for a heterogeneous membrane with uniform composition and spherical shape. This problem is of practical importance, as many experiments with multi-component vesicles study the composition landscape of spherical (or quasi-spherical) membranes, and how uniform and spherical vesicles respond to external stimuli by altering their composition landscape and shape. We have demonstrated that the response of a heterogeneous, yet uniform, membrane is fundamentally different from that of a homogeneous (single phase) membrane. For example, single phase spherical membranes are always stable with positive pressure. Nevertheless, in the case of multi-component, chemical instabilities can drive mechanical instabilities even at relatively high pressures.

The focus of the numerical examples has been the calculation of critical pressure, under

Table 2.1: Effects of phase interaction and shape-composition coupling parameters on the stability and mode.

	Higher k_c	Higher f''	Higher H_0'
Stability	Stabilize	Stabilize	Non-monotonous
Mode	Lower l	Non-monotonous	Higher l

which the vesicle destabilizes, and the corresponding mode. Specifically, we performed a parametric study in order to gain insight into how the characteristics of the interaction between the phases and the strength of the coupling between composition and shape affect the membrane stability. The results are summarized in Table 1. Furthermore, we have demonstrated that the range of excited modes depends on a delicate and non-intuitive interplay between the properties of the membrane and external conditions, such as temperature and osmotic pressure. The excitation of modes with a certain range of wavelengths corresponds to a composition landscape that has a typical morphological correlation length that depends on the level of stimulation, in qualitative agreement with experimental observations.

We emphasize that our numerical results are limited to linear stability analysis, which provides important insight regarding conditions of stability and the excited modes, but does not provide information regarding the post-stability behavior. This can be achieved by extending the current analysis to higher variations of the energy functional. Note that deriving these higher variations is technical in principle, as it is does not require any special techniques or derivations besides the ones used for calculating the first and second variations.

Chapter 3

Open Single-component Membranes

We now turn to open membranes. This investigation is motivated by periodic membranes that are observed when nerve fibers are under stretch [OPJJF97], and by tubular membranes that are under laser-induced tension [BZTM97]. In these situations, the entire vesicle is extremely long and studying them as a closed vesicle is prohibitively difficult. However, it is convenient to consider each period as an open membrane. Further, it turns out that building a general model for open membrane itself is theoretically interesting and challenging. In particular, not every contributor of the energy functional can be explicitly written in as a potential. Besides, narrowing down the domain of the problem to the axisymmetric shapes, as it is usually done, can significantly lose many solutions.

In this chapter, we first derive a model for open single-component membranes; second, we investigate the equilibrium equations and boundary conditions; third, we study the linear stability of a uniform cylindrical membrane; and finally we find the beading shapes by solving the axisymmetric equilibrium equations. Study of open multi-component membranes will be in the next chapter.

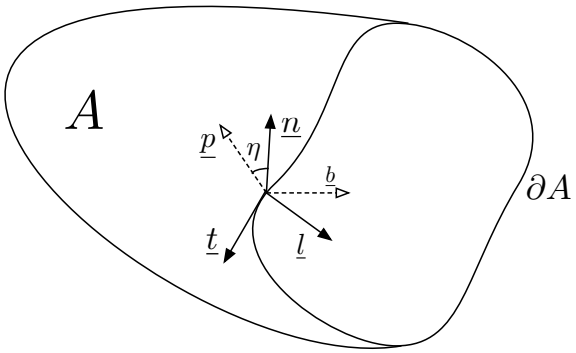

Figure 3.1: An open membrane A with boundary ∂A. The Frenet-Serret frame of ∂A is plotted in dashed arrows. The angle between the normals of the surface and the curve is denoted by η.

3.1 The Energy Functional and Its Variations

Consider an open bounded membrane (surface) A with a boundary ∂A as shown in Fig. 3.1. Let ρ denote the density of lipid molecules per unit area. The energy functional for an open single-component membrane can be written as the sum of the mechanical energy, the work of external loads and chemical energy:

$$\mathcal{F} = \mathcal{F}_{\text{mech}} + \mathcal{F}_{\text{ext}} + \mathcal{F}_{\text{chem}}. \tag{3.1}$$

As shown below, the mechanical energy and the chemical energy have explicit characterization, whereas the work done by external force does not. Therefore, we use the principle of virtual work to derive the governing equations.

3.1.1 Mechanical Potentials

There are three mechanical contributions to the total energy that can be expressed in terms of potentials: bending, stretching, and line-tension. The first two are similar to those introduced for closed membranes while the final one is different. Specifically, the bending

energy is assumed to be in the form of the classical Helfrich bending energy

$$F_{\text{bending}} = \frac{1}{2} k_H \int_A (2H - H_0)^2 dA, \tag{3.2}$$

where k_H is the bending stiffness and H is the mean curvature. The stretching energy is

$$F_{\text{stretching}} = \int_A \zeta(\rho) dA, \tag{3.3}$$

where the surface free energy $\zeta(\rho)$ controls both the membrane stretching by regulating the molecular density ρ, and the membrane chemical properties by choosing the number of molecules on the membrane. The variations of the bending and stretching energies are similar to those of closed membranes presented in Chapter 2.

The third potential is associated with the line-tension σ of the edge (boundary) and can be written as

$$F_\sigma = \int_{\partial A} \sigma \, ds. \tag{3.4}$$

To calculate the variation of F_σ, we consider a transformation

$$\underline{z}(s) = \underline{y} + \epsilon \, \underline{v}(s) \tag{3.5}$$

of the edge from position $\underline{y} = \underline{y}(s)$, where s is the arc length of the curve. The arbitrary pertubation $\underline{v}$ can be expressed in intrinsic coordinates as

$$\underline{v}(s) = v_t \underline{t} + v_p \underline{p} + v_b \underline{b}, \tag{3.6}$$

where

$$\underline{t} = \frac{d\underline{y}}{ds}, \qquad \underline{p} = \frac{1}{k}\frac{d\underline{y}}{ds}, \qquad \underline{b} = \underline{t} \times \underline{p}, \tag{3.7}$$

and k is the curvature of the curve $\underline{y}(s)$ (see Fig. 3.1). Using the Frenet-Serret formulas, it can be calculated that

$$\frac{d\underline{z}}{ds} = \underline{t} + \epsilon(v_t k\underline{p} + v_p[-k\underline{t} + k_1\underline{b}] - k_1 b v_b \underline{p}) + \epsilon\left(\dot{v}_t\underline{t} + \dot{v}_p\underline{p} + \dot{v}_b\underline{b}\right), \tag{3.8}$$

up to the first order of ϵ[1]. Therefore, the unit length element in the transformed configuration can be written as

$$ds_z = \left\|\frac{d\underline{z}}{ds}\right\| ds = (1 - \epsilon k v_p + \epsilon\dot{v}_t)\, ds. \tag{3.9}$$

Because we are interested in the membrane as a surface, it is more convenient to transform ds_z into the coordinates associated with the surface $\{\underline{t}, \underline{n}, \underline{l}\}$, where $\underline{n}$ is the surface unit normal at the edge and $\underline{l} = \underline{t} \times \underline{n}$ is the binormal (see Fig. 3.1). Let η be the angle between the two normal vectors $\underline{p}$ and $\underline{n}$, then we have

$$\begin{aligned} & v_p = v_n\underline{n}\cdot\underline{p} + v_l\underline{l}\cdot\underline{p} \\ \Rightarrow\quad & v_p = v_n\cos\eta + v_l\sin\eta \\ \Rightarrow\quad & ds_z = (1 + \epsilon[-v_n k\cos\eta - v_l k\sin\eta] + \epsilon\dot{v}_t)\, ds. \end{aligned} \tag{3.10}$$

By definition,

$$K_n = -k\cos\eta \qquad \text{and} \qquad K_g = k\sin\eta \tag{3.11}$$

are the normal and geodesic curvatures of the edge. Accordingly, we can write the unit

[1]Because we will only calculate the second variation for the surface part, we will not need the second order of ϵ here.

length of the transformed configuration as

$$ds_z = (1 + \epsilon[v_n K_n + v_l K_g])\, ds + \epsilon \dot{v}_t ds, \tag{3.12}$$

and the corresponding edge energy as

$$F_\sigma(\epsilon) = \int_{\partial A} \sigma(1 + \epsilon[v_n K_n + v_l K_g]) ds + \epsilon \int_{\partial A} \sigma \dot{v}_t ds. \tag{3.13}$$

As ∂A is a closed curve, we have

$$\begin{aligned} \int_{\partial A} \sigma \dot{v}_t ds &= \sigma v_t|_{\partial(\partial A)} - \int_{\partial A} \dot{\sigma} v_t ds \\ &= -\int_{\partial A} \dot{\sigma} v_t ds. \end{aligned} \tag{3.14}$$

Therefore, $F_\sigma(\epsilon)$ can be simplified to

$$F_\sigma(\epsilon) = \int_{\partial A} \sigma(1 + \epsilon[v_n K_n + v_l K_g]) ds - \epsilon \int_{\partial A} \dot{\sigma} v_t ds. \tag{3.15}$$

It follows that the variation of the line tension energy can be written as

$$\delta^{(1)} F_\sigma = \int_{\partial A} \sigma(v_n K_n + v_l K_g) ds - \int_{\partial A} \dot{\sigma} v_t ds. \tag{3.16}$$

3.1.2 The Work Done by External Forces

The second term in (3.1) is the work of external forces, which include the forces and moments at the edge as well as the pressure over the surface. Denote by $\underline{N}$ and $\underline{\tau}$ the forces in the normal and binormal directions respectively; M the bending moment; and P the pressure.

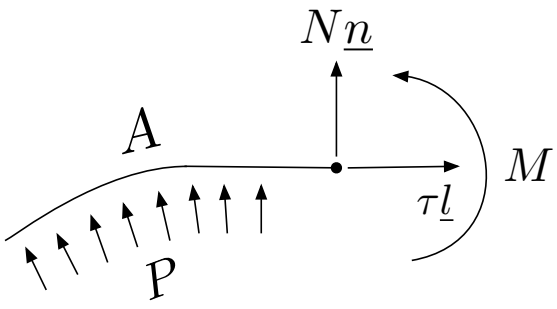

Figure 3.2: External forces and moment acting on the membrane.

The work of the external forces and moments at the edge can be calculated as

$$W_{\text{ext}} = -\int_{\partial A} M\dot{\underline{n}} \cdot \underline{l}\, ds - \int_{\partial A} N\underline{v} \cdot \underline{n}\, ds - \int_{\partial A} \tau\underline{v} \cdot \underline{l}\, ds, \tag{3.17}$$

where $\underline{n}$ and $\underline{l}$ are the normal and binormal unit vector of the edge associated with the surface.

Because pressure is always normal to the surface, calculating the corresponding work needs special care. Consider the transformation

$$\underline{z}(t) = \underline{y} + t\underline{u} \tag{3.18}$$

of the surface from time $t = 0$ to time $t = 1$ [Pea59]. The work done by pressure on this transformation can be calculated as

$$\begin{aligned} W(P) &= \int_0^1 dt \int_{A^{(t)}} \left[-P\frac{d}{dt}(u_i t)(n_i)^{(t)} dA^{(t)} \right] \\ &= -Pu_i \int_0^1 dt \int_{A^{(t)}} (n_i)^{(t)} dA^{(t)}. \end{aligned} \tag{3.19}$$

The surface area elements at position $\underline{y}$ and position $z(t)$ are

$$dA_i^0 = n_i^0 dA^0 = e_{ijk} dy_j^{(1)} dy_k^{(2)} \tag{3.20}$$

and

$$dA_i^{(t)} = n_i dA^{(t)} = e_{ijk} dz_j^{(1)} dz_k^{(2)}, \tag{3.21}$$

where

$$dz_i^{(1)} = \frac{\partial z_i}{\partial y_j} dy_j^{(1)} \qquad \text{and} \qquad dz_i^{(2)} = \frac{\partial z_i}{\partial y_j} dy_j^{(2)}. \tag{3.22}$$

The two surface area elements are related as

$$\begin{aligned} dA_i^t =& e_{ijk} \frac{\partial z_j}{\partial y_s} \frac{\partial z_k}{\partial y_t} dy_s^{(1)} dy_t^{(2)} \\ =& \frac{1}{2} e_{ijk} \frac{\partial z_j}{\partial y_s} \frac{\partial z_k}{\partial y_t} e_{mst} e_{mpq} dy_p^{(1)} dy_q^{(2)} \\ =& \frac{1}{2} e_{ijk} e_{mst} \frac{\partial z_j}{\partial y_s} \frac{\partial z_k}{\partial y_t} dA_m^{(0)}. \end{aligned} \tag{3.23}$$

Accordingly, the relationship between the directional area elements can be written as

$$n_i^{(t)} dA^{(t)} = \frac{1}{2} e_{ijk} e_{mst} \frac{\partial z_j}{\partial y_s} \frac{\partial z_k}{\partial y_t} n_m^{(0)} dA^{(0)}. \tag{3.24}$$

Plugging (3.24) into (3.19), we have

$$\begin{aligned} W(P) =& - P u_i \int_0^1 \int_{A^{(0)}} \frac{1}{2} e_{ijk} e_{rpq} \frac{\partial (y_j + u_j t)}{\partial x_p} \frac{\partial (y_k + u_k t)}{\partial x_q} n_r dA^{(0)} \\ =& - P u_i \int_{A^{(0)}} \left\{ \frac{1}{2} e_{ijk} e_{rpq} \delta_{jp} \delta kq + \frac{1}{4} e_{ijk} e_{rpq} (\delta_{jp} u_{k,q} + \delta_{kq} u_{j,p}) + \frac{1}{6} e_{ijk} e_{rpq} u_{j,p} u_{k,q} \right\} n_r dA^{(0)} \end{aligned}$$

or

$$W(P) = -P \int_{A^{(0)}} \left\{ u_i n_i + \frac{1}{2}(u_{k,k} n_i - u_{k,i} n_k) u_i + \frac{1}{6} e_{ijk} e_{rpq} u_{j,p} u_{k,q} u_i n_r \right\} dA^{(0)}. \tag{3.25}$$

It can be easily seen from equation (3.25) that the first variation of the "pressure potential" involves only the normal component of the transformation, i.e.

$$\delta^{(1)} F_p := W_p = -\int_A P u_i n_i \, dA. \tag{3.26}$$

Moreover, we can show that the second order term

$$\begin{aligned} II &= -\frac{P}{2} \int_A (u_{k,k} n_i - u_{k,i} n_k) u_i dA \\ &= -\frac{P}{2} \int_A \{ (\nabla \cdot \underline{u})(\underline{u} \cdot \underline{n}) - [(\nabla \underline{u}) \cdot \underline{n}] \cdot \underline{u} \} \, dA, \end{aligned} \tag{3.27}$$

where $\nabla \underline{u} = \frac{\partial}{\partial x_i} \underline{e}_i \otimes u_k \underline{e}_k = u_{k,i} \, \underline{e}_i \otimes \underline{e}_k$, does not depend on the tangential perturbations either. Let $\underline{g}^{\alpha,\, \alpha=\overline{1,2}}$ be the curvilinear coordinate basis of the surface and consider an arbitrary transformation

$$\underline{u} = u_\alpha \underline{g}^\alpha \tag{3.28}$$

in the tangential direction. Since $\underline{u} \cdot \underline{n} = 0$, the first term in (3.27) vanishes and the second order term then becomes

$$II = \frac{P}{2} \int_A [(\nabla \underline{u}) \cdot \underline{n}] \cdot \underline{u} \, dA. \tag{3.29}$$

From equation (3.28) we have

$$\begin{aligned}\nabla \underline{u} &= \frac{\partial}{\partial x_i}\underline{e}_i \otimes u_\alpha \underline{g}^\alpha \\ &= u_{\alpha,i}\,\underline{e}_i \otimes \underline{g}^\alpha \qquad (\alpha = \overline{1,2},\ i = \overline{1,3}),\end{aligned} \tag{3.30}$$

$$\Rightarrow (\nabla \underline{u}) \cdot \underline{n} = u_{\alpha,i}\,\underline{e}_i \otimes \underline{g}^\alpha \cdot \underline{n} = 0. \tag{3.31}$$

Hence, II vanishes for any tangential perturbations. In other words, both the first and second variations depend only on the normal perturbation.

Therefore, without loss of generality, we can use normal perturbations

$$\underline{u} = \psi \underline{n}. \tag{3.32}$$

to simplify (3.25). The work of pressure can then be written as

$$W(P) = -P \int_{A^{(0)}} \left\{ \psi + \frac{1}{2}\left[(\psi n_k)_{,k}\psi - (\psi n_k)_{,i} n_k \psi n_i \right] + \text{h.o.t} \right\} dA^{(0)}. \tag{3.33}$$

Notice that $\underline{n}$ is the normal unit vector, so

$$n_i n_i = 1, \qquad (n_i n_i)_{,k} = 0, \qquad \text{and} \qquad n_{k,k} = \nabla \cdot \underline{n} = -2H. \tag{3.34}$$

Changing the notation $v_n \equiv \psi$, the first and second variations related to pressure are

$$\delta^{(1)} F_p = -\int_A P v_n \, dA, \tag{3.35}$$

and

$$\delta^{(2)} F_p = P \int_A 2H v_n^2 dA, \tag{3.36}$$

respectively.

3.1.3 Chemical Potential

Lastly, we consider the last term in (3.1) which accounts for the number of molecules on the membrane. Since we have an open system, it can exchange molecules with the environment. We will investigate three cases: isolated membranes, membranes connected to a lipid bath, and periodic membranes.

First, if the membrane is chemically isolated, the number of molecules is conserved. To address this conservation constraint, we use the Lagrange multiplier method by adding

$$-\lambda \left(\int_A \rho \, dA - N_0 \right), \tag{3.37}$$

where λ is a Lagrange multiplier constant, to the energy functional. Because N_0 and λ are constants, they do not affect other quantities in the variation, and can be dropped from the energy functional. As a result, the chemical contribution can be written as

$$-\lambda \int_A \rho \, dA, \tag{3.38}$$

where λ is the Lagrange multiplier.

Second, if the membrane is connected to a lipid reservoir, the total number of molecules from the reservoir and the membrane is conserved. The chemical energy of the whole system

together with the constraint can be written as

$$\mathcal{F}_c = \int_A \zeta(\rho) dA + \int_{\mathcal{A}\setminus A} \bar{\zeta}(\rho) dA - \lambda \left(\int_A \rho \, dA + \int_{\mathcal{A}\setminus A} \rho \, dA - N_0 \right), \tag{3.39}$$

where A and $\mathcal{A} \setminus A$ are the spaces occupied by the membrane and the reservoir, respectively. The first variation of $\mathcal{F}_c$ can be calculated as

$$\begin{aligned} \delta^{(1)}\mathcal{F}_c = &\int_A \left\{ \zeta'(\rho) - \lambda \right\} \delta\rho \, dA + \int_{\mathcal{A}\setminus A} \left\{ \bar{\zeta}'(\rho) - \lambda \right\} \delta\rho \, dA \\ &+ \int_{\partial A} \left\{ \zeta(\rho) - \bar{\zeta}(\rho) - \lambda [\![\rho]\!] \right\} \underline{v} \cdot \underline{l} \, dA. \end{aligned} \tag{3.40}$$

In the above expression, $\underline{l}$ is the unit normal of the boundary ∂A and $[\![\rho]\!] = \rho_{\text{membrane}} - \rho_{\text{reservoir}}$.

The first variation calculated at an equilibrium state should vanish for any $\delta\rho$, the perturbations in density, and any $\underline{v}$, the displacement of the boundary. Therefore, the chemical equilibrium conditions are

$$\lambda = \zeta'(\rho) \qquad (\text{on } A), \tag{3.41}$$

$$\lambda = \bar{\zeta}'(\rho) \qquad (\text{on } \mathcal{A} \setminus A), \tag{3.42}$$

and

$$\zeta(\rho) - \bar{\zeta}(\rho) = \lambda [\![\rho]\!] \qquad (\text{on } \partial A). \tag{3.43}$$

Because the reservoir is considered to have an infinite number of lipid molecules, exchanging molecules with the membrane will not change its chemical potential. As a result, its surface energy density should have the form $\bar{\zeta}(\rho) = \lambda\rho$, and the constant λ in equation (3.42) is the

given chemical potential of the reservoir, which does not change during the experiment. The membrane and the reservoir should have the same chemical potential, as they are chemically equilibrial. From equation (3.41), we can see that the molecular density in the membrane will be adjusted such that its chemical potential $\zeta'(\rho)$ is equal to λ, the chemical potential of the reservoir. The shape of the boundary ∂A can be found from equation (3.43). In conclusions, the chemical contribution to the total energy can be written as

$$-\lambda \int_A \rho \, dA \tag{3.44}$$

where λ is the chemical potential of the lipid bath.

Third, if the membrane is very long and periodic, the total number of molecules is conserved but the number of molecules in each period can change. The constraint can be added to the energy functional *of each period* as in the following form

$$-\lambda \left(\int_{A_{period}} \rho dA - \frac{N_0}{n} \right). \tag{3.45}$$

Again, λ, N_0, and n are the Lagrange multiplier, the total number of molecules of the membrane, and the number of period respectively. We allow the period to prefer any number of molecules as long as it minimizes the total energy. The number of periods can be found from the conservation of the number of molecules of the whole system

$$n = \frac{N_0}{\int_{A_{\text{period}}} \rho \, dA} \tag{3.46}$$

when the number of molecules in each period $\int_{A_{\text{period}}} \rho \, dA$ is known. Similar to the Lagrange multiplier, n depends on other quantities of the problem, but it is a constant. Therefore,

the last term in (3.45) can be dropped out from the energy functional and the chemical potential in this case can be written as

$$-\lambda \int_A \rho \, dA, \tag{3.47}$$

where λ is the Lagrange multiplier.

More importantly, equations (3.38), (3.44), and (3.47) have exactly the same form. Therefore, we have the general energy functional of an open membrane as follow:

$$\mathcal{F} = \frac{1}{2} k_H \int_A (2H - H_0)^2 dA + \int_A \zeta(\rho) \, dA - \int_A \lambda\rho \, dA + \int_{\partial A} \sigma \, ds + F_P + F_{N,\tau} + F_M. \tag{3.48}$$

3.2 The Equilibrium Equations

3.2.1 General Formulation

Using the principle of virtual work and the first variations calculated as in (3.16), (3.17), and (3.35); we can write the first variation of the energy functional (3.48) as

$$\begin{aligned}
\delta^{(1)}\mathcal{F} = & \int_A \{k_H \Delta(2H - H_0) + (2H - H_0)(2H^2 - 2K + H_0 H) - P - 2H[\zeta(\rho) - \lambda\rho])\} v_n dA \\
& + \int_A \{\zeta'(\rho) - \lambda\} v_\rho dA \\
& + \int_{\partial A} \{\sigma K_n - N + k_H \nabla(2H - H_0) \cdot \underline{l}\} \, \underline{v} \cdot \underline{n} \, ds \\
& + \int_{\partial A} \left\{ \frac{1}{2} k_H (2H - H_0)^2 + [\![\zeta(\rho)]\!] - \lambda [\![\rho]\!] - \tau \right\} \underline{v} \cdot \underline{l} \, ds \\
& + \int_{\partial A} \{M - k_H(2H - H_0)\} \nabla v_n \cdot \underline{l} \, ds \\
& - \int_{\partial A} \dot{\sigma} \underline{v} \cdot \underline{t} \, ds.
\end{aligned} \tag{3.49}$$

At equilibrium, $\delta^{(1)}\mathcal{F}$ vanishes for all shape perturbations $\underline{v}$ and density perturbations v_ρ. Therefore, we have the equilibrium equations and boundary conditions as follow

$$k_H\Delta(2H-H_0)+(2H-H_0)(2H^2-2K+H_0H) \\ -P-2H[\zeta(\rho)-\lambda\rho]=0, \qquad \text{in A} \tag{3.50}$$

$$\zeta'(\rho)-\lambda=0, \qquad \text{in } A \tag{3.51}$$

$$\sigma K_n - N + k_H\nabla(2H-H_0)\cdot\underline{l}=0, \qquad \text{on } \partial A \tag{3.52}$$

$$\frac{1}{2}k_H(2H-H_0)^2+[\![\zeta(\rho)]\!]-\lambda[\![\rho]\!]-\tau=0, \qquad \text{on } \partial A \tag{3.53}$$

$$M-k_H(2H-H_0)=0, \qquad \text{on } \partial A \tag{3.54}$$

and

$$\dot{\sigma}=0. \qquad \text{on } \partial A \tag{3.55}$$

Equations (3.50) and (3.51) can be rearranged to

$$k_H\Delta(2H-H_0)+(2H-H_0)(2H^2-2K+H_0H)-P-2H\Sigma=0 \quad \text{in } A \tag{3.56}$$

and

$$\lambda=\zeta'(\rho), \qquad \text{in } A \tag{3.57}$$

where $\Sigma := \zeta(\rho)-\rho\zeta'(\rho)$.

Equation (3.56) is the balance of forces on the surface including bending, pressure, and surface tension. Therefore, the force per unit length Σ is identified as the surface tension. Equation (3.57) is the chemical equilibrium equation. If the membrane is isolated, its chemical potential will adjust such that the constraint on the number of molecule is

satisfied. If the membrane is connected to a reservoir, the molecular density changes such that the membrane chemical potential equals to that of the reservoir. Because (3.57) holds at every point on the surface and λ is a constant, the molecular density is uniform on the surface. This result implies that the surface tension, a mechanical force, needs to be uniform as long as the surface is in chemical equilibrium. Moreover, the non-uniform forces due to bending do not lead to non-uniformity in surface tension.

Equations (3.52), (3.53), and (3.54) are the balances of forces and moments at the edge. They allow us to find either the surface geometry at the edge, given the applied forces or vice versa. The external force τ in the binormal direction plays both as a real force stretching the membrane and as a configurational force adding or removing lipids. Equation (3.55) shows that the line tension needs to be uniform over the edge. Those boundary conditions together with the equilibrium equation (3.56) form a complete system of equations to describe open membranes.

Notice that the equilibrium equations obtained here have the same forms as the ones derived for closed single-component membranes. However, the interpretation of λ and the boundary conditions are different.

3.2.2 The Uniform Cylindrical Solution

The equilibrium solution of a uniform cylindrical shape can be obtained from equation (3.56) by letting $H = -\frac{1}{2R_0}$ to have

$$\frac{k_H}{2R_0^3}\left(R_0^2H_0^2 - 1\right) + \frac{\Sigma}{R_0} - P = 0. \tag{3.58}$$

We are interested in the tension-controlled experiments, and specifically, how the stability of the cylindrical shape of a certain radius depends on the membrane tension. Therefore, it is convenient to eliminate the pressure from the second variation in order to have the relationship between the membrane radius and the membrane tension. Equation (3.58) give us

$$P = \frac{k_H}{2R_0^3}\left(R_0^2 H_0^2 - 1\right) + \frac{\Sigma}{R_0}. \tag{3.59}$$

This equation describes the pressure that has to be applied to maintain a cylindrical vesicle of a certain radius and subject to a certain tension at equilibrium. We note that we can proceed alternately and equivalently by eliminating the radius and using tension and the pressure as defining parameters.

3.3 Linear Stability

3.3.1 General Formulation

Generally, an equilibrium state is stable if the energy functional is convex at that point. This is ascertained by applying small perturbations in shape and density to the energy functional and checking the positive-definiteness of the second variation denoted by $\delta^{(2)}\mathcal{F}$. Alternatively, bifurcation method can also be used to study the linear stability. These methods happen to be equivalent in our problem, as we have demonstrated in Appendix D.

In this thesis, we assume that any bifurcated solution also satisfies the same boundary conditions as does the original equilibrium solution. The following second variations are

calculated by letting $v_n|_{\partial A} = 0$ and $\nabla v_n \cdot \underline{l}|_{\partial A} = 0$.

$$\begin{aligned}\delta^{(2)}\mathcal{F} = \int_A \Big\{ & \left(k_H \left[8H^4 - 10H^2K + \frac{H_0^2 K}{2} + 2K^2 \right] + HP + K\Sigma \right) v_n^2 \\ & + 2K_H(2H - H_0) v_n \nabla H \cdot \nabla v_n + \left(k_H \left[3H^2 - 2HH_0 + \frac{H_0^2}{4} \right] + \frac{\Sigma}{2} \right) |\nabla v_n|^2 \\ & + 2k_H(4H^2 - HH_0 - K) v_n \Delta v_n + \frac{k_H}{2} (\Delta v_n)^2 \\ & - k_H(2H - H_0) \nabla v_n \cdot \overline{\nabla} v_n - 2k_H(2H - H_0) v_n \overline{\Delta} v_n + \zeta''(\rho) v_\rho^2 \Big\} dA.\end{aligned} \tag{3.60}$$

The equilibrium state under consideration is stable if the above expression is positive for any trial function v_n and v_ρ. Notice that the cross term between perturbations in shape and density vanishes. Moreover, the term associated with v_ρ^2 is always positive. Therefore, we only need to investigate the term associated with v_n^2 for arbitrary v_n.

3.3.2 Linear Stability of Uniform Cylindrical Membranes

We investigate the stability of a uniform cylinder by taking periodic perturbations of the form

$$v_n = A_{km} \exp\left[2\pi i \left(k \frac{s}{L} + m\theta \right) \right], \qquad L > 0,\ s \in [0, L],\ \theta \in [0, 2\pi],\ k, m \in \mathbb{Z}, \tag{3.61}$$

where k and m are the wave numbers in the longitudinal and radial directions. Note that the wavelength L can vary. Also, we can easily calculate the differential operators that are needed for the second variations as follow

$$\Delta y(s, \theta) = \frac{\partial^2 y}{\partial s^2} + \frac{1}{R_0^2} \frac{\partial^2 y}{\partial \theta^2}, \quad |\nabla y|^2 = \frac{\partial y}{\partial s} \frac{\partial z}{\partial s} + \frac{1}{R^2} \frac{\partial y}{\partial \theta} \frac{\partial z}{\partial \theta}, \quad \nabla y \cdot \overline{\nabla} z = -\frac{1}{R_0} \frac{\partial y}{\partial s} \frac{\partial z}{\partial s}. \tag{3.62}$$

Using these operators, we plug the trial functions (3.61) into the second variation (3.60) to obtain

$$\begin{aligned}\frac{2}{\pi L^5 R_0^4}\delta^{(2)}\mathcal{F} =& 2k_H L^4 m^4 + \left(k_H[16\pi^2 R_0^2 + L^2(H_0^2 R_0^2 - 5)] + 2L^2 R_0^2 \Sigma\right) L^2 m^2 \\ &+ k_H(32\pi^4 R_0^4 + L^4[3 - H_0^2 R_0^2] + 4L^2\pi^2 R_0^2[H_0^2 R_0^2 + 4H_0 R_0 - 1]) \\ &- 2L^2 R_0^2(L^2 - 4\pi^2 R_0^2)\Sigma.\end{aligned} \tag{3.63}$$

The above expression is a polynomial of order 4 in both the longitudinal wave number k and the radial wave number m. Moreover, the expression contains only even power of k and m. Therefore, we can change the variables to $y = (L/k)^2$ and $b = m^2$. The uniform cylindrical membrane is stable if the second variation is positive $\forall y \in \mathbb{R}; b \in \mathbb{Z}; y, b > 0$.

We now show that the single component membrane can only show two types of periodic instability–axisymmetric beading and non-axisymmetric coiling. First, the second variation is a quadratic polynomial of b with a positive coefficient of b^2. Therefore, $\lim_{b\to\infty} \delta^{(2)}\mathcal{F} > 0$, and there are only limited number of wave numbers that will make the second variation negative. Second, the zero points of the second variation in b direction can be calculated as

$$\begin{aligned}b_{1,2} =& -\frac{4\pi R_0^2}{y} + \frac{5 - H_0^2 R_0^2}{4} - \frac{\Sigma R_0^2}{2k_H} \\ &\pm \frac{1}{4}\sqrt{(H_0^2 R_0^2 - 1)^2 - \frac{128\pi^2 R_0^2(1 + H_0 R_0)}{y} + \frac{4R_0^2(H_0^2 R_0^2 - 1)\Sigma}{k_H} + \frac{4R_0^4\Sigma^2}{k_H^2}}.\end{aligned} \tag{3.64}$$

We will show that the larger solution b_2 is always less than or equal to 2; equivalently, the unstable radial wave number m (recall that $b = m^2$) can only be either 0 or 1.

Assume that

$$b_2 > 2 \tag{3.65}$$

which is equivalent to

$$\sqrt{(H_0^2R_0^2-1)^2-\frac{128\pi^2R_0^2(1+H_0R_0)}{y}+\frac{4R_0^2(H_0^2R_0^2-1)\Sigma}{k_H}+\frac{4R_0^4\Sigma^2}{k_H^2}}> \frac{1}{4}\left(3+H_0^2R_0^2+\frac{16\pi^2R_0^2}{y}+\frac{2R_0^2\Sigma}{k_H}\right). \tag{3.66}$$

Since both sides of (3.66) are positive, we can square both sides and obtain the equivalent inequality

$$-\frac{16\pi^4R_0^4}{y^2}-\frac{2\pi^2R_0^2\left(k_H([H_0R_0+2]^2+3)+2\Sigma R_0^2\right)}{k_Hy}-\frac{k_H(H_0^2R_0^2+1)+2\Sigma R_0^2}{2k_H}>0. \tag{3.67}$$

However, it is easy to see that each of the terms on the left hand side of (3.67) is negative. Therefore, the assumption (3.65) can not hold. It means that the second variation is positive for all radial perturbations with wave numbers larger than 2, regardless of the perturbed wavelength in the longitudinal direction. Therefore, the possible unstable periodic perturbations only include radial expansion with $m = 0$ and coiling with $m = 1$.

Beading If $m = 0$, the second variation (3.63) becomes

$$\begin{aligned}\frac{2}{\pi L^5R_0^4}\delta^{(2)}\mathcal{F}=&L^4(k_H[3-H_0^2R_0^2]-2R_0^2\Sigma)+32\pi^4k_HR_0^4\\&+4\pi^2L^2R_0^2(k_H[H_0^2R_0^2+4H_0R_0-1]+2R_0^2\Sigma).\end{aligned} \tag{3.68}$$

To simplify the expression, we change the variable to $z=\frac{\pi^2R_0^2}{L^2}$ to have

$$\begin{aligned}\frac{1}{\pi L^9R_0^4}\delta^{(2)}\mathcal{F}=&16k_Hz^2+(2k_H[H_0^2R_0^2+4H_0R_0-1]+4R_0^2\Sigma)z\\&+\frac{1}{2}k_H(3-H_0^2R_0^2)-R_0^2\Sigma\end{aligned} \tag{3.69}$$

so that the coefficient of the highest order of z is positive. The membrane is stable if the roots $z_{1,2}$ of $\delta^{(2)}\mathcal{F}$ are either not real or negative.

First, let us consider the case when $z_{1,2}$ are not real. Equation (3.69) allows us to calculate the minimum point of $\delta^2\mathcal{F}$ over all z as

$$\begin{aligned}\min_{z\in\mathbb{R}} \delta^2\mathcal{F} = &-\frac{R_0^4}{4k_H}\Sigma^2 - \frac{R_0^2}{4}(3 + 4H_0R_0 + H_0^2R_0^2)\Sigma \\ &- \frac{k_H}{16}\left(H_0^4R_0^4 + 8H_0^3R_0^3 + 22H_0^2R_0^2 - 8H_0R_0 - 23\right).\end{aligned} \tag{3.70}$$

Notice that $\min_{z\in\mathbb{R}} \delta^2\mathcal{F}$ is a quadratic polynomial of Σ with a negative coefficient of Σ^2. It means that there will be only a limited range of Σ such that $\min_{z\in\mathbb{R}} \delta^2\mathcal{F} > 0$. Moreover, we have

$$\max_{\Sigma}\min_{z\in\mathbb{R}} \delta^2\mathcal{F} = 2k_H(1 + H_0R_0) \qquad \text{at} \qquad \Sigma_m = \frac{k_H}{2R_0^2}(1 - [H_0R_0 + 2]^2) \tag{3.71}$$

and

$$\min_{z\in\mathbb{R}} \delta^2\mathcal{F} = 0 \qquad \text{at} \qquad \Sigma_0^{(p,m)} = -\frac{k_H}{2R_0^2}(H_0^2R_0^2 + 4H_0R_0 + 3 \pm 4\sqrt{2}\sqrt{1 + H_0R_0}). \tag{3.72}$$

Also note that the two roots $z_{1,2}$ are not real if

$$\max_{\Sigma}\min_{z\in\mathbb{R}} \delta^2\mathcal{F} > 0, \qquad \Sigma_0^{(m)} < \Sigma < \Sigma_0^{(p)}, \qquad \text{and} \qquad \Sigma > 0. \tag{3.73}$$

Combining (3.71–3.73), we have the first stability condition when $z_{1,2}$ are not real in the form of

$$-1 < H_0R_0 < 1, \qquad 0 < \Sigma < \Sigma_0^p, \tag{3.74}$$

in which $\Sigma_0^m < 0$ for $-1 < H_0 R_0 < 1$.

Second, consider the case when $z_{1,2}$ are real. In order for $z_{1,2} < 0$, we need

$$\begin{aligned} z_1 z_2 =& \frac{k_H(H_0^2 R_0^2 - 3) - 2R_0^2\Sigma}{32 k_H} > 0, \qquad \text{and} \\ z_1 + z_2 =& \frac{k_H(1 - 4H_0 R_0 - H_0^2 R_0^2) - 2R_0^2\Sigma}{8 k_H} < 0 \end{aligned} \tag{3.75}$$

provided that $z_{1,2}$ are real. The system of two inequalities (3.75) is equivalent to

$$-\frac{1}{2} \le H_0 R_0 \le 0, \qquad \Sigma_r^{(1)} < \Sigma < \Sigma_r^{(2)}, \tag{3.76}$$

and

$$0 < H_0 R_0 \le \sqrt{5} - 2 \qquad \Sigma_r^{(1)} < \Sigma < \Sigma_r^{(2)}, \tag{3.77}$$

and

$$\sqrt{5} - 2 < H_0 R_0 \le \sqrt{3} \qquad 0 < \Sigma < \Sigma_r^{(2)}, \tag{3.78}$$

where

$$\Sigma_r^{(1)} = \frac{k_H}{2R_0^2}(1 - 4H_0 R_0 - H_0^2 R_0^2) \qquad \text{and} \qquad \Sigma_r^{(2)} = \frac{k_H}{2R_0^2}(3 - H_0^2 R_0^2). \tag{3.79}$$

Moreover, notice that

$$\begin{aligned} & \Sigma_0^{(p)} \le \Sigma_r^{(2)} \qquad \text{for all} \qquad H_0 R_0 \ge -1, \\ & \Sigma_0^{(p)} \ge \Sigma_r^{(1)} \qquad \text{for all} \qquad H_0 R_0 \le -\frac{1}{2}, \\ \text{and} \quad & \Sigma_0^{(p)} \ge \Sigma_r^{(1)} \qquad \text{for all} \qquad H_0 R_0 \ge -\frac{1}{2}. \end{aligned} \tag{3.80}$$

Putting all this together, we have $\delta^2\mathcal{F}$ is positive definite for all positive z when either

$$\begin{cases} -1 < H_0R_0 < -1/2 \\ \Sigma < \Sigma_c^{(1)} \quad \text{where} \quad \Sigma_c^{(1)} = \frac{k_H}{2R_0^2}\left(4\sqrt{2}\sqrt{H_0R_0+1} - H_0^2R_0^2 - 4H_0R_0 - 3\right) \end{cases} \tag{3.81}$$

or

$$\begin{cases} -1/2 \le H_0R_0 < \sqrt{3} \\ \Sigma < \Sigma_c^{(2)} \quad \text{where} \quad \Sigma_c^{(2)} = \frac{k_H}{2R_0^2}\left(3 - H_0^2R_0^2\right). \end{cases} \tag{3.82}$$

When there is no spontaneous curvature, the above conditions reduce to the previous reported result [BZTM97], i.e., the uniform cylinder is stable when

$$\Sigma < \Sigma_c = \frac{3k_H}{2R_0^2}. \tag{3.83}$$

We can see from Fig. 3.3 that spontaneous curvature de-stablizes the straight shape regardless of its sign.

We also utilize these instability results to find the initial guesses for numerical calculations of beading shapes. The minimum of the second variation (3.69) with respect to the inverse wavelength z is archived at

$$z_{\min} = \frac{5}{16} - \frac{1}{16}(H_0R_0+2)^2 - \frac{R_0^2}{8k_H}\Sigma. \tag{3.84}$$

First, beading with large wavelengths is likely to appear when $\delta^{(2)}\mathcal{F}(z_{\min}) < 0$ and $z_{min} \le 0$ because the most unstable mode has infinitely long wavelength (Fig. 3.5a). On the contrary, beading with shorter length is favorable when $z_{\min} > 0$ (Fig. 3.5b). The numerical

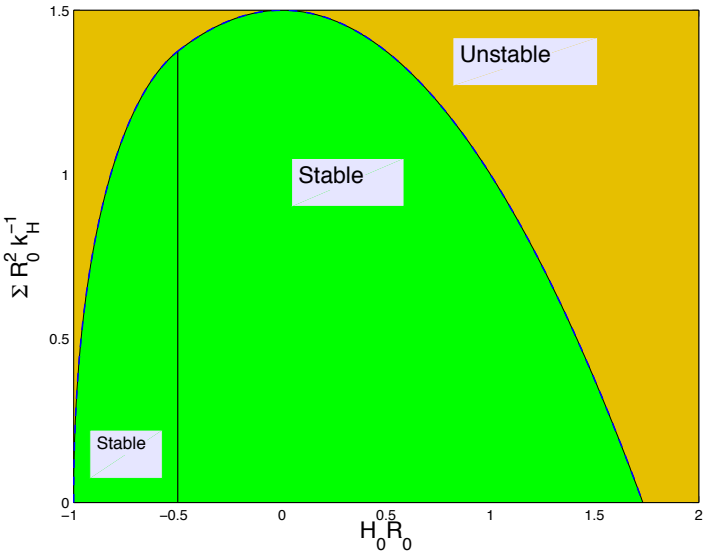

Figure 3.3: Beading stability diagram on $\Sigma - H_0$ plane for a uniform cylindrical membrane. Beadings are preferred at high tension.

calculation shows that the beading solution is easiest to obtain (and the algorithm is fastest to converge) with an initial guess at the most unstable wavelength

$$R_{\text{guess}}(s) = A\cos\left(\frac{2\pi s}{L_{\min}}\right) + B\sin\left(\frac{2\pi s}{L_{\min}}\right), \tag{3.85}$$

where $L_{\min} = \frac{\pi R_0}{\sqrt{z_{\min}}}$. Second, equation (3.84) shows that increasing the tension Σ will lower z_{min} resulting in the larger range of unstable wavelengths. Therefore, many types of beading can be observed when the tension is large. However, the most unstable wavelength goes to infinity as the tension increases.

Coiling The second unstable case is with $b = 1$. We have

$$\frac{1}{2\pi^3 L^5 R_0^6}\delta^{(2)}\mathcal{F}\Big|_{b=1} = (k_H[H_0^2R_0^2 + 4H_0R_0 + 3] + 2R_0^2\Sigma)y + 8k_H\pi^2R_0^2 < 0 \tag{3.86}$$

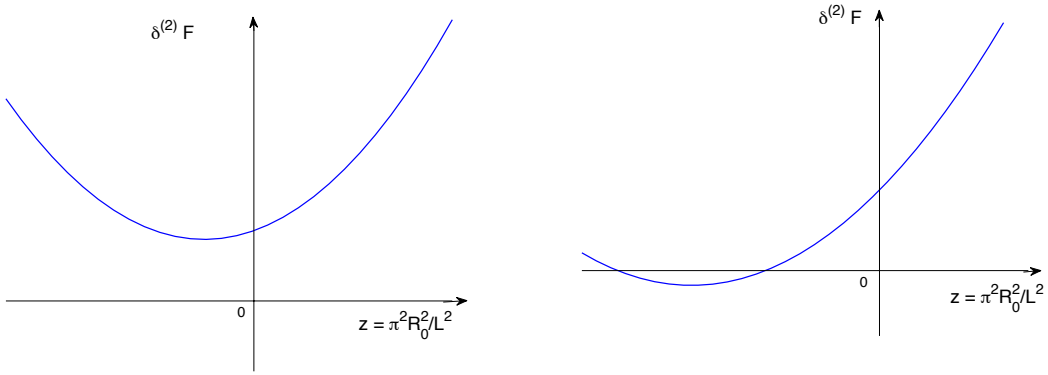

(a) $\delta^{(2)}\mathcal{F}$ is positive for all y.

(b) $\delta^{(2)}\mathcal{F}$ is positive for all $y > 0$.

Figure 3.4: Two cases of $\delta^{(2)}\mathcal{F}$ vs. $z = \frac{\pi^2 R_0^2}{L^2}$ such that the cylindrical membrane is stable.

for some $y > 0$ if

$$\Sigma < \Sigma_{coil} = \frac{k_H(1 - [H_0R_0 + 2]^2)}{2R_0^2}, \quad -3 \leq H_0R_0 \leq -1. \tag{3.87}$$

So, coiling will appear with longitudinal wavelengths

$$L_{coiling} \geq \sqrt{y_{coiling}} = \frac{2\pi\sqrt{2k_H}R_0}{\sqrt{k_H(1 - [H_0R_0 + 2]^2) - 2R_0^2\Sigma}}. \tag{3.88}$$

The uniform cylinder is stable under coiling perturbations if conditions (3.87) are not satisfied. In other words, coiling is preferred when the tension is small and the spontaneous curvature is moderate as shown in Fig. 3.6. Interestingly, if the membrane has zero spontaneous curvature, coiling will not appear. However, it can still be unstable under axisymmetric perturbations as presented in Fig. 3.3.

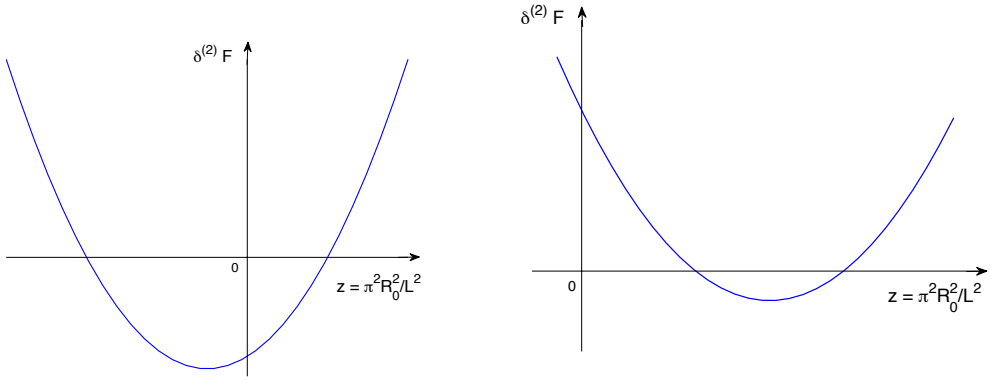

(a) Long wavelength is more favorable. (b) Shorter wavelength is more favorable.

Figure 3.5: The cylindrical membrane is unstable when there exists $y > 0$ such that $\delta^{(2)}\mathcal{F} < 0$.

Summary The uniform cylindrical membrane is stable under any type of periodic perturbations except beading and coiling. It is *stable* under beading perturbations if

$$\begin{cases} -1 < H_0R_0 < -1/2, \\ \Sigma < \Sigma_c^{(1)}, \end{cases} \quad \text{or} \quad \begin{cases} -1/2 \le H_0R_0 < \sqrt{3}, \\ \Sigma < \Sigma_c^{(2)}, \end{cases} \tag{3.89}$$

and *unstable* under coiling perturbations if

$$\begin{cases} -3 \le H_0R_0 \le -1, \\ \Sigma < \Sigma_{coil}. \end{cases} \tag{3.90}$$

The critical values $\Sigma_c^{(1,2)}$ and Σ_{coil} are given in (3.81), (3.82), and (3.87). These stability conditions show that coiling is preferred when tension is small, while beading is preferred when tension is large. However, note that the stability also depends on the membrane radius. A too large or too small tube radius prevents coiling, whereas a large radius guarantees the appearance of beading.

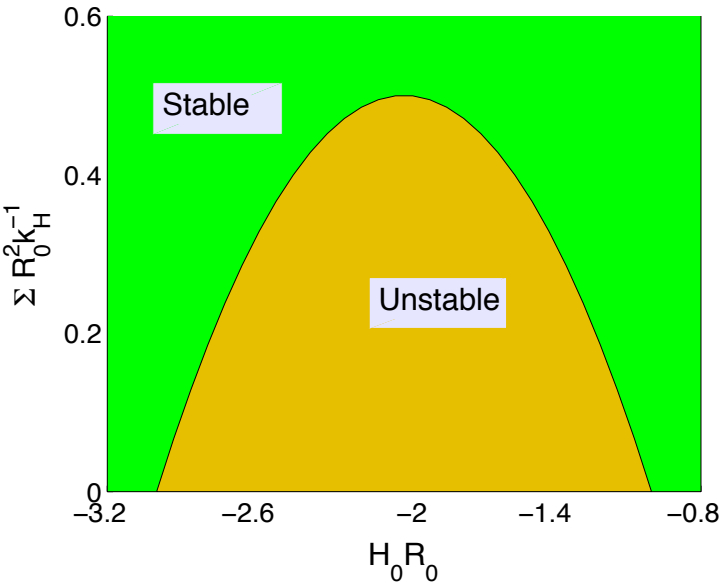

Figure 3.6: Coiling stability diagram on $\Sigma - H_0$ plane for a uniform cylindrical membrane. Coiling is preferred at small tension.

The prediction on how tension actually affects stability are observed in experiments done on neural cells [POJ94]. Nerves at the relaxed state, or even under moderate stretch, are observed to have waved/coiled nerve fibers which are called the bands of Fontana. As the stretch increases, the bands of Fontana disappear, giving the nerve fibers a straight shape. When the stretch continues to increase beyond some critical points, beading appear to replace the straight shape (Fig. 3.7 and Fig. 3.8).

3.4 Axisymmetric Solutions of the Equilibrium Equations

While linear stability tells us about critical points, and the potential onset of instability; it does not tell us whether the solution is in fact unstable or is simply the nature of a bifurcated solution. We need to solve the nonlinear equilibrium equations to understand this. We do so now under the restriction that the shape is axisymmetric.

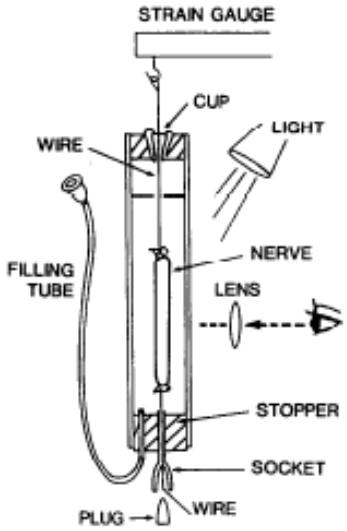

(a) Experiment setup

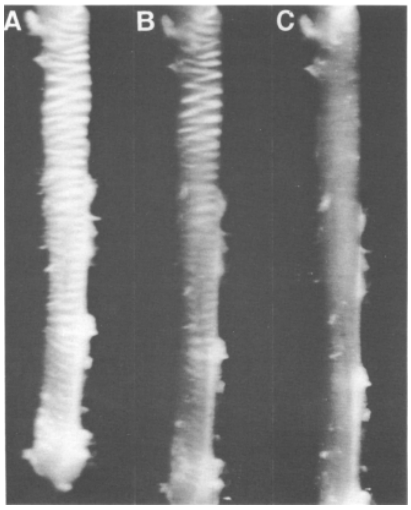

(b) A. The band of Fontana in a relaxed nerve; B. Some loss of banding on moderate stretch; C. Banding completely gone at 14% elongation.

Figure 3.7: The bands of Fontana. Images and observation of Pourmand *et al.* [POJ94]. (Reprinted from [POJ94], Copyright (2013), with permission from Elsevier.)

3.4.1 Axisymmetric Equations

Recall that equation (3.56) and the boundary conditions (3.52–3.55) form a complete set of equations for open membranes. Assuming that the shape is axisymmetric and using the parametrization

$$\dot{R} := \frac{dR}{ds} = \cos\psi(s), \qquad \dot{z} := \frac{dz}{ds} = -\sin\psi, \tag{3.91}$$

where s is the arc length and $\psi(s)$ is the azimuthal angle as shown in Fig. 3.9, we can calculate the mean and Gauss curvature

$$H = -\frac{\sin\psi(s) + R(s)\dot{\psi}(s)}{2R(s)}, \qquad K = \frac{\sin\psi(s)\dot{\psi}(s)}{R(s)}. \tag{3.92}$$

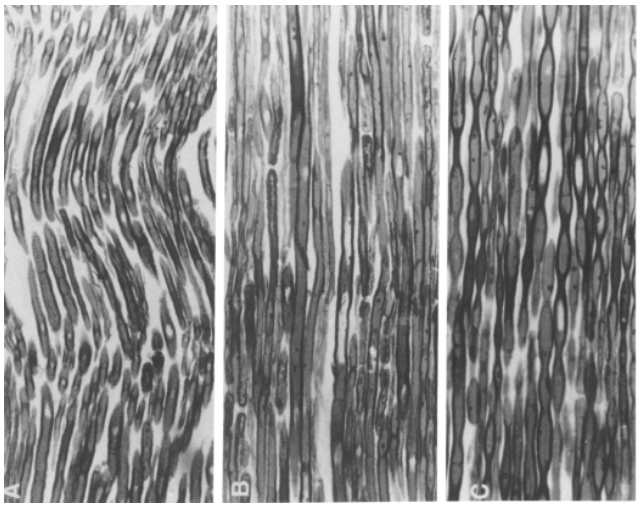

Figure 3.8: A. Long waves giving rise to the bands of Fontana; B. Nerve straightened to the point where not all the banding had gone; C. Nerve stretched to the point where the bands completely disappeared. Numerous beads are present in most of these cold-fixed fibers. Images and observation of Pourmand *et al.* [POJ94]. (Reprinted from [POJ94], Copyright (2013), with permission from Elsevier.)

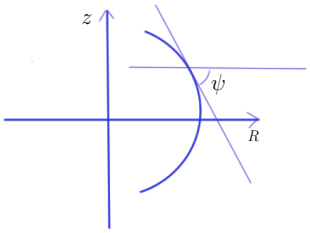

Figure 3.9: Axisymmetric parametrization.

The equilibrium equation (3.56) becomes

$$-k_H\dddot{\psi} - \frac{2k_H\cos\psi\ddot{\psi}^2}{R} + \frac{1}{4R^2}\left(4\Sigma R^2 + k_H\left[2R^2H_0^2 + 1 + 3\cos(2\psi) + 8RH_0\sin\psi\right]\right)\dot{\psi}$$
$$-\frac{1}{2}k_H\dot{\psi}^3 + \frac{3k_H\sin\psi\dot{\psi}^2}{2R} + \frac{k_H}{8R^3}\left(4R^2H_0^2\sin\psi - 5\sin\psi - \sin(3\psi)\right) + \frac{\sin\psi}{R}\Sigma - P = 0 \tag{3.93}$$

3.4.2 Boundary Conditions

We describe the boundary conditions for three practical problems: isolated membranes, membranes with attached rings, and periodic membranes. However, only periodic mem-

brane problem will be numerically calculated in the next section as we are interested in studying the beading of tubular membranes.

Isolated membrane with *free edges*. Generally, the boundary conditions (3.52-3.54) give us six equations because each condition is applied at both end $s = 0$ and $s = L$. However, at equilibrium, the total external force vanishes. Therefore, the boundary conditions give us five independent equations. We also have other three independent equations including the density equation (3.51), the constraint on the number of molecules, and the axis origin equation $z(0) = 0$. Correspondingly, this problem has eight unknowns: five integration constants of $\dddot{\psi}, \dot{R}$, and $\dot{z}$; the Lagrange multiplier λ; the density ρ; and the arc length L. Therefore, the problem is complete with eight unknowns and eight equations.

Chemically isolated membrane with two *attached rings* . In addition to the eight unknowns, as in the free edge problem, the applied forces (4) and moments (2) at the two edges are also unknown. It means that we need fourteen equations to solve this problem. Besides the eight equations above, we have the ninth and tenth equations from the given radii of the rings. The last four equations come from the pulling force which is known, i.e.

$$\tau\Big|_{0,L} = f\cos\psi\Big|_{0,L}, \quad \text{and} \quad N\Big|_{0,L} = f\sin\psi\Big|_{0,L}. \tag{3.94}$$

In short, we have fourteen equations to solve for fourteen unknowns.

***Periodic* membrane with controlled number of molecules.** This problem has seven unknowns including five integration constants of $\dddot{\psi}, \dot{R}$, and $\dot{z}$; the density ρ; and the arc length L. Likewise, the periodicity of $\psi, \dot{\psi}, \ddot{\psi}$, and R gives us four equations. The fifth one is the fixing axis origin equation $z(0) = 0$. Because the shape is periodic, the balance of forces

along z direction will give us how τ depends on the total pulling force f. Therefore, the sixth equation is the boundary condition (3.53), which is the relationship between surface tension $\Sigma(\rho)$ and the external force. Lastly, the seventh equation comes from prescribing the angle at the edge. This does not affect the final results because we can always slide the period along z direction such that the $\psi(0)$ matches the prescribed value. As a result, we have a complete system with seven equations for seven unknowns.

It is worth pointing out that we are able to obtain the completeness of the periodic problem because our calculation uses 3D perturbations on the general energy functional. Here, we only need to prescribe the angle at the edge, unlike with previous works where both the angle and the radius need to be prescribed. This is because the previous works on axisymmetric membranes use 2D perturbations on the axisymmetric energy functional, which causes extra geometrical constraints [JS94]. Consequently, these constraints reduce the solution space of the problem.

3.4.3 Algorithm to Find Periodic Solutions

As stated above, we can assume that the value of the azimuthal angle at the beginning of each period is ψ_0 without loss of generality. Also, instead of calculating the shapes at each given pulling force f, we will calculate the shape for each given tension Σ. After having the shapes, we compute the corresponding pulling force f. This allows us to reduce the number of unknowns to six. Hence, the complete set of boundary conditions for axisymmetric equations is

$$\begin{aligned} &\psi(0) = \psi_0, \qquad \psi(L) = \psi_0, \qquad \dot{\psi}(0) = \dot{\psi}(L), \\ &\ddot{\psi}(0) = \ddot{\psi}(L), \quad R(0) = R(L), \quad z(0) = 0. \end{aligned} \tag{3.95}$$

We use a modified shooting method to solve this boundary valued problem on a variable domain. The algorithm is divided into two steps,

Step 1: *Intermediate solution.* Solve (3.91) and (3.93) on a fixed domain $s \in [0, L_0]$ with the boundary conditions

$$\begin{aligned} &\psi(0) = \psi_0, \qquad \psi(L_0) = \psi_0, \qquad \dot{\psi}(0) = \dot{\psi}(L_0), \\ &\ddot{\psi}(0) = \ddot{\psi}(L_0), \quad R(0) = R(L_0), \quad z(0) = 0, \end{aligned} \tag{3.96}$$

where L_0 is a chosen unstable wavelength and ψ_0 is unknown.

Step 2: *Beading solution.* Without loss of generality, assume that the azimuthal angle at the ends is ψ_0 from Part 1. Use the solution in Step 1 as an initial guess to solve(3.91) and (3.93) on a variable domain $s \in [0, L]$ with boundary conditions

$$\begin{aligned} &\psi(0) = \psi_0, \qquad \psi(L) = \psi_0, \qquad \dot{\psi}(0) = \dot{\psi}(L), \\ &\ddot{\psi}(0) = \ddot{\psi}(L), \quad R(0) = R(L), \quad z(0) = 0. \end{aligned} \tag{3.97}$$

3.4.4 Numerical Results

Applying the algorithm described in the previous section and utilizing the most unstable wavelength as the initial guess, we are able to obtain the beading shapes of open single-component membranes as shown in Fig. 3.12.

First, the numerical calculations agree with the stability analysis in that the beading solutions are only observed in the unstable regime of parameters. Second, the intermediate beading solutions in Step 1 can be found at various unstable wavelength L_0, but the algorithm converges faster and with wider range of initial guess shapes around the most

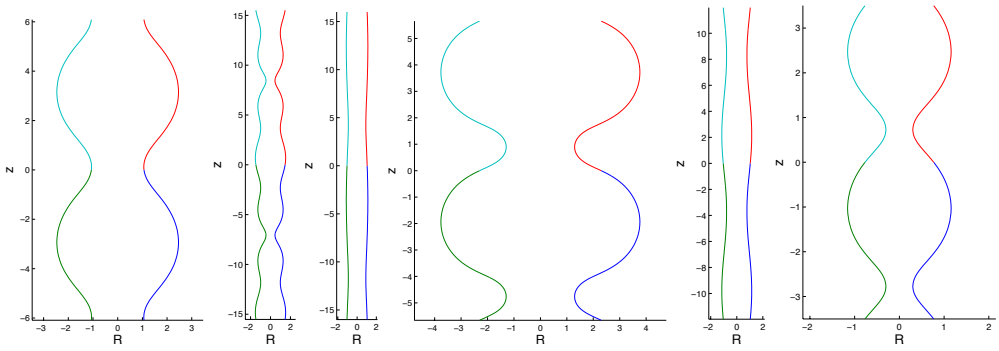

(a) (b) (c) (d) (e) (f)

Figure 3.10: Intermediate beading solutions. The first three intermediate solutions make Step 2 of the algorithm converge (shown in Fig. 3.12).(a) $L = L_{\min} = 6.85R_0$, (b, c) $L = 16R_0$, (d) $L = 8R_0$, (e) $L = 12R_0$, (f) $L = 4R_0$. The unstable wavelength regime is $[5.1, 14.5]$.

unstable wavelength $L_{\min}$. Third, the beading solutions are mostly found when the initial guess wavelength is $L_0 = L_{\min}$. One drawback of this algorithm is that the shooting method is not efficient when the wavelength L is too large.

The existence of the numerical beading shapes is a proof that beadings can occur purely as a mechanical response of the membrane.

3.5 Conclusions

In this chapter, we have built a framework to study open single-component membranes. The general derivation using arbitrary 3D perturbations allows us to obtain a complete system of equations. Several boundary conditions have been discussed. Numerical calculations have been performed to solve the axisymmetric periodic problems. The numerical results show that beading shape can occur purely due to the mechanical response of the membrane.

Additionally, our linear stability shows that the uniform cylindrical membrane are quite stable under periodic perturbations. The only types of periodic perturbations that are able to make the cylindrical single-component membrane unstable are beading and coil-

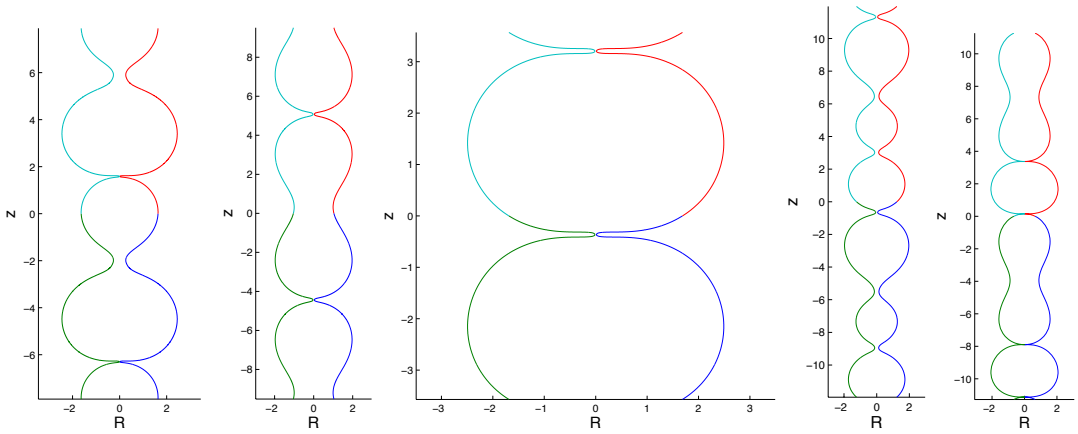

Figure 3.11: Intermediate, narrow neck solutions. (a, b) $L = 12R_0$, (c) $L = 6.85R_0$, (d, e) $L = 16R_0$.

ing. Furthermore, our linear stability suggests that coiling is preferred at small tension, while beading is preferred at high tension. These features are observed in nerve-stretching-experiments where nerve fibers have coiling shapes under small stretch, cylindrical shapes under moderate stretch, and beading shapes under large stretch.

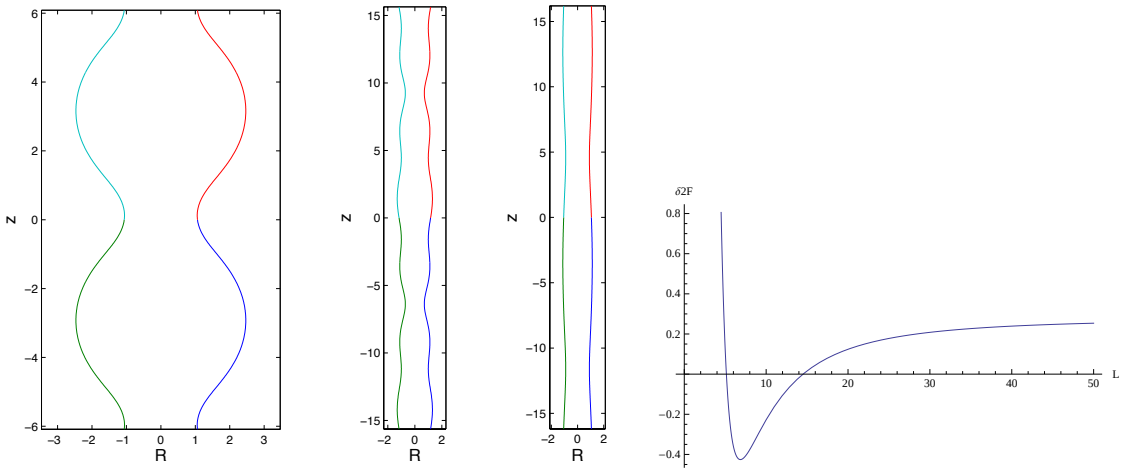

(a) (b) (c) (d)

Figure 3.12: Beading solutions with initial guesses from the first three intermediate solutions in Fig.3.10. Guesses from other intermediate solutions do not make the algorithm converge. (a) Initial guess L_0 is taken to be the most unstable wavelength $L_{\min}$. The varied-domain-problem converges to the intermediate solution. (b) and (c) The initial guess L_0 is slightly larger than the unstable wavelengths. Solution (b) is the same as the intermediate solution while solution (c) is straightened (stabilized) to the cylindrical solution.(d) The non-dimensional second variation $\delta^2\mathcal{F}$ as a function of the non-dimensional wavelength L.

Chapter 4

Open Multi-component Membranes

We now consider open multi-component membranes. In this chapter, we will derive a general framework, and then study the linear stability of a uniform cylindrical membrane as an example. We will show that the open multi-component membranes have similar instability behavior to the single-component ones, in that they prefer radial instability modes at small tension and longitudinal instability modes at high tension. However, in addition to the coiling instability as in the single-component case, they also experience other radial instability modes such as peanut and pear modes.

4.1 Energy Functional and General Equations

We consider an open, bounded membrane A as shown in Fig. 3.1. We assume that membrane is made of two types of molecules with total density ρ and (relative) composition c as in Chapter 2. The multi-component features of the membrane here are captured by using the interactions and the couplings between the membrane geometry, chemistry, and mechanics that we used to study the closed multi-component membranes in Chapter 2. Likewise, the openness of the membrane is taken care of by using the same approach that

we have in Chapter 3. Specifically, we use the energy functional in the form of

$$\mathcal{F} = \int_A \frac{1}{2} k_H(c)(2H - H_0(c))^2 dA + \int_A \zeta(\rho)\, dA + \int_{\partial A} \sigma\, ds + F_P + F_f + F_M + \int_A f(c)\, dA + \int_A k_c |\nabla c|^2\, dA - \lambda_1 \int_A \rho\, dA - \lambda_2 \int_A \rho c\, dA \tag{4.1}$$

to model an open membrane composed of two types of lipids. In (4.1), the first three terms are mechanical potentials including bending, stretching, and line-tension; the next three terms are the work done by external forces; the seventh and eighth terms are the interaction energy and the penalty for sharp change in concentration. The last two terms account for the conservation of molecules of the system. If the membrane is isolated or periodic, then λ_1 and λ_2 are the Lagrange multipliers. If the membrane is connected to a lipid reservoir, those two constants can be found from the properties of the reservoirs (see Appendix E).

Using similar variations as described in Chapter 2 and Chapter 3, we can calculate the first variation of the energy functional (4.1) as

$$\begin{aligned}
\delta^{(1)}\mathcal{F} = \int_A \{ & \Delta[k_H(2H - H_0)] + k_H(c)(2H - H_0)(2H^2 - 2K + H_0 H) - P \\
& - 2H[\zeta(\rho) - \lambda_1 \rho - \lambda_2 \rho c]) - 2k_c \nabla c \cdot \overline{\nabla} c + 2k_c H |\nabla c|^2 - 2H f(c)\} v_n dA \\
& + \int_A \{\zeta'(\rho) - \lambda_1 - \lambda_2 c\} v_\rho dA \\
& + \int_A \left\{ f'(c) - \lambda_2 \rho - 2k_c \Delta c - k_H H_0'(c)(2H - H_0) + \frac{1}{2} k_H'(c)(2H - H_0(c))^2 \right\} v_c dA \\
& + \int_{\partial A} \{\sigma K_n - N + \nabla[k_H(c)(2H - H_0(c))] \cdot \underline{l}\}\, \underline{v} \cdot \underline{n}\, ds \\
& + \int_{\partial A} \left\{ \frac{1}{2} k_H(c)(2H - H_0(c))^2 + \zeta(\rho) - \lambda_1 \rho - \lambda_2 \rho c - \tau \right\} \underline{v} \cdot \underline{l}\, ds \\
& + \int_{\partial A} \{M - k_H(c)(2H - H_0(c))\}\, \nabla v_n \cdot \underline{l}\, ds - \int_{\partial A} \dot{\sigma} \underline{v} \cdot \underline{t}\, ds + \int_{\partial A} 2k_c (\nabla c \cdot \underline{l})\, v_c\, ds,
\end{aligned} \tag{4.2}$$

where $\underline{t}, \underline{n}$, and $\underline{l}$ are the unit tangent, normal, and binormal vectors as illustrated in Fig. 3.1. The first variation $\delta^{(1)}\mathcal{F}$ vanishes for all shape perturbations $\underline{v}$, density perturbations v_ρ, and concentration perturbations v_c for any equilibrium state. Therefore, the equilibrium equations and boundary conditions of the open multi-component membrane are

$$\begin{aligned}&\Delta[k_H(2H-H_0)]+k_H(c)(2H-H_0)(2H^2-2K+H_0H)-P\\&\quad-2H[\zeta(\rho)-\lambda_1\rho-\lambda_2\rho c])-2k_c\nabla c\cdot\overline{\nabla}c+2k_cH|\nabla c|^2-2Hf(c)=0,\qquad\text{in } A\end{aligned}\tag{4.3}$$

$$\zeta'(\rho)-\lambda_1-\lambda_2 c=0,\qquad\text{in } A\tag{4.4}$$

$$f'(c)-\lambda_2\rho-2k_c\Delta c-k_HH_0'(c)(2H-H_0)+\frac{1}{2}k_H'(c)(2H-H_0(c))^2=0,\qquad\text{on } A\tag{4.5}$$

$$\sigma K_n-N+\nabla[k_H(c)(2H-H_0(c))]\cdot\underline{l}=0,\qquad\text{on } \partial A\tag{4.6}$$

$$\frac{1}{2}k_H(c)(2H-H_0(c))^2+[\![\zeta(\rho)]\!]-\lambda_1[\![\rho]\!]-\lambda_2[\![\rho c]\!]-\tau=0,\qquad\text{on } \partial A\tag{4.7}$$

$$M-k_H(c)(2H-H_0(c))=0,\qquad\text{on } \partial A\tag{4.8}$$

$$\dot{\sigma}=0,\qquad\text{on } \partial A\tag{4.9}$$

and

$$k_c\nabla c\cdot\underline{l}=0.\qquad\text{on } \partial A\tag{4.10}$$

First, we notice that equations (4.3-4.5) have the same forms as the shape, density, and concentration equations obtained from Chapter 2 when using the Lagrange multiplier method. However, the interpretation of $\lambda_{1,2}$ here are different, because the open membrane is allowed to exchange molecules with the reservoir. Moreover, the boundary conditions (4.6-4.10) fundamentally distinguish between the two problems.

Second, it can be noticed from equation (4.4) that single component membrane must have uniform tension while multi-component membrane can have non-uniform tension due to the non-uniformity in composition. In other words, the bending of membrane does not lead to the non-uniformity of the tension, but the chemistry of the membrane does.

Third, the equilibrium equation (4.3) can be simplified to

$$\begin{aligned} &k_H\Delta(2H-H_0)+k_H(2H-H_0)(2H^2-2K+H_0H)-P-2H[\zeta(\rho)-\rho\zeta'(\rho)]) \\ &\quad -2k_c\nabla c\cdot\overline{\nabla}c+2k_cH|\nabla c|^2-2Hf(c)=0 \end{aligned} \tag{4.11}$$

by using the density equation (4.4). Again, the term $\Sigma := \zeta(\rho)-\rho\zeta'(\rho)$ is identified as the membrane tension since it balances with pressure when there are no bending and chemistry forces.

Fourth, our last remark is about the boundary condition of the composition. From equation (4.10)

$$k_c\nabla c\cdot\underline{l}=0, \qquad \text{on } \partial A \tag{4.12}$$

we can see that the composition does not change in the direction that is normal to the boundary. If the membrane is isolated, condition (4.10) is a Neumann boundary condition for the composition. If the membrane is connected to a reservoir, it means that the composition is continuous across the boundary from the reservoir to the membrane. If the membrane is periodic, this boundary condition is automatically satisfied.

4.2 Axisymmetric Equations and Boundary Conditions

In this section, we will derive the axisymmetric equations and the boundary conditions to study open multi-component membranes. Using the parametrization

$$\dot{R} = \frac{dR}{ds} = \cos\psi, \qquad \dot{z} = \frac{dz}{ds} = -\sin\psi, \tag{4.13}$$

where s is the arc length and $\psi(s)$ is the azimuthal angle as shown in Fig. 3.9, we can calculate the mean and Gauss curvature as

$$H = -\frac{\sin\psi(s) + R(s)\dot{\psi}(s)}{2R(s)}, \qquad K = \frac{\sin\psi(s)\dot{\psi}(s)}{R(s)}. \tag{4.14}$$

The shape equation (4.11) becomes

$$\begin{aligned} k_H \Bigg\{ & -\dddot{\psi} - \frac{2\cos\psi\ddot{\psi}}{R} - H_0''(c)\dot{c}^2 - H_0'(c)\ddot{c} - \frac{1}{2}\dot{\psi}^3 + \frac{3\sin\psi\dot{\psi}^2}{2R} \\ & + \dot{\psi}\left(\frac{2H_0\sin\psi}{R} + \frac{1+3\cos(2\psi)}{4R^2} + \frac{H_0^2}{2}\right) \\ & + \frac{H_0^2\sin\psi}{2R} - \frac{5\sin\psi + \sin(3\psi)}{8R^3} - \frac{\cos\psi H_0'(c)\dot{c}}{R}\Bigg\} + k_c\left\{\frac{\sin\psi(\dot{c})^2}{R} - (\dot{c}\dot{\psi})^2\right\} \\ & + \left\{\frac{\sin\psi}{R} + \dot{\psi}\right\}\{\zeta(\rho) - \rho\zeta'(\rho) + f(c)\} - P = 0. \end{aligned} \tag{4.15}$$

We also have the density and composition equations as follow

$$\zeta'(\rho) - \lambda_1 - \lambda_2 c = 0, \tag{4.16}$$

$$2k_c\left\{\ddot{c} + \frac{\dot{c}\cos\psi}{R}\right\} - f'(c) + \lambda_2\rho - k_H H_0'(c)\left\{\dot{\psi} + \frac{\sin\psi}{R} + H_0\right\} = 0. \tag{4.17}$$

Let us consider the tethering experiment as an example. Because the tether part is

very small compared to the source vesicle, we can assume that the vesicle serves as a lipid reservoir. Consequently, the two constants λ_1 and λ_2 are the "adjusted" chemical potentials defined by the vesicle's properties as in equation (E.13). Integrating equations (4.15-4.17) gives us the shape, density, and composition. Specifically, the problem has eight unknowns: the arc length L and seven integration constants for $\dddot{\psi}, \dot{R}, \dot{z}$, and $\ddot{c}$. Correspondingly, we have eight equations to form a complete system. The first two equations are the geometrical condition

$$\psi(L) = \pi/2 \tag{4.18}$$

and the fixing axis origin condition

$$z(0) = 0. \tag{4.19}$$

The third and the fourth equations come from the boundary conditions in the normal direction (4.6)

$$(\ddot{\psi} + \dot{c}H_0'(c))\Big|_{0,L} = 0, \tag{4.20}$$

in which we have assumed that there are no boundary forces in the normal direction, that is

$$N(0) = N(L) = 0 \qquad \text{and} \qquad M(0) = M(L) = 0. \tag{4.21}$$

Those assumptions also give us the fifth equation by simplifying the boundary condition (4.8), which is associated with $\nabla\psi_1 \cdot \underline{l}$, as

$$\dot{\psi}(0) + \frac{\sin\psi(0)}{R(0)} + H_0(c(0)) = 0. \tag{4.22}$$

The sixth equation is the boundary condition (4.7) in the binormal direction

$$-\frac{1}{2}k_H\left(\dot{\psi}(L)+\frac{1}{R(L)}+H_0(c(L))\right)^2+\zeta(\rho(L))-\rho(L)\zeta'(\rho(L))-\tau=0, \tag{4.23}$$

where τ is known from the pulling force. The seventh and eighth equations are from the boundary condition (4.10) for the composition,

$$c(0)=c_b, \qquad \text{and} \qquad \dot{c}(L)=0. \tag{4.24}$$

So we have a complete system with eight equations for eight unknowns, which allows us to study the tethering experiments.

4.3 Uniform Cylindrical Solution

For a uniform cylindrical, the shape equation (4.11) gives us the balance of force in normal direction

$$P=\frac{k_H(c)(R_0^2H_0(c)^2-1)}{2R_0^3}+\frac{\zeta(\rho)-\rho\zeta^{'}(\rho)}{R_0}+\frac{f(c)}{R_0}. \tag{4.25}$$

Above, the first two terms on the right hand side are mechanical forces (per unit area) from bending and stretching, while the last term is the chemical force. The other two equilibrium equations (4.4) and (4.5) give us the relations of the Lagrange multipliers with other parameters of the problem as follow

$$\lambda_1=\zeta^{'}(\rho)-\frac{k_HH_0^{'}(c)c(R_0H_0+1)}{R_0\rho}-\frac{k_H^{'}(c)(R_0H_0+1)^2}{2R_0^2\rho}-\frac{cf^{'}(c)}{\rho}, \tag{4.26}$$

$$\lambda_2=\frac{f^{'}(c)}{\rho}+\frac{(R_0H_0+1)(2k_HH_0^{'}(c)R_0+k_H^{'}(c)[R_0H_0+1])}{2R_0^2\rho}. \tag{4.27}$$

4.4 Linear Stability

4.4.1 General Formulation

We consider a normal shape perturbation ψ_1, a density perturbation ψ_2, and a composition perturbation ψ_3. Following the methods introduced in Chapters 2 and 3, we find that the second variation of the energy functional under small perturbations can be written as

$$\delta^{(2)}\mathcal{F} = \int_A D_{ij}\psi_i\psi_j dA, \tag{4.28}$$

where D_{ij} are symmetric differential operators defined as follow

$$\begin{aligned} D_{11}\psi_1\psi_1 =& \frac{1}{2}k_H(\Delta\psi_1)^2 + \psi_1^2\left\{k_H\left[8H^4 - 10H^2K + 2K^2 + \frac{1}{2}KH_0^2\right]\right. \\ &+2k_c\left[(2H^2-K)|\nabla c|^2 - H\nabla c\cdot\bar{\nabla}c\right] + K[\zeta(\rho) - \rho\zeta'(\rho) + f(c)] + HP\Big\} \\ &+ 2k_H\left\{(2H-H_0)(\nabla H\cdot\nabla\psi_1 - \bar{\Delta}\psi_1 + H\Delta\psi_1)\psi_1\right. \\ &+(2H^2-K)\psi_1\Delta\psi_1\Big\} + \frac{1}{2}|\nabla\psi_1|^2\left\{\frac{1}{2}k_H(12H^2 - 8HH_0 + H_0^2)\right. \\ &\left.+\zeta(\rho) - \rho\zeta'(\rho) + f(c) + k_c|\nabla c|^2\right\} - k_c(2H-H_0)\nabla\psi_1\cdot\bar{\nabla}\psi_1 - k_c(\nabla c\cdot\nabla\psi_1)^2, \end{aligned} \tag{4.29}$$

$$D_{12}\psi_1\psi_2 = 0, \qquad \text{(taking into account the density equilibrium equation)} \tag{4.30}$$

$$\begin{aligned} D_{13}\psi_1\psi_3 =& 2k_c\psi_1\nabla\psi_3\cdot(H\nabla c - \bar{\nabla}c) + \frac{1}{2}\psi_3\Delta\psi_1\left\{k_H'(c)(2H-H_0) - k_HH_0'(c)\right\} \\ &+\psi_1\psi_3\left\{H(\lambda_2\rho - f'(c)) + k_HH_0'(c)(K - HH_0)\right. \\ &\left.+k_H'(c)\left[2H^3 - 2HK + KH_0 - \frac{1}{2}HH_0^2)\right]\right\} \end{aligned} \tag{4.31}$$

$$D_{22}\psi_2\psi_2 = \frac{1}{2}\zeta''(\rho)\psi_2^2, \tag{4.32}$$

$$D_{23}\psi_2\psi_3 = -\lambda_2\psi_2\psi_3, \tag{4.33}$$

and

$$D_{33}\psi_3\psi_3 = k_c|\nabla\psi_3|^2 + \frac{1}{2}\psi_3^2\left\{Q + k_H H_0'^2(c) - 2k_H'(c)H_0'(c)(2H - H_0)\right\}. \tag{4.34}$$

Above,

$$Q = f''(c) - k_H H_0''(c)(2H - H_0) + \frac{1}{2}k_H''(c)(2H - H_0)^2 \tag{4.35}$$

is the unique combination of the second derivatives of the terms coupling the shape and composition, and is called the miscible parameter.

Furthermore, the Lagrange multipliers λ_1 and λ_2 can be eliminated by using the density equations to have

$$\lambda_1 = -\frac{1}{\rho}\left\{2k_c\Delta c - f'(c) + k_H H_0'(c)(2H - H_0) - \frac{1}{2}k_H'(c)(2H - H_0)^2\right\} \tag{4.36}$$

and

$$\lambda_2 = \zeta'(\rho) + \frac{c}{\rho}\left\{2k_c\Delta c - f'(c) + k_H H_0'(c)(2H - H_0) - \frac{1}{2}k_H'(c)(2H - H_0)^2\right\}. \tag{4.37}$$

After substituting the Lagrange multipliers' expressions into the second variation, we observe that the coefficient D_{12} coupling the perturbations in shape and density vanishes. This reinforces the observation from the previous section that the bending of the membrane does not cause the non-uniformity of the tension. In contrast, notice that coefficient D_{23}

coupling the density and composition does not vanish ($D_{23} = -\lambda_2$), and neither does D_{13} coupling shape and composition. Therefore, the shape and density are individually coupled to the composition, but there is no direct coupling between the shape and the density.

4.4.2 Stability of Uniform Cylindrical Membranes

4.4.2.1 Longitudinal Perturbations

To study the stability of a uniform cylindrical membrane under longitudinal perturbations, we apply the following perturbations

$$\psi_1 = Ae^{\frac{2\pi is}{L}}, \quad \psi_2 = Be^{\frac{2\pi is}{L}}, \quad \psi_3 = Ce^{\frac{2\pi is}{L}}, \tag{4.38}$$

to the second variation (4.28). The resulting expression has the form

$$\delta^{(2)}\mathcal{F} = (A, B, C)J(A, B, C)^T, \tag{4.39}$$

where J is a 3×3 matrix whose components are as follow

$$\begin{aligned}
\frac{J_{11}}{2\pi L} &= k_H \left(\frac{8\pi^4}{L^4} + \frac{3}{4R_0^4} - \frac{H_0(c)^2}{4R_0^2} - \frac{\pi^2}{L^2 R_0^2} + \frac{4\pi^2 H_0(c)}{L^2 R_0} + \frac{\pi^2 H_0(c)^2}{L^2} \right) \\
&\quad + (\zeta(\rho) - \rho\zeta'(\rho)) \left(\frac{2\pi^2}{L^2} - \frac{2}{2R_0^2} \right), \\
\frac{J_{12}}{2\pi L} &= 0, \\
\frac{J_{13}}{2\pi L} &= \left(\frac{2\pi^2}{L^2} - \frac{1}{2R_0^2} \right) \left(k_H(c) H_0^{'}(c) + \left[\frac{1}{R_0} + H_0(c) \right] k_H^{'}(c) \right), \\
\frac{J_{22}}{2\pi L} &= \frac{\zeta''(\rho)}{2}, \\
\frac{J_{23}}{2\pi L} &= -\frac{(1 + R_0 H_0)(2k_H(c) R_0 H_0^{'}(c) + k_H^{'}(c)[1 + R_0 H_0(c)])}{4R_0^2 \rho}, \\
\frac{J_{33}}{2\pi L} &= \frac{1}{2} \left(k_c H_0^{'}(c)^2 + 2 \left[\frac{1}{R_0} + H_0 \right] H_0^{'}(c) k_0^{'}(c) + \frac{8\pi^2 k_c}{L^2} + Q \right), \\
Q &= f''(c) - k_H H_0^{''}(2H - H_0) + \frac{1}{2} k_H^{''}(c)(2H - H_0)^2.
\end{aligned} \tag{4.40}$$

Above, the pressure has been eliminated using the shape equation of the uniform solution (4.25). The equilibrium concentration has also been assumed to correspond to $f(c) = f'(c) = 0$.

We find the stability conditions by investigating the eigenvalues of J. Specifically, if the eigenvalue changes its sign, then the uniform membrane changes its stability. Therefore, we are interested in finding the roots of the equation

$$\det \Big(J(L; k_H(c), H_0(c), k_{ri,i=1,2,3}, \rho, k_c, Q) \Big) = 0. \tag{4.41}$$

In order to do that, we assume that the surface energy takes the form

$$\zeta(\rho) = k_{r0} + k_{r1}\rho(\log\rho - 1) + k_{r2}(\rho - 1)^2. \tag{4.42}$$

This form of the surface energy allows us to calculate how surface tension depends on the membrane density as

$$\Sigma = k_{r0} - k_{r1}\rho + k_{r2}(1-\rho^2). \tag{4.43}$$

Because surface tension is the quantity that is usually measured in experiments, we investigate if there exists a critical tension and how it depends on other parameters of the membrane. We begin by examining (4.41), and interpret it as a relationship between the wavelength L and the membrane properties, as well as the membrane density. Further, a long calculation shows that $\det(J)$ is a six order even polynomial in L. Thus, the existence of a root corresponds to an instability. Therefore, for a given set of parameters of the membrane, (4.41) gives $L = L(\rho)$. Using this relationship, together with the tension expression (4.43) where $\Sigma = \Sigma(\rho)$, we can parametrically plot Σ as a function of L. The plot allows us to find the critical tension if it exists.

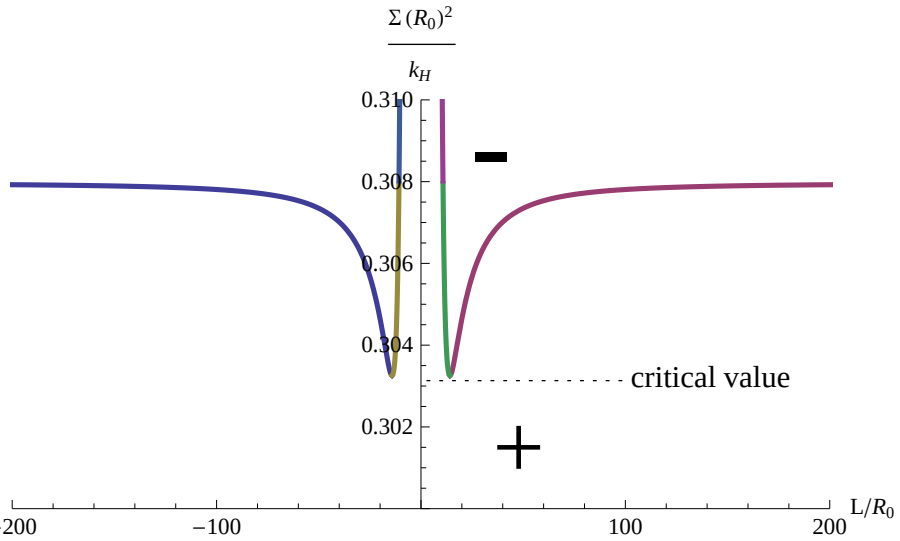

Figure 4.1: Stability diagram in $\Sigma - L$ space. The eigenvalues of the second variation vanish at the lines. Different colors correspond to different roots of $\det(J)$. The second variation is positive definite in the region under the lines, denoted by the + sign.

Fig. 4.1 shows typical roots of $\det(J)$ in the Σ–L space where different color lines

correspond to the six different roots. The number of real roots can be 0, 2, 4, or 6, depending on the value of tension. The region above the curve is unstable and denoted by the negative sign; the region below the curve is stable and denoted by the positive sign. As seen in the figure, there exists a critical tension Σ_c such that there does not exist any unstable wavelength when $\Sigma < \Sigma_c$.

We proceed to investigate how this critical tension depends on the properties of the membranes. The first property to be studied is the coupling between geometry and chemistry, $H_0(c)$. For simplicity, the calculation is done by using the value of $H_0(c)$ and $H_0^{'}(c)$ such that $H_0 = H_0^{'}(c)c$ where $c = 1/2$. Since the effect of the second derivative $H_0^{''}(c)$ is included in the miscibility parameter Q, this assumption does not necessarily mean that $H_0(c)$ is linear.

The coupling $H_0(c)$ has great influence on both the critical tension and critical wavelength. The critical tension is plotted as a function of $H_0(c)$ in Fig. 4.2a as the line connected by red + signs. Note that this critical tension is 0 when $H_0(c)R_0 \geq -1/2$. Thus, we conclude that the region shaded in green is the only stable region in the $\Sigma - H_0$ space and the rest is unstable. Moreover, the influence tends to destabilize the multi-component membrane, as its critical tension is much smaller than that of the single-component one. The difference between the two critical tensions vanishes at $H_0(c)R_0 = -1/2$, which happens to be the curvature of the cylinder. This vanishing is expected because the membrane is at its most preferable curvature at that point, i.e. the spontaneous curvature term does not want to alternate the membrane curvature. More importantly, we observe that the multi-component membrane suddenly changes to completely unstable once the spontaneous curvature is smaller than the membrane curvature: $H_0(c)R_0 > -1/2$. This is very different from single-component membrane, in which the membrane can be stable even when the

spontaneous curvature wants the membrane to curve outward ($H_0 > 0$).

Another remark on the effects of the spontaneous curvature is that the critical wavelength increases very rapidly when the spontaneous curvature decreases, as shown in Fig. 4.2b. This is similar to the observation on single-component membranes, although the increase starts at a larger spontaneous curvature for multi-component membranes.

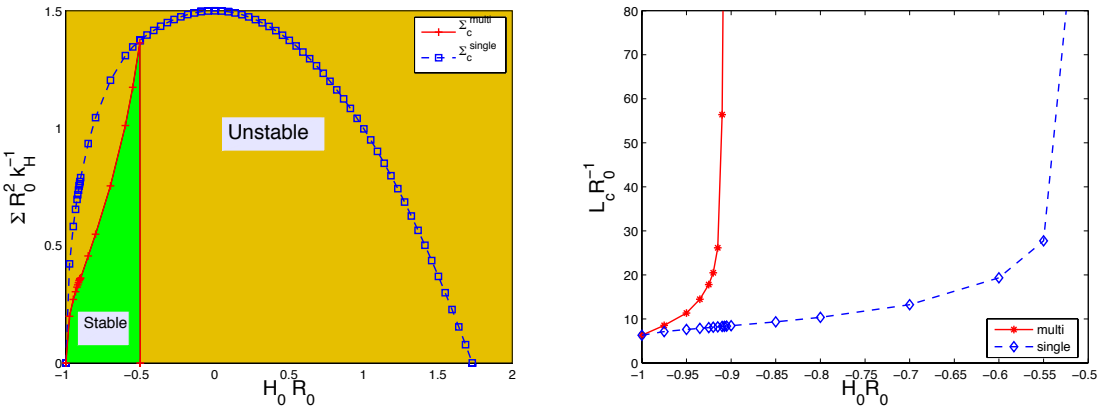

(a) Critical tension (b) Critical wavelength

Figure 4.2: Effects of the spontaneous curvature on the stability of an open multi-component membrane under longitudinal perturbations. The critical values of single-component and multi-component membranes are plotted in blue and red, respectively. The multi-component membrane has significantly (a) smaller stable regime but (b) larger critical wavelength than the single-component one does. In (a), the stable and unstable regimes are shaded in green and yellow, respectively. The multi-component membrane becomes completely unstable when its curvature is larger than the spontaneous curvature. The figures are calculated at $Qk_H R_0^{-2} = 1$ and $k_c k_H^{-1} = 0.2$.

The second property to be studied is the miscibility of the membrane. We systematically calculate the stability diagram for different values of Q as plotted in Fig. 4.3. We observe that, even when $Q > 0$, the critical tension is still smaller than that of the single-component membrane. As $Q \to +\infty$, the two critical tensions approach each other. On the other side of the graph, we see that there are $Q < 0$ where the membrane can still be stable as long as the membrane tension is small enough. Likewise, the critical wavelength is larger than that of the single-component one.

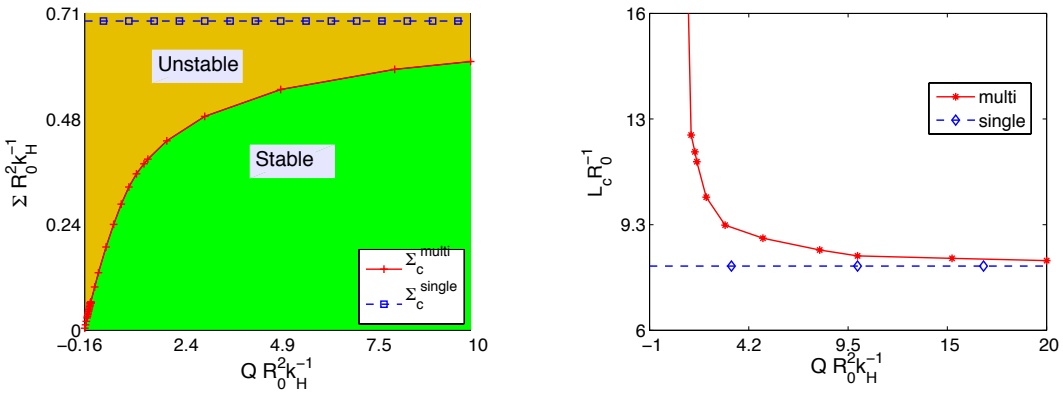

(a) Critical tension (b) Critical wavelength

Figure 4.3: Effects of the membrane miscibility on the critical tension and critical wavelength of an open multi-component membrane under longitudinal perturbations. Calculation is done with $H_0(c)R_0 = -0.925$.

While the experimental value of Q is not well known, the range that we used to study multi-component vesicles in Chapter 2 is between -10^{-7} to -10^{-9} Jm^{-2}. Applying the same range of Q for a cylindrical membrane of radius 0.6 μm, we obtain that the critical tension is from 10^{-9} to 10^{-8} Jm^{-2}, as shown in Fig. 4.4a. Furthermore, we calculate the critical tension for another membrane with larger radius as shown in Fig. 4.4b. The two figures show that the critical tensions of both multi-component and single-component membranes increase as their radii decrease. However, the critical value of the former is always one order of magnitude smaller than that of the latter. It will be interesting to verify this result experimentally.

Lastly, we study the combined effect of the spontaneous curvature and the membrane miscibility on the stability of the open multi-component membrane. Fig. 4.5 shows the effects of the spontaneous curvature on the critical tension when the membrane is miscible (the star green line) and immiscible (the plus blue line). Notice that when the membrane is miscible ($Q > 0$), the instability is dominated by the effects of the spontaneous curvature,

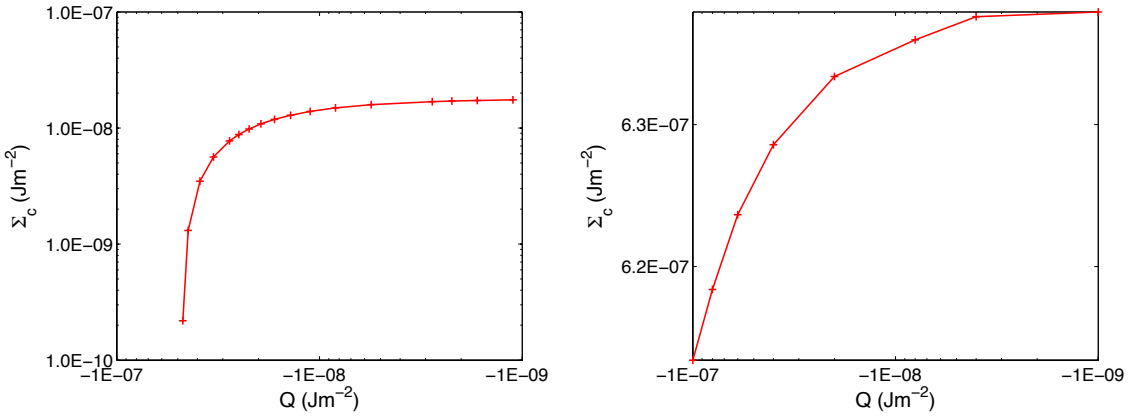

(a) $R_0 = 0.6$ μm, $\Sigma_c^{(single)} = 1.9\text{E}{-7}$ Jm^{-2} (b) $R_0 = 0.1$ μm, $\Sigma_c^{(single)} = 7\text{E}{-6}$ Jm^{-2}

Figure 4.4: Effects of the membrane miscibility Q on the critical tension of an open multi-component membrane under longitudinal perturbations. A membrane of smaller radius (b) has higher critical tension than the one of larger radius (a).

i.e., the membrane becomes completely unstable once the spontaneous curvature is larger than the membrane radius. Whereas, when the membrane is immiscible ($Q < 0$), the stability is dominated by the chemical stability, and the critical tension gradually goes to zero. Also, notice that when $QR_0^2k_H^{-1}$ changes from 1 to -0.08, the critical tension reduces one to two order of magnitude, depending on the value of the spontaneous curvature.

In conclusion, there exists a critical tension for open multi-component membrane beyond which it becomes unstable to longitudinal perturbations. The coupling between shape and chemistry has a negative effect on the membrane stability in that the critical tension of the multi-component membranes is smaller. If the coupling is weak and the lipids are highly chemically miscible, then the membrane stability approaches that of single-component one. However, the critical tension of a typical multi-component cylindrical membrane is one order of magnitude smaller than that of a single-component one.

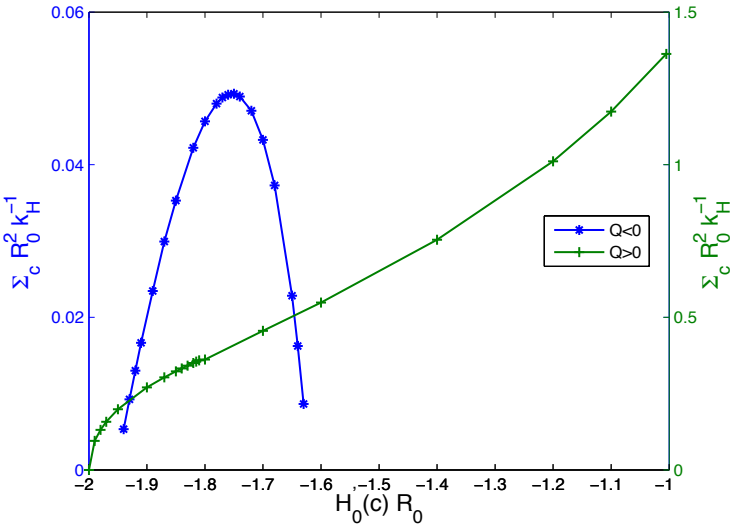

Figure 4.5: Combined effects of the spontaneous curvature and the membrane miscibility on the stability of an open multi-component membrane under longitudinal perturbations. The star blue line is calculated at $QR_0^2k_H^{-1} = -0.08$ and the plus green line is calculated at $QR_0^2k_H^{-1} = 1$. The stability is dominated by geometry instability when the membrane is miscible while it is dominated by the chemistry when the membrane is immiscible.

4.4.2.2 Radial Perturbations

The calculation process is similar to what we did in the previous section with the longitudinal perturbations. Instead of the z-dependent perturbations, we take the trial perturbations to be of in the form

$$\psi_1 = Ae^{2\pi im\theta}, \quad \psi_2 = Be^{2\pi im\theta}, \quad \psi_3 = Ce^{2\pi im\theta}. \tag{4.44}$$

Inserting this into the second variation (4.28), we have

$$\delta^{(2)}\mathcal{F} = (A, B, C)J(A, B, C)^T, \tag{4.45}$$

where J is a 3×3 matrix whose components are as follow

$$\begin{aligned}
\frac{J_{11}}{2\pi L} &= \frac{1}{4R_0^2}(m^2-1)\Big\{k_H(c)(2m^2+R_0^2H_0(c)^2-3)+2R_0^2(\zeta(\rho)-\rho\zeta'(\rho))\Big\},\\
\frac{J_{12}}{2\pi L} &= 0,\\
\frac{J_{13}}{2\pi L} &= \frac{(m^2-1)\left(k_H(c)H_0^{'}(c)+k_H^{'}(c)\left[\frac{1}{R_0}+H_0(c)\right]\right)}{2R_0^2},\\
\frac{J_{22}}{2\pi L} &= \frac{\zeta''(\rho)}{2},\\
\frac{J_{23}}{2\pi L} &= -\frac{1}{4R_0^2\rho}(1+R_0H_0(c))\Big\{2R_0k_H(c)H_0^{'}(c)+k_H^{'}(c)(1+R_0H_0(c))\Big\},\\
\frac{J_{33}}{2\pi L} &= \frac{1}{2}\left(k_H(c)H_0^{'}(c)^2+2H_0^{'}(c)k_H^{'}(c)\left[\frac{1}{R_0}+H_0(c)\right]+\frac{2k_cm^2}{R_0^2}+Q\right).
\end{aligned} \tag{4.46}$$

Again, the pressure has already been eliminated, assuming mechanical equilibrium and the equilibrium concentration is assumed to be at the well in the above expression. We are interested in finding the unstable wavenumber m from the solution of the equation

$$\det(J) = 0. \tag{4.47}$$

The first observation is that the components in the first row of matrix J are all multiplied by m^2-1. Therefore, $m = \pm 1$ are two roots of $\det(J)$, regardless of other coefficients. Second, all components of J contain only m^2, so $\det(J)$ is an even function of m; and we change variable from m to $b = m^2$ for simplicity. Third, $\det(J)$ is a third order polynomial of b with the highest coefficient

$$\frac{C_{b^3}}{2\pi L} = \frac{k_H(c)k_c\zeta''(\rho)}{4R_0^2} > 0. \tag{4.48}$$

Therefore, $\lim_{b\to\pm\infty} = \pm\infty$ and there are only limited number of unstable radial wavenum-

ber. Typical graphs of $\det(J)$ is plotted in Fig. 4.6.

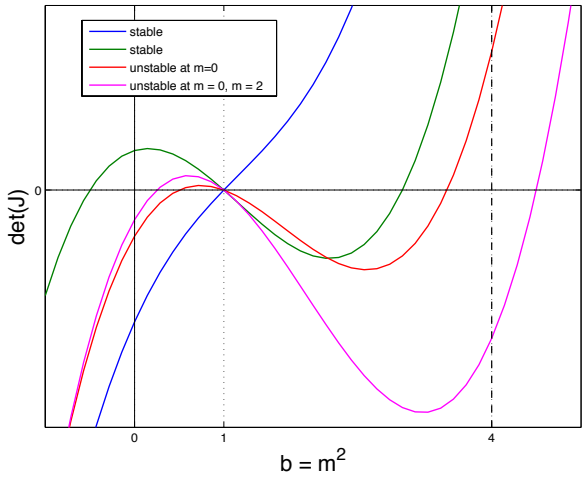

Figure 4.6: Typical graph of $\det(J)$ vs. b. Blue: stable because $\det(J)$ has only one root $b = 1$. Green: stable even though $\det(J)$ has multiple roots, but it is positive at all integer m. Red: unstable for expansion perturbations ($m = 1$). Magenta: unstable at $m = 1$ and $m = 2$.

Let us denote the three roots of $\det(J)$ as $b_\pm$ and b_1 where $b_- < b_1 = 1 < b_+$. First, the membrane is stable at $m = 0$ if b_- is not real or $b_- < 0$, as shown by the blue and green graphs in Fig. 4.6. Second, it is stable for non-axisymmetric perturbations if b_+ is not real or $b_+ < 4$, i.e. the blue, green, and red graphs in Fig. 4.6. On the other hand, it has unstable non-axisymmetric modes if $b_+ \geq 4$. Because $C_{b^3} > 0$, the radial perturbations lead to a limited number of unstable wavelengths with small wave numbers. These behaviors are very different from the longitudinal perturbations, which can result in an infinite number of unstable long wavelengths.

Having the three roots of $\det(J)$ in hand, we study the critical values at which the membrane changes from a stable state to an unstable one. Specifically, the solutions $b = b(\rho)$ and the surface tension $\Sigma = \Sigma(\rho)$ is parametrically plotted through parameter ρ. The resulting graphs, Fig. 4.7, allows us to investigate the critical values. As seen in Fig. 4.7a, there exists a critical tension such that the membrane is stable for $\Sigma > \Sigma_c$. Moreover, the

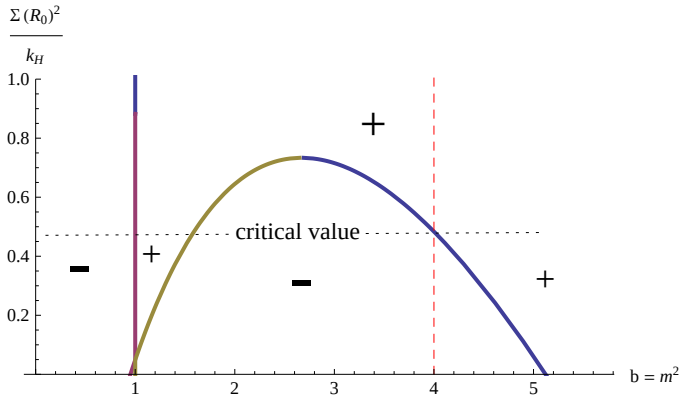

(a) Stable for $\Sigma > \Sigma_c$

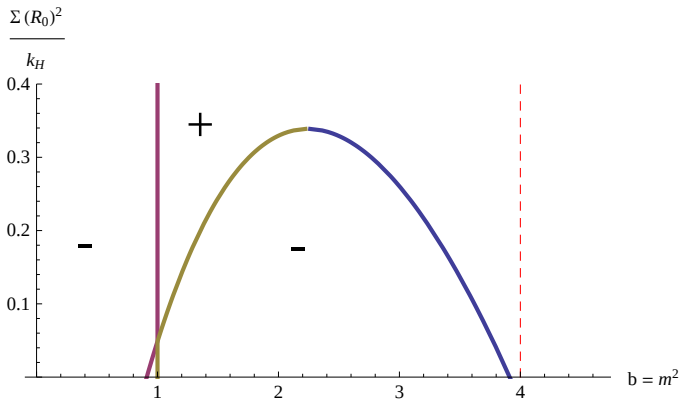

(b) Always stable

Figure 4.7: Typical stability diagrams in $\Sigma - b$ space where different colors correspond to different roots of $\det(J)$. (a) and (b) are calculated for the same set of parameters, except that (a) with $\frac{QR_0^2}{k_H} = -2$ is more immiscible than (b) with $\frac{QR_0^2}{k_H} = -1.5$.

critical tension can even reach zero; that is, there is not any radial wave number such that the second variation is negative, as in Fig. 4.7b. Recall from the previous section that the membrane is stable under the longitudinal perturbations if $\Sigma < \Sigma_c^l$. It means that the membrane prefers the radial instability at small tension, but the longitudinal instability at large tension. This preference of the membrane on the instability modes is also observed for single-component membranes in Chapter 3.

However, there is a significant difference in that the multi-component membrane experiences more modes of instability, other than just the beading and coiling, as the single-component one does. In fact, the coiling ($m = 1$) is an inflection point of $\det(J)$ instead of

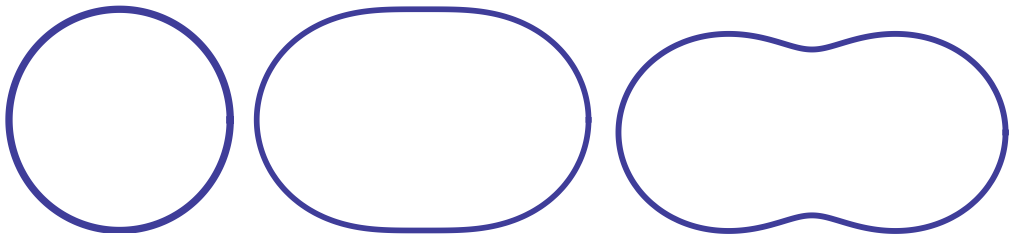

(a) Circle (b) Ellipse-like (c) Peanut-like

Figure 4.8: An unstable cylinder (a) can be transformed to the ellipse-like shape (b) or peanut-like shape (c) at the peanut critical mode $m = 2$.

a real unstable mode. The membrane's critical mode is at $m = 2$, at which the instability shape takes the appearance of either an ellipse for very small perturbations or a peanut for larger perturbations as shown in Fig. 4.8 (b) and (c).

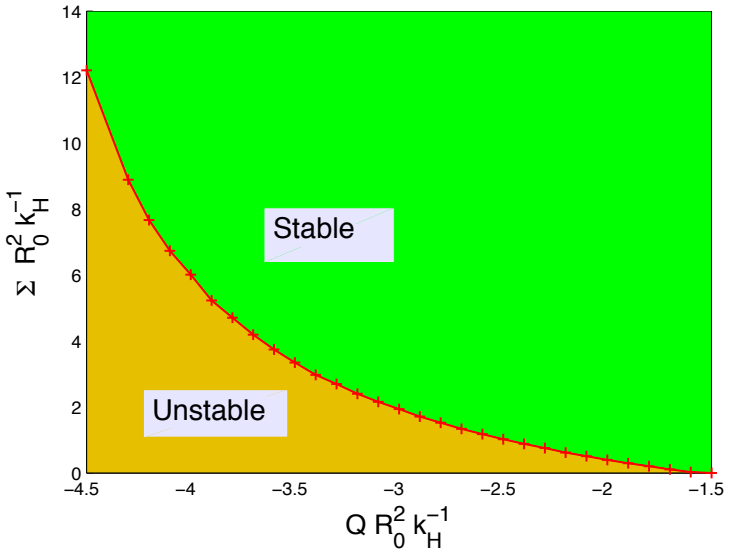

Figure 4.9: Effects of membrane miscibility on the stability of an open multi-component membrane under radial perturbations. When $QR_0^2k_H^{-1} < -3$, there appears an unstable mode at $m = 3$ beside the critical mode $m = 2$. Results shown for $H_0^{'}R_0 = -1.95$ and $k_ck_H^{-1} = 0.2$.

Fig. 4.9 shows that the open multi-component membranes becomes less stable when Q decreases. This result is expected because the membrane itself is chemically unstable as Q becomes more negative. The interesting result is that we observe another mode of

instability beside the critical mode $m = 2$ when the miscibility is low enough. Particularly, when $QR_0^2 k_H^{-1} < -3$, the instability modes also include the pear-like shapes with $m = 3$. Illustrations of this mode are presented in Fig. 4.10.

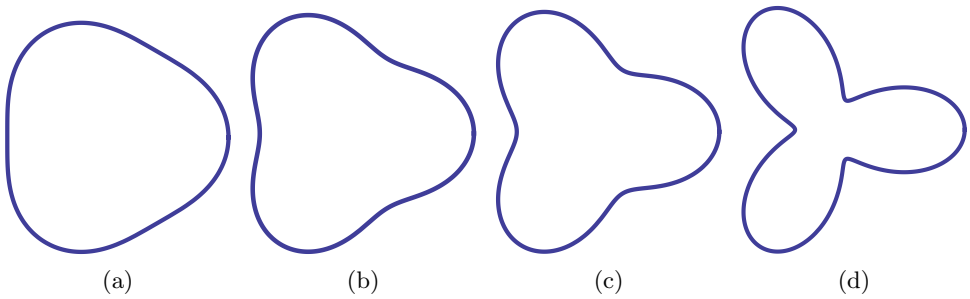

Figure 4.10: Pear instability mode ($m = 3$).

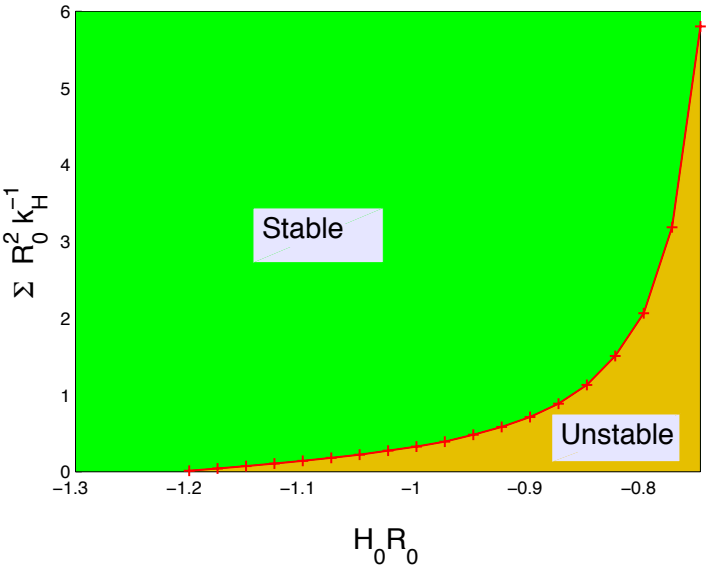

Figure 4.11: Influence of the spontaneous curvature on the stability of an open multi-component membrane under radial perturbations. Calculation is done with $QR_0^2 k_H^{-1} = -0.2$ and $k_c k_H^{-1} = 0.2$.

Another factor that has large influences on the stability is the spontaneous curvature. We plot how the critical tension depends on this quantity in Fig. 4.11. We observe that the membrane becomes stable for all tension as H_0 decreases. This is in contrast to the effects of H_0 under the longitudinal perturbations, in that the membrane is stable only at

moderate spontaneous curvature (Fig. 4.2). Notice that the unstable shapes with $m > 1$ have sections of positive and sections of negative curvatures; however, the curvature of a cylindrical membrane is always negative. Therefore, when $H_0R_0 < -1.2$, the cylindrical shape with negative curvature is more preferable than other shapes of $m > 1$. Additionally, when the spontaneous curvature is moderate, it cannot prevent the membrane from curving outward, and the instability modes with positive curvature (peanut and pear shapes) appear.

In conclusions, the open multi-component membranes prefer the radial instability shapes when tension is small and the longitudinal instability shapes when tension is large. These features are similar to that of the single-component ones, except that the radial instability shapes here include peanut-like and pear-like shapes. Because of the positive curvature of these shapes, the cylindrical shape is actually very stable when the spontaneous curvature is negative enough.

4.4.2.3 Combined Perturbations

In the previous two sections, we identified various instabilities by taking perturbations in the radial and the longitudinal directions separately. In this section we will allow mixed modes of perturbations in both directions. The trial perturbation is taken to be of the form

$$\psi_1 = Ae^{2\pi i\left(\frac{z}{L}+m\theta\right)}, \quad \psi_2 = Be^{2\pi i\left(\frac{z}{L}+m\theta\right)}, \quad \psi_3 = Ce^{2\pi i\left(\frac{z}{L}+m\theta\right)}. \tag{4.49}$$

Apply the above trial perturbations to the second variation (4.28) to obtain

$$\delta^{(2)}\mathcal{F} = (A, B, C)J(A, B, C)^T, \tag{4.50}$$

where J is a 3×3 matrix whose components are as follow

$$
\begin{aligned}
\frac{J_{11}}{2\pi L} =& \frac{k_H(c)}{R_0}\left(\frac{2m^4-5m^2+3}{4R_0^3}+\frac{4\pi^2 H_0(c)}{L^2}\right)+\frac{k_H(c)\pi^2}{L^4R_0^2}(L^2[4m^2-1]+8\pi^2R_0^2) \\
&+\frac{1}{4L^2R_0^2}(L^2(m^2-1)+4\pi^2R_0^2)(k_H(c)H_0(c)^2+2[\zeta(\rho)-\rho\zeta'(\rho)]), \\
\frac{J_{12}}{2\pi L} =& 0, \\
\frac{J_{13}}{2\pi L} =& \frac{\left\{L^2(m^2-1)+4\pi^2R_0^2\right\}\left(k_H(c)H_0^{'}(c)+k_H^{'}(c)\left[\frac{1}{R_0}+H_0(c)\right]\right)}{2L^2R_0^2}, \\
\frac{J_{22}}{2\pi L} =& \frac{\zeta''(\rho)}{2}, \\
\frac{J_{23}}{2\pi L} =& -\frac{1}{4R_0^2\rho}(1+R_0H_0(c))\left\{2R_0k_H(c)H_0^{'}(c)+k_H^{'}(c)(1+R_0H_0(c))\right\}, \\
\frac{J_{33}}{2\pi L} =& \frac{1}{2}\left(k_H(c)H_0^{'}(c)^2+2H_0^{'}(c)k_H^{'}(c)\left[\frac{1}{R_0}+H_0(c)\right]+2k_c\left[\frac{4\pi^2}{L^2}+\frac{m^2}{R_0^2}\right]+Q\right).
\end{aligned}
\tag{4.51}
$$

Similar to the previous sections, the pressure has already be eliminated and the equilibrium concentration is assumed to be at the well in the above expression. We are interested in finding the longitudinal unstable wavelength L and the radial unstable wavenumber m from the solution of the equation

$$\det(J(L,m)) = 0. \tag{4.52}$$

The expression $\det(J)$ is an even polynomial of order six in both L and m when it is multiplied by $64L^6R_0^8\rho$; therefore, we change the variables to $y = L^2$ and $b = m^2$. The coefficient of b^3 is

$$C_{b^3} = 16k_H(c)k_c\zeta''(\rho)\rho^2R_0^2y^3 > 0, \qquad \forall y > 0 \tag{4.53}$$

and for all set of the membrane's parameters. However, the coefficient of y^3 can be positive or negative, so $\det(J(y,b))$ can be quite complicated.

Fig. 4.12 shows a typical plot of $\det(J)$ as a function of y and b. We see that there are a

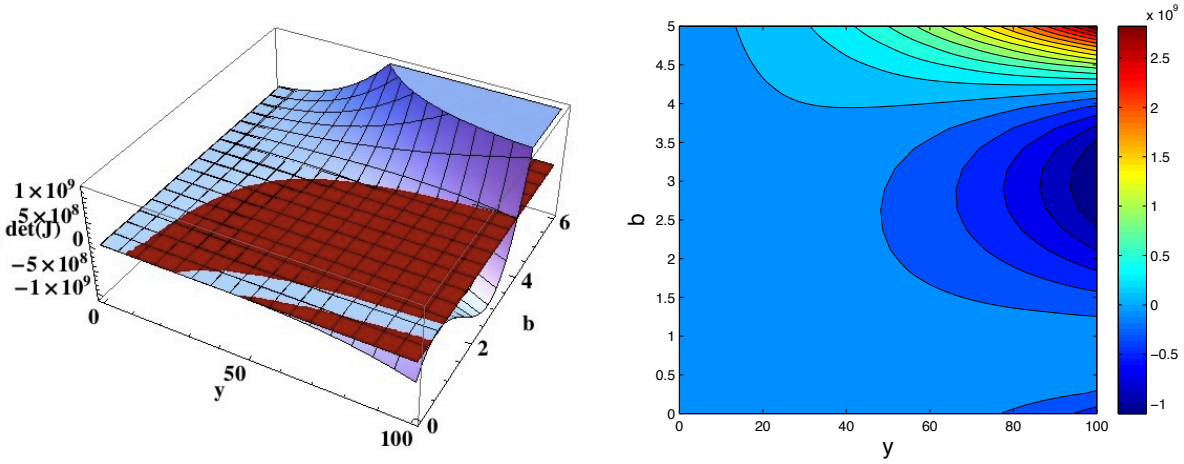

(a) A 3D plot of det(J) at a given tension. The the zero plane plotted in red is added to check where det(J) is negative.

(b) A contour plot of det J at a given tension

Figure 4.12: Typical graph of det(J) vs the radial wavenumber square b and the longitudinal wavelength square y.

number of mixed unstable modes that have $L < \infty$ and $m \neq 0$. However, the mixed modes seems to include only the peanut mode with $m = 2$ and the pear mode with $m = 3$. Also, it seems that the instability behaviors of det(J) at each given y are most clearly exhibited at $y \to \infty$. By contrast, the instability behaviors at each given b can be either at $b = 0$ or $b = 4$. In Fig. 4.12, the determinant is smaller at $b = 4$ than at $b = 0$, or correspondingly at $m = 0$ than $m = 2$. It would be interesting to investigate how the mixed modes play out with the critical values. This work will be done in the future.

4.5 Conclusions

In this chapter, we built a framework to study open multi-component membranes. Investigating the equilibrium equations, we show that it is possible for a membrane connected to a reservoir to have different lipid density and concentration from the reservoir. We also derive the linear stability conditions for open multi-component membranes, assuming that

there are no shape perturbations at the boundary. We then use these conditions to study the stability of a uniform cylindrical membrane. Critical tension and critical wavelengths are found for the membrane under pure longitudinal perturbations and pure radial perturbations. The results show that the uniform cylindrical membrane prefers radial instability modes when tension is low and longitudinal instability modes when tension is large. We observe that small spontaneous curvature destabilizes the membrane under both radial and longitudinal perturbations. However, large spontaneous curvature destabilizes the membrane under longitudinal perturbations, but does not affect the membrane stability under radial perturbations. The effects of spontaneous curvature are dominated by the chemical instability when the membrane becomes immiscible. We predict that the critical tension of a multi-component membrane is one to two orders of magnitude smaller than that of a single-component one, depending on the miscibility of the membrane. We also predict that the critical tension increases as the membrane radius decreases.

Chapter 5

Summary, Discussion, and Future Work

5.1 Summary of results

General framework This thesis provides a framework to study both open and closed membranes. Our general derivations allow us to identify and understand how the surface tension and surface energy are related, as well as the role of tension as a configurational force in controlling the membrane molecular density. With the help of the non-conventional differential operators and their related integral theorems, the derived second variations for both types of membranes which allow us to study the linear stability of the systematically. Moreover, we are able to identify a miscibility parameter Q of the membrane, which depends not only on the temperature but also on the coupling between geometry and chemistry, $H_0^{''}(c)$, between mechanics and chemistry, $k_H^{''}(c)$, as well as the system size H. We elaborate on these using case studies of the stability of uniform spherical and uniform cylindrical membranes.

Stability of closed multi-component membranes Our linear stability study on a uniform multi-component spherical vesicle shows that the multi-component vesicle is highly

unstable, even at high pressure. Moreover, its stability is very sensitive to the membrane miscibility, which includes temperature, the coupling, and the system size (Fig. 2.3). In addition, the instability modes have very high frequency, which is in contrast to single-component vesicles where the critical mode is always two [ZCH89]. This high frequency prediction is completely consistent with experimental observations [BHW03, VK03]. Likewise, the high frequency instability is also consistent with (flat) spinodal decomposition. Yet, unlike (flat) spinodal decomposition, the critical temperature, pressure and mode depend on system size through the miscible parameter Q.

We also study how the vesicle stability depends on other parameters of the problem, including the $H_0(c)$, k_c, $k_H(c)$, and H; of these parameters, the spontaneous curvature H_0 (Fig. 2.4) and the system size H (Fig. 2.5) have the most interesting influence. We observe that the critical pressure varies non-monotonically with H_0 in which the membrane is unstable for very high or very low spontaneous curvature.

Stability of open single-component membranes We have also studied the linear stability of a uniform cylindrical membrane. We prove that there are only two types of unstable periodic modes, which are beading and coiling instabilities. We observe that coiling is preferred when the tension is small while beading is preferred when the tension is large (Fig. 3.3 and Fig. 3.6). The observation of how tension affects stability agrees well with experiments done on neural cells [POJ94]. Specifically, nerves at the relaxed state, or even under moderate stretch, are observed to have coiled nerve fibers, which are called the bands of Fontana. As the stretch increases, the bands of Fontana disappear, giving the nerve fibers a straight shape. When the stretch continues to increase beyond some critical points, beadings appear to replace the straight shape (Fig. 3.7 and Fig. 3.8).

Stability of open multi-component membranes Our linear stability calculations for an open multi-component membrane show that the membrane prefers the radial instability when tension is small (Fig. 4.9 and Fig. 4.11) and the longitudinal instability when the tension is large (Fig. 4.2 and Fig. 4.3). This feature is also observed in single-component membranes. Moreover, the coupling between shape and chemistry has a negative effect on the membrane stability, in that the stable regime of the multi-component membranes is smaller compared to that of a single-component one. If the coupling is weak and the lipids are highly chemically miscible, then the membrane stability approaches that of a single-component one. However, the critical tension of a typical multi-component cylindrical membrane is one order of magnitude smaller than that of a single-component one (Fig. 4.4). We also show that the multi-component one has more instability modes, including not only beading and coiling, but also peanut and pear shapes.

5.2 Discussion

Comparison of the effects of the membrane miscibility Fig. 5.1 shows the effects of the miscibility on the stability of open and closed membranes. We observe that all membranes are less stable when the miscibility decreases. However, their critical wave numbers behave very differently. As the membrane immiscibility increases, the critical wave number of a closed vesicle increases (Fig. 5.1a) while that of the open membrane decreases (Fig. 5.1d). It means that, at low temperature, the multi-component vesicle segregate into small domains while the multi-component cylinder segregate into long cylindrical segments with alternative large and small radii.

Another interesting observation is that the critical wave number of the open membrane under radial perturbations is always two. Recall that the critical wave number of a single-

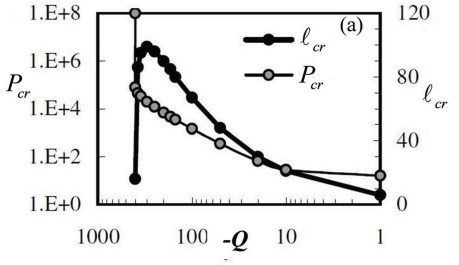

(a) Shown in Fig. 2.3, stable when $P > P_c$.

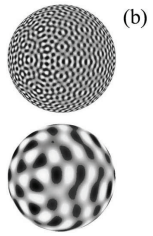

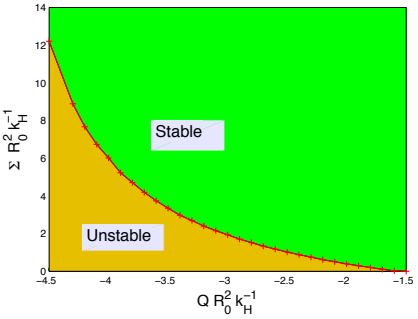

(b) Shown in Fig. 4.9.

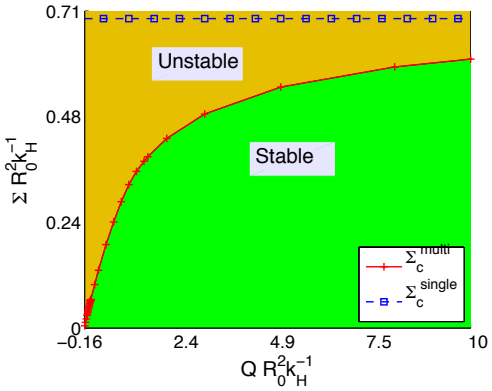

(c) Shown in Fig. 4.3a.

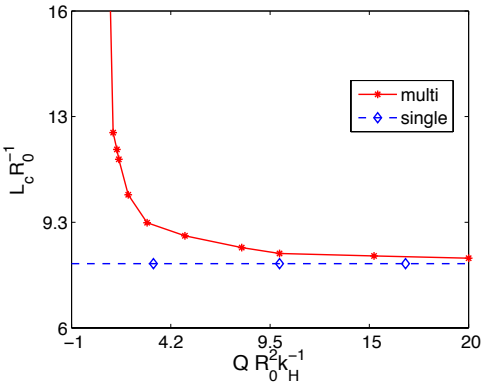

(d) Shown in Fig. 4.3b.

Figure 5.1: Comparison of the effects of the membrane miscibility Q on the stability of (a) a closed membrane, (b) an open membrane under radial perturbations, and (c, d) open membrane under longitudinal perturbations. The critical mode in (b) is at $m = 2$ while the unstable modes include include $m = 0, 1, 2$, and 3 (beading, coiling, peanut, and pear shapes.)

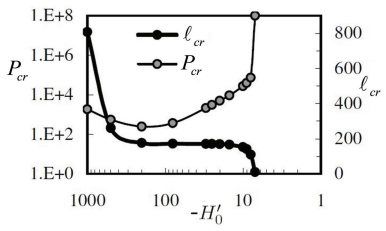

(a) Shown in Fig. 2.4

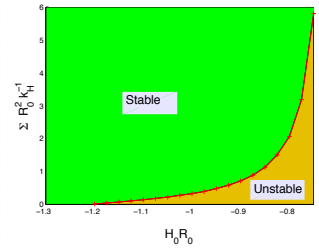

(b) Shown in Fig. 4.11

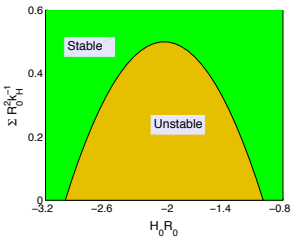

(c) Shown in Fig. 3.6;

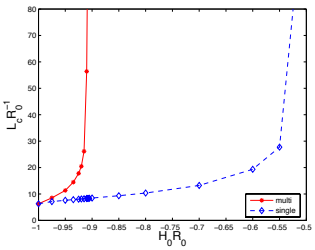

(d) Shown in Fig. 4.2

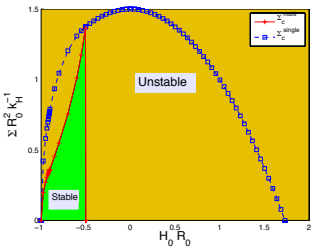

(e) Shown in Fig. 4.2

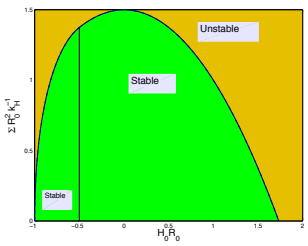

(f) Shown in Fig. 3.3

Figure 5.2: Comparison of the effects of H_0 on stability of (a) a closed multi-component membrane, (b) an open single-component membrane under radial perturbations, (c) an open multi-component membrane under radial perturbations, (d) an open single-component membrane under longitudinal perturbations, and (e, f) an open multi-component membrane under longitudinal perturbations.

component vesicle is also two [ZCH89]. This can be understand as follow. There are two reasons leading to instability: the constraint in geometry and multi-component features. The single-component vesicle has geometrical constraint in two directions, whereas, the multi-component open (cylindrical) membrane has geometrical constraint in one direction and the multi-component features. In the multi-component cylinder, the larger dimension (the longitudinal direction) is more flexible and stabilizes potential multi-component instabilities, leaving the radial direction to behave as if it is a single-component with geometrical constraint in two directions, i.e. the single-component vesicle. Therefore, they both have the same critical wave number.

Comparison of the effects of spontaneous curvature Fig. 5.2 shows the effects of the spontaneous curvature on both open and closed membranes under various types of per-

turbations. As seen in Fig. 5.2a, the closed membrane is most stable when the spontaneous curvature is moderate and becomes very unstable when the spontaneous curvature is very large or very small. This feature is similar to what observed in Fig. 5.2e and f for open single- and multi-component membranes under longitudinal perturbations. By contrast, the open membrane under radial perturbation is very stable at high spontaneous curvature (Fig. 5.2b and c). In short, the stability of the multi-component vesicle is similar to that of open membranes under longitudinal perturbations, but different from that of open membranes under radial perturbations. This observation is very similar to the observation of critical wave numbers equaling two noted above. Thus, we propose the same explanation as in the previous paragraph.

Another possible explanation for the stability of the open membranes under radial perturbations at high spontaneous curvature is based on the nature of the perturbed shapes. Any perturbed shape with wave number $m > 1$ has sections of positive and sections of negative curvature; by contrast, the curvature of a cylindrical membrane is negative. Therefore, when the spontaneous curvature is (negatively) large, the cylindrical shape is more preferable and stable than other shapes. When the spontaneous curvature is small or positive, it cannot prevent the membranes from curving outward. Thus, the cylindrical membrane can be unstable with respect to radial perturbations, and adapt to shapes with positive curvatures such as the peanut and pear shapes.

Another interesting effect of the spontaneous curvature is that it can make the membrane suddenly change from stable to completely unstable as seen in Fig. 5.2e. The drop point is where the spontaneous curvature begins to be smaller than the membrane curvature. This means that the open multi-component membrane is (geometrically) unstable when its curvature is larger than the spontaneous curvature. This effect of the spontaneous curvature

can be observed only when the membrane is miscible ($Q > 0$). When the membrane becomes immiscible ($Q < 0$), the instability is dominated by the chemical instability and the membrane becomes unstable before it reaches the geometrically unstable point. An illustration is presented in Fig. 4.5 which plots the critical tensions vs. the spontaneous curvature at different values of Q. In this figure, we can see that the critical tension drops to zero at $H_0R_0 = -1/2$ when $QR_0^2k_H^{-1} = 1$, but gradually goes to zero when $QR_0^2k_H^{-1} = -0.08$.

Our last remark is about the range of the critical wave numbers. We notice that the most appealing instability characteristics of the closed multi-component membrane is that its critical wave number is extremely high. However, the critical wave number of the open membrane is either less than one (for longitudinal perturbations) or of order one (for radial perturbations). One possible explanation for this is that the open membrane is more flexible in moving the molecules around, and it can thus avoid the sharp changes in shape and composition.

5.3 Potential Future Work

General framework for open membranes We have derived the equilibrium and stability conditions for open membranes (Chapter 3 and 4). However, we did not take into account the stability effects of the boundary. It is possible that the perturbations of the edges ($v_n\big|_{\partial A}$ and $\nabla v_n \cdot \underline{l}\big|_{\partial A}$) lead to the instability of the membranes. Therefore, we want to investigate how the edge perturbations can affect the membrane stability in our future work. Also, we have justified the equivalence between different methods of calculating the second variations (Appendix D); however, we want to prove this equivalence for a more general case.

Complete linear stability analysis on the open multi-component membranes We want to study the effects of other parameters ($k_H(c), k_c$, and the system size) on the stability of open multi-component membranes more thoroughly. Comparing these effects with the results on the stability of multi-component vesicles (presented in Chapter 2) would be interesting and provide deeper understandings on both of these classes of membranes. We also want to numerically solve the axisymmetric equations provided in Section 4.2 to study the tether and protein sorting experiments.

Theoretical predictions and experimental studies The presented results are theoretically interesting, and we have shown that many of these are consistent with previously reported experimental observations. We want to give more intuitive interpretations of the predictions and implications of these results. Furthermore, it would be more useful to suggest new experimental studies, as well as to predict the parameters ranges, such as the geometry-chemistry coupling strength ($H_0^{'}(c)$), and the dependence of the bending modulus on composition ($k_H(c)$), based on our linear stability analysis.

Appendix A

Useful Relations

In this appendix we list useful relations and identities that we have used in deriving the equilibrium equations and stability conditions. Throughout this appendix, f and ψ denote arbitrary scalar functions. In addition, we consider S to be a closed surface.

The integral theorems and identities listed below are a direct consequence of the divergence theorems (2.10) and (2.13). Nevertheless, we list them here for completeness. Specifically, proofs for the identities associated with the conventional gradient operator A.1-A.8) can be found in [Sto69], while those related to the non-conventional gradient operator in [YCN+05, YYW07]:

$$\nabla f \cdot \mathbf{n} = 0; \qquad \overline{\nabla} f \cdot \mathbf{n} = 0. \tag{A.1}$$

$$\nabla \cdot (\overline{\nabla} f) = \overline{\nabla} \cdot (\nabla f); \qquad \nabla f \cdot \overline{\nabla} \psi = \overline{\nabla} f \cdot \nabla \psi. \tag{A.2}$$

$$\int_S \nabla^2 f \, dS = 0; \qquad \int_S \overline{\nabla}^2 f \, dS = 0. \tag{A.3}$$

$$\int_S \nabla \cdot (f\nabla\psi)\, dS = 0; \qquad \int_S \overline{\nabla} \cdot (f\nabla\psi)\, dS = 0. \tag{A.4}$$

$$\int_S f\nabla^2\psi\, dS = -\int_S \nabla f \cdot \nabla\psi\, dS; \qquad \int_S f\overline{\nabla}^2\psi\, dS = -\int_S \nabla f \cdot \overline{\nabla}\psi\, dS. \tag{A.5}$$

$$\int_S (f\nabla^2\psi - \psi\nabla^2 f)dS = 0; \qquad \int_S (f\overline{\nabla}^2\psi - \psi\overline{\nabla}^2 f)dS = 0. \tag{A.6}$$

$$\nabla^2\psi = g^{ij}(\psi_{,ij} - \Gamma^m_{ij}\psi_{,m}); \qquad \overline{\nabla}^2\psi = K\overline{L}^{ij}(\psi_{,ij} - \Gamma^m_{ij}\psi_{,m}). \tag{A.7}$$

$$L_{im}g^{mn}L_{nj} = 2HL_{ij} - Kg_{ij}; \qquad K\overline{L}^{ij} = 2Hg^{ij} - L^{ij}. \tag{A.8}$$

$$|\overline{\nabla} f|^2 = -K|\nabla f|^2 + 2H\nabla f \cdot \overline{\nabla} f \tag{A.9}$$

$$\overline{\nabla} f \cdot \overline{\nabla} f = 2H\nabla f \cdot \overline{\nabla} f - K\nabla f \cdot \nabla f.$$

Appendix B

Variations of Various Quantities

Perturbing the shape in the normal direction

$$\delta \mathbf{x} = \epsilon \psi_1 \mathbf{n} \tag{B.1}$$

one can shown that [ZCH89]

$$\begin{aligned}
\delta \mathbf{g}_i =& (\mathbf{n}\psi_{1,i} - L_{ij}\mathbf{g}^j\psi_1)\epsilon, \\
\delta g_{ij} =& -2L_{ij}\psi_1\epsilon + [\psi_{1,i}\psi_{1,j} + \psi_1^2 L_{im}L_{jn}g^{mn}]\epsilon^2 + \mathcal{O}(\epsilon^3), \\
\delta g =& -4gH\psi_1\epsilon + g[|\nabla\psi_1|^2 + 2\psi_1^2(2H^2 + K)]\epsilon^2 + \mathcal{O}(\epsilon^3), \\
\delta g^{ij} =& 2\psi_1[2Hg^{ij} - K\overline{L}^{ij}]\epsilon + [(\frac{1}{g}e_{3i\alpha}e_{3i\beta} - g^{ij}g^{ab})\psi_{1,\alpha}\psi_{1,\beta} \\
& - 3\psi_1^2(Kg^{ij} - 4H^2 g^{ij} + 2HK\overline{L}^{ij})]\epsilon^2 + \mathcal{O}(\epsilon^3), \\
\delta \mathbf{n} =& -\nabla\psi_1\epsilon - \left[\psi_1\psi_{1,i}L_{\alpha\beta}g^{\beta i}\mathbf{g}^\alpha + \frac{1}{2}g^{ij}\psi_{1,i}\psi_{1,j}\mathbf{n}\right]\epsilon^2 + \mathcal{O}(\epsilon^3), \\
\delta L_{\alpha\beta} =& \left[\psi_{1,\alpha\beta} - \Gamma^\gamma_{\alpha\beta}\psi_{1,\gamma} - (2HL_{\alpha\beta} - Kg_{\alpha\beta})\psi_1\right]\epsilon \\
& + \Big[\psi_1\psi_{1,i}\{(L_{n\alpha}g^{ni})_{,\beta} + L_{\alpha n}g^{mn}\Gamma^i_{m\beta} - L_{mn}g^{ni}\Gamma^m_{\alpha\beta}\} \\
& + \psi_{1,i}\psi_{1,\alpha}L_{\beta\gamma}g^\gamma g^i - \frac{1}{2}g^{ij}\psi_{1,i}\psi_{1,j}L_{\alpha\beta} + \psi_{1,\beta}\psi_{1,i}g^{ni}L_{n\alpha}\Big]\epsilon^2 \\
& + \mathcal{O}(\epsilon^3),
\end{aligned} \tag{B.2}$$

and consequently

$$
\begin{aligned}
\delta L =& \Big[\overline{\nabla}^2\psi_1 - 2HK\psi_1\Big]g\epsilon + \Big[\{4H^2K + 2K(K-4H^2)\}\psi_1^2 \\
&- \frac{1}{2}K|\nabla\psi_1|^2 + K\psi_1\Delta\psi_1 - 2H\psi_1\overline{\Delta}\psi_1 - \{(L_{\alpha n}g^{ni})_{,\beta}KL^{\alpha\beta} \\
&+ g^{ni}KL_{mn}L^{\alpha\beta}\Gamma^m_{\alpha\beta} - g^{nm}KL_{\alpha n}L^{\alpha\beta}\Gamma^i_{m\beta}\}\psi_1\psi_{1,i} \\
&+ e_{3\alpha\beta}(\psi_{1,1a} - \Gamma^m_{1\alpha}\psi_{1,m})(\psi_{1,2\beta} - \Gamma^n_{2\beta}\psi_{1,n})/g\Big]g\epsilon^2 + \mathcal{O}(\epsilon^3), \\
\delta H =& \Big[(2H^2 - K)\psi_1 + \frac{1}{2}\nabla^2\psi_1\Big]\epsilon + \Big[\psi_1(2H\nabla^2\psi_1 - \overline{\nabla}^2\psi_1) \\
&+ \frac{1}{2}\nabla\psi_1\cdot(H\nabla\psi_1 - \overline{\nabla}\psi_1) + \psi_1^2H(4H^2 - 3K) \\
&+ \psi_1\nabla H\cdot\nabla\psi_1\Big]\epsilon^2 + \mathcal{O}(\epsilon^3), \\
\delta K =& \Big[2HK\psi_1 + \overline{\nabla}^2\psi_1\Big]\epsilon + \Big[\{4H^2 - K\}K\psi_1^2 - \{(L_{\alpha n}g^{ni})_\beta \\
&+ g^{ni}L_{mn}\Gamma^m_{\alpha\beta} - g^{mn}L_{\alpha n}\Gamma^i_{m\beta}\}KL^{\alpha\beta}\psi_1\psi_{1,i} + \frac{3}{2}K|\nabla\psi_1|^2 \\
&+ \{K\Delta\psi_1 + 2H\overline{\Delta}\psi_1\}\psi_1 \\
&+ e_{3\alpha\beta}(\psi_{1,1a} - \Gamma^m_{1\alpha}\psi_{1,m})(\psi_{1,2\beta} - \Gamma^n_{2\beta}\psi_{1,n})/g\Big]\epsilon^2 + \mathcal{O}(\epsilon^3), \\
\delta dS =& -2H\psi_1 dS\,\epsilon + \left[\frac{1}{2}|\nabla\psi_1|^2 + K\psi_1^2\right]\epsilon^2 + \mathcal{O}(\epsilon^3), \\
\delta V_S =& \epsilon\int_S \psi_1\,dS - \epsilon^2\int_S H\psi_1^2 dS + \mathcal{O}(\epsilon^3).
\end{aligned}
\tag{B.3}
$$

Importantly, the variation of the gradient does not equal the gradient of the variation, as in flat space. In particular, $\delta(\nabla c) \neq \nabla(\delta c)$. Also, the variation of the term in the energy

function which penalizes composition gradients is

$$\begin{aligned}\delta(|\nabla c|^2) =& 2\nabla c \cdot \Big[\psi_1(H\nabla c - \overline{\nabla} c) + \nabla\Psi_3\Big]\epsilon \\ &+ \Big[|\nabla\psi_1|^2|\nabla c|^2 + 2|\nabla\Psi_3|^2 - 2(\nabla\psi_1\cdot\nabla c)^2 \\ &+ \psi_1^2(8H^2|\nabla c|^2 - 4K|\nabla c|^2 - 4H\nabla c\cdot\overline{\nabla} c) \\ &+ 8H\psi_1\nabla\Psi_3\cdot\nabla c - 8\nabla\Psi_3\cdot\overline{\nabla} c\Big]\epsilon^2 + \mathcal{O}(\epsilon^3).\end{aligned} \tag{B.4}$$

where $\Psi_3 = (\Delta\psi_3 - c\Delta\psi_2)/\rho$. Above, $\delta\eta$ means $\eta(\mathbf{x}+\delta\mathbf{x}) - \eta(\mathbf{x})$, and e_{ijk} is a cyclic permutation of $(1,2,3)$, i.e.

$$e_{ijk} = \begin{cases} 1, & \text{if } (ijk) \text{ is an even permutation of } (123) \\ -1, & \text{if } (ijk) \text{ is an odd permutation of } (123) \\ 0, & \text{otherwise.} \end{cases} \tag{B.5}$$

Also, note the difference between L^{ij} and $\overline{L}^{ij}$: while L_{ij} and L^{ij} are the covariant and contravariant components associated with the second fundamental tensor $\mathbf{L}$, $\overline{L}^{ij}$ are the contravariant components of $\mathbf{L}^{-1}$, i.e.

$$L^{ij} = g^{im}g^{jn}L_{mn}; \quad L_{im}\overline{L}^{mj} = \delta_{ij}. \tag{B.6}$$

Appendix C

The Equivalence Between the Tangential Perturbation Method and the Lagrange Multiplier Method

In order to solve our constrained optimization problem, the Lagrange multiplier method may be used [Zei84]. By this method, the equilibrium solutions of (2.1, 2.3) nullify the first variation of the Lagrange functional

$$\mathcal{L} = \mathcal{F} - \lambda_1 \int_S c\rho \, dS - \lambda_2 \int_S \rho \, dS \tag{C.1}$$

with respect to any perturbations in shape, concentration, and density, which take the form

$$\delta \mathbf{x} = \epsilon \psi_1 \mathbf{n}, \quad \delta\rho = \epsilon\psi_2, \quad \delta c = \epsilon \psi_3. \tag{C.2}$$

The constants λ_1 and λ_2 in (C.1) are Lagrange multipliers, ψ_i in (C.2) are arbitrary functions, and ϵ is a small infinitesimal quantity. The equilibrium solutions are stable if the

second variation is positive for any perturbations in the tangent space of the constraints:

$$\delta\mathbf{x} = \epsilon\psi_1\mathbf{n}, \quad \delta\rho = \epsilon\left(2H\rho\psi_1 + \Delta\psi_2\right), \quad \delta c = \epsilon\left(\frac{\Delta\psi_3 - c\Delta\psi_2}{\rho}\right). \tag{C.3}$$

Calculating the first variation of the Lagrange functional $\mathcal{L}$ under arbitrary perturbation (C.2) and letting it equal to zero for any ψ_i, $i = \overline{1,3}$, we have the corresponding three equilibrium equations

$$\begin{aligned}&\Delta(k_H(c)(2H - H_0(c))) + 4k_H(c)H(H^2 - K) + k_H(c)H_0(c)(2K - HH_0(c))\\ &- 2Hf(c) + k_c(H|\nabla c|^2 - \nabla c\cdot\widetilde{\nabla}c) - 2H\left(k_\rho(\rho-1)^2 - \lambda_1 c\rho - \lambda_2\rho\right) - P = 0,\end{aligned} \tag{C.4a}$$

$$2k_\rho(\rho - 1) - \lambda_2 - \lambda_1 c = 0, \tag{C.4b}$$

$$k_c\Delta c - f^{'}(c) + k_H(2H - H_0(c))H_0^{'}(c) + \lambda_1\rho - \frac{1}{2}k_H^{'}(c)(2H - H_0(c))^2 = 0. \tag{C.4c}$$

Let us manipulate (C.4) and (2.23) to show that they are equivalent. Solving (C.4b) and (C.4c) for λ_1 and λ_2 and substituting them into (C.4a), we have

$$\begin{aligned}&\Delta(k_H(c)(2H - H_0(c))) + 4k_H(c)H(H^2 - K) + k_H(c)H_0(c)(2K - HH_0(c))\\ &- 2Hf(c) + k_c(H|\nabla c|^2 - \nabla c\cdot\widetilde{\nabla}c) + 2k_\rho H(\rho^2 - 1) - P = 0,\end{aligned} \tag{C.4a$\star$}$$

$$\lambda_2 = 2k_\rho(\rho - 1) - \lambda_1 c, \tag{C.4b$\star$}$$

$$\lambda_1 = -\frac{k_H(2H - H_0(c))H_0^{'}(c) - f^{'}(c) + k_c\Delta c}{\rho} + \frac{1}{2\rho}k_H^{'}(c)(2H - H_0(c))^2. \tag{C.4c$\star$}$$

Also, using the fact that $\Delta\varphi = 0$ on a closed surface implies that φ is a constant function, we may combine (2.23b) and (2.23c) to obtain

$$\begin{aligned}\Delta(k_H(2H - H_0(c))) + 4k_H H(H^2 - K) + k_H H_0(c)(2K - HH_0(c)) \\ - 2Hf(c) + k_c(H|\nabla c|^2 - \nabla c \cdot \widetilde{\nabla} c) + 2k_\rho H(\rho^2 - 1) - P = 0,\end{aligned} \tag{2.23a$\star$}$$

$$\alpha_2 = 2k_\rho(\rho - 1) - \alpha_1 c, \tag{2.23b$\star$}$$

$$\alpha_1 = -\frac{k_H(2H - H_0(c))H_0'(c) - f'(c) + k_c\Delta c}{\rho} + \frac{1}{2\rho}k_H'(c)(2H - H_0(c))^2, \tag{2.23c$\star$}$$

where α_1 and α_2 are constants. We can see that (C.4$\star$) and (2.23$\star$) are exactly the same. A more general proof can be found in [Zei84].

Similarly, calculating $\delta^2\mathcal{L}$ at the tangential perturbations (C.3) and eliminating the Lagrange multipliers λ_1 and λ_2 by using the equilibrium equations (C.4), we also get

$$\delta^{(2)}\mathcal{L} = \int_S \sum_{i,j=1}^{3} D_{ij}\psi_i\psi_j \, dS, \tag{C.7}$$

D_{ij} are defined as in (2.28).

Appendix D

Justification of Different Methods in Calculating the Second Variations for Open Membranes

To study the stability of an open membrane, we can use the bifurcation method instead of calculating the second variation (3.60), as done in Chapter 3. The bifurcation theory states that an equilibrium state is linearly stable if the small perturbed system does not have any solution; instead, if there exists a solution, the system is unstable and the extra solution is called the bifurcated solution. Therefore, the bifurcation method involves in calculating the perturbations of equilibrium equations (3.56–3.57) and boundary conditions (3.52–3.55) at the interested state.

We can also obtain an equivalent bifurcation condition by first integrating the equilibrium equations over the surface and the boundary conditions over the boundary to have the first variation (3.49); and second, perturbing the first variation expression. We will denote the perturbation of the first variation by $\delta(\delta\mathcal{F})$. Somewhat differently, we can further push the first variation back to the expression that we had before applying the integral theorem on the term associated with the second derivative of the perturbation. We will denote the resulting expression by $\delta(\delta\mathcal{F}_{\Delta v_n})$, where the subscript Δv_n means that the first variation contains Δv_n instead of $\Delta(2H - H_0)$. In short, $\delta(\delta\mathcal{F})$ is different from $\delta(\delta\mathcal{F}_{\Delta v_n})$ in that

the former contains the variation of $v_n\Delta(2H-H_0)$ while the latter contains the variation of $(2H-H_0)\Delta v_n$. We will justify the equivalence between $\delta(\delta\mathcal{F})$, $\delta(\delta\mathcal{F}_{\Delta v_n})$, and $\delta^{(2)}\mathcal{F}$ in this section.

Taking into account the equilibrium equation in density, $\delta^{(2)}\mathcal{F}$ can be written as in (3.60), and the other two are as follow

$$\begin{aligned}\delta(\delta\mathcal{F}) = \int_A \Big\{ \Big(k_H \left[8H^4 - 10H^2K + \frac{H_0^2K}{2} + 2K^2 + H\Delta(2H-H0) - \overline{\Delta}(2H-H_0) \right] \\ + HP + K\Sigma \Big) v_n^2 + \left(k_H \left[3H^2 - \frac{H_0^2}{4} - K \right] - \frac{\Sigma}{2} \right) v_n \Delta v_n \\ + 2k_H v_n \nabla H \cdot \nabla(Hv_n) + k_H v_n \Delta \left(v_n \left[2H^2 - K + \frac{1}{2}\Delta v_n \right] \right) \\ - k_H v_n \nabla v_n \cdot \overline{\nabla}(2H-H_0) - k_H(2H-H_0) v_n \Delta v_n + \zeta''(\rho) v_\rho^2 \Big\} dA,\end{aligned} \tag{D.1}$$

and

$$\begin{aligned}\delta(\delta\mathcal{F}_{\Delta v_n}) = \int_A \Big\{ \left(k_H \left[8H^4 - 10H^2K + \frac{H_0^2K}{2} + 2K^2 \right] + HP + K\Sigma \right) v_n^2 \\ + k_H(2H-H_0)\nabla v_n \cdot (\nabla(Hv_n) - \overline{\nabla} v_n) \\ + \left(\left[7H^2 - HH_0\frac{H_0^2}{4} - 2K \right] - \frac{\Sigma}{2} \right) v_n \Delta v_n \\ + \frac{1}{2} k_H (\Delta v_n)^2 - 2k_H(2H-H_0) v_n \overline{\Delta} v_n + \zeta''(\rho) v_\rho^2 \Big\} dA.\end{aligned} \tag{D.2}$$

To justify the equivalence between the three variations, let us consider the differences between $\delta^{(2)}\mathcal{F}$ and the other two. From equations (3.60) and (D.2) we have

$$\begin{aligned}\delta^{(2)}\mathcal{F} - \delta(\delta\mathcal{F}_{\Delta v_n}) - = \int_A k_H \Big\{ (2H-H_0) v_n \nabla v_n \cdot \nabla H \\ + \frac{1}{2} \left(\frac{1}{2}(2H-H_0)^2 + \Sigma \right) \left(v_n \Delta v_n + |\nabla v_n|^2 \right) \Big\} dA.\end{aligned} \tag{D.3}$$

The right hand side of (D.3) can be transformed so that the equation can be written as

$$\delta^{(2)}\mathcal{F} - \delta(\delta\mathcal{F}_{\Delta v_n}) = \frac{1}{2}\int_{\partial A}\left\{\frac{1}{2}k_H(2H-H_0)^2+\Sigma\right\} v_n \nabla v_n \cdot \underline{l}\, dL. \tag{D.4}$$

If we assume that there is no perturbation at the boundary, i.e. $v_n|_{\partial A} = 0$ and $\nabla v_n \cdot \underline{l}|_{\partial A} = 0$, then $\delta^{(2)}\mathcal{F}$ and $\delta(\delta\mathcal{F}_{\Delta v_n})$ are identical. Similarly, from (3.60) and (D.1) we have

$$\begin{aligned}\delta(\delta\mathcal{F}) - \delta^{(2)}\mathcal{F} = \int_A \Big\{ &\left(k_H\left[-3H^2+2HH_0-\frac{H_0^2}{4}\right]-\frac{\Sigma}{2}\right)|\nabla v_n|^2 + \frac{k_H}{2}(\Delta v_n)^2 \\ &+ k_H v_n\left[\nabla(Hv_n)\cdot\nabla(2H-H_0)+\Delta(v_n[2H^2-K+1/2\Delta v_n])\right] \\ &+ k_H v_n \nabla v_n \cdot \left[\overline{\nabla}(2H-H_0)-2(2H-H_0)\nabla H\right] + k_H(2H-H_0)\nabla v_n\cdot\overline{\nabla}v_n \\ &+ k_H\left[H\Delta(2H-H_0)-\overline{\Delta}(2H-H_0)\right]v_n^2 + k_H(2H-H_0)v_n\overline{\Delta}v_n\Big\} dA.\end{aligned} \tag{D.5}$$

Again, using the integral theorems for both the conventional and non-conventional gradient operators, we have

$$\begin{aligned}\delta(\delta\mathcal{F}) - \delta^{(2)}\mathcal{F} = &\int_A k_H\Big\{2v_n\nabla v_n\cdot([H+H_0]\nabla H-\nabla K)+v_n^2\left(4|\nabla H|^2+4H\Delta H-\Delta K\right) \\ &\quad -\left(3H^2-2HH_0+\frac{H_0^2}{4}+\frac{\Sigma}{2k_H}\right)\left(v_n\Delta v_n+|\nabla v_n|^2\right)\Big\}dA \\ &+\int_{\partial A} k_H\Big\{\frac{1}{2}\left(v_n\nabla(\Delta v_n)-\Delta v_n\nabla v_n\right)+2(H\nabla H-\overline{\nabla}H)v_n^2 \\ &\quad + v_n(2H\overline{\nabla}v_n-H_0\nabla v_n)\Big\}\cdot\underline{l}\, dL.\end{aligned} \tag{D.6}$$

It is easy to see from (D.6) that if the shape is uniform and the perturbations at the boundary is zero, both the surface and and line integrals vanish. Note that we limit ourselves to justifying the equivalence between the variations for uniform solutions when there is no boundary perturbations. Proof of the more general cases will be in our future works.

Appendix E

Detailed Derivations for an Open Multi-component Membrane Connected to a Reservoir

The multi-component features of the membrane are captured by using the interactions and couplings between the membrane geometry, chemistry, and mechanics that we used to study the closed multi-component membranes in Chapter 2. Likewise, the openness of the membrane is taken care of by using the same approach that we have in Chapter 3. Specifically, we consider a membrane composed of two types of lipids and connected to a lipid reservoir as shown in Fig. E.1a. The energy functional of the system can be written as

$$\begin{aligned}\mathcal{F} = &\int_A \frac{1}{2} k_H(c)(2H - H_0(c))^2 dA + \int_A \zeta(\rho)\, dA + \int_{\partial A} \sigma\, ds + F_P + F_f + F_M + \int_A f(c)\, dA \\ &+ \int_A k_c |\nabla c|^2\, dA - \lambda_1 \left(\int_A \rho\, dA + \int_{\mathcal{A}\setminus A} \rho\, dA \right) - \lambda_2 \left(\int_A \rho c\, dA + \int_{\mathcal{A}\setminus A} \rho c\, dA \right) \\ &+ \int_{\mathcal{A}\setminus A} \overline{\zeta}(\rho)\, dA + \int_{\mathcal{A}\setminus A} \overline{f}(c)\, dA,\end{aligned} \tag{E.1}$$

in which the first three terms are mechanical potentials including bending, stretching, and line-tension; the next three terms are the work done by external forces; the seventh and eighth terms are the interaction energy and the penalty for sharp change in concentration.

The two terms multiplied by $\lambda_{1,2}$ account for the conservation of molecules of the system. The last two terms are the surface and interaction energies of the reservoir. We will

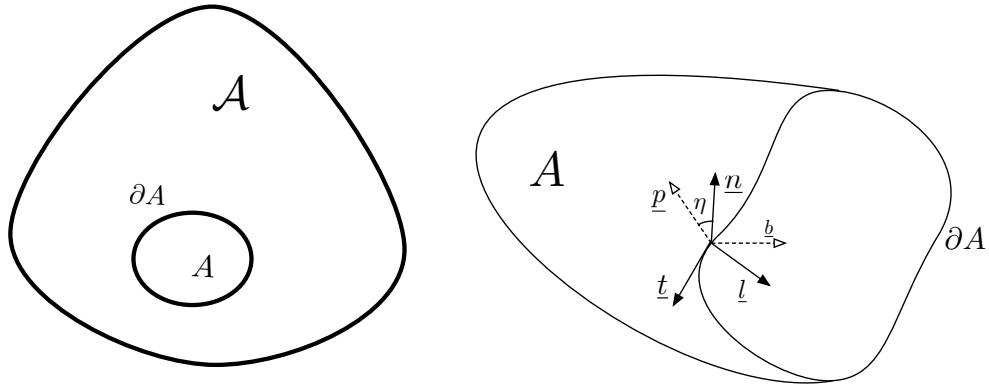

(a) (b)

Figure E.1: (a)Open membrane A is connect reservoir $\mathcal{A}$. (b) Vector notations on ∂A.

show that the open multi-component membrane has slightly different chemical potentials compared to the one we defined for the single-component membranes.

Using similar variations as described in Chapter 2 and Chapter 3, we can calculate the

first variation of the energy functional (E.1) as

$$\begin{aligned}\delta^{(1)}\mathcal{F} = \int_A \{&\Delta[k_H(2H-H_0)] + k_H(c)(2H-H_0)(2H^2-2K+H_0H) - P \\ &- 2H[\zeta(\rho)-\lambda_1\rho-\lambda_2\rho c]) - 2k_c\nabla c\cdot\overline{\nabla}c + 2k_cH|\nabla c|^2 - 2Hf(c)\}v_n dA \\ &+ \int_A \{\zeta'(\rho)-\lambda_1-\lambda_2 c\}v_\rho dA \\ &+ \int_A \left\{f'(c)-\lambda_2\rho - 2k_c\Delta c - k_H H_0'(c)(2H-H_0) + \frac{1}{2}k_H'(c)(2H-H_0(c))^2\right\} v_c dA \\ &+ \int_{\mathcal{A}\setminus A}\{\overline{\zeta}'(\rho)-\lambda_1-\lambda_2 c\}v_\rho dA + \int_{\mathcal{A}\setminus A}\{\overline{f}'(c)-\lambda_2\rho\}v_c dA \\ &+ \int_{\partial A}\{\sigma K_n - N + \nabla[k_H(c)(2H-H_0(c))]\cdot\underline{l}\}\,\underline{v}\cdot\underline{n}\,ds \\ &+ \int_{\partial A}\left\{\frac{1}{2}k_H(c)(2H-H_0(c))^2 + [\![\zeta(\rho)]\!] - \lambda_1[\![\rho]\!] - \lambda_2[\![\rho c]\!] - \tau\right\}\underline{v}\cdot\underline{l}\,ds \\ &+ \int_{\partial A}\{M - k_H(c)(2H-H_0(c))\}\,\nabla v_n\cdot\underline{l}\,ds \\ &- \int_{\partial A}\dot{\sigma}\underline{v}\cdot\underline{t}\,ds + \int_{\partial A} 2k_c(\nabla c\cdot\underline{l})\,v_c\,ds.\end{aligned} \tag{E.2}$$

This first variation $\delta^{(1)}\mathcal{F}$ vanishes for all shape perturbations $\underline{v}$, density perturbations v_ρ, and concentration perturbations v_c for any equilibrium state. Therefore, the equilibrium equations and boundary conditions can be written as

$$\begin{aligned}&\Delta[k_H(2H-H_0)] + k_H(c)(2H-H_0)(2H^2-2K+H_0H) - P \\ &\quad - 2H[\zeta(\rho)-\lambda_1\rho-\lambda_2\rho c]) - 2k_c\nabla c\cdot\overline{\nabla}c + 2k_cH|\nabla c|^2 - 2Hf(c) = 0, \qquad \text{in } A\end{aligned} \tag{E.3}$$

$$\zeta'(\rho)-\lambda_1-\lambda_2 c = 0, \qquad \text{in } A \tag{E.4}$$

$$\overline{\zeta}'(\rho)-\lambda_1-\lambda_2 c = 0, \qquad \text{on } \mathcal{A}\setminus A \tag{E.5}$$

$$f'(c)-\lambda_2\rho - 2k_c\Delta c - k_H H_0'(c)(2H-H_0) + \frac{1}{2}k_H'(c)(2H-H_0(c))^2 = 0, \qquad \text{on } A \tag{E.6}$$

$$\overline{f}'(c) - \lambda_2 \rho = 0, \qquad \text{on } \mathcal{A} \setminus A \tag{E.7}$$

$$\sigma K_n - N + \nabla[k_H(c)(2H - H_0(c))] \cdot \underline{l} = 0, \qquad \text{on } \partial A \tag{E.8}$$

$$\frac{1}{2} k_H(c)(2H - H_0(c))^2 + [\![\zeta(\rho)]\!] - \lambda_1 [\![\rho]\!] - \lambda_2 [\![\rho c]\!] - \tau = 0, \qquad \text{on } \partial A \tag{E.9}$$

$$M - k_H(c)(2H - H_0(c)) = 0, \qquad \text{on } \partial A \tag{E.10}$$

$$\dot{\sigma} = 0, \qquad \text{on } \partial A \tag{E.11}$$

and

$$k_c \nabla c \cdot \underline{l} = 0. \qquad \text{on } \partial A \tag{E.12}$$

We observe that the Lagrange multipliers λ_1 and λ_2 are defined by the properties of the lipid reservoir. Specifically, equations (E.5) and (E.7) give us the dependence on the chemical potentials, the density, and concentration of the reservoir, i.e.

$$\lambda_1 = \overline{\zeta}'(\rho_b) - \overline{f}'(c_b)\frac{c_b}{\rho_b} \quad \text{and} \quad \lambda_2 = \overline{f}'(c_b)\frac{1}{\rho_b}. \tag{E.13}$$

In equation (E.13), ρ_b and c_b are the density and composition of the reservoir which is reasonably assumed to be uniform. This equation shows that the Lagrange multipliers are known constants and can be independently found from the reservoir's properties. As a result, we can drop those terms that are integrated over the reservoir in equation (E.1) from the energy functional. It can be re-written as

$$\begin{aligned}\mathcal{F} = &\int_A \frac{1}{2} k_H(c)(2H - H_0(c))^2 dA + \int_A \zeta(\rho)\, dA + \int_{\partial A} \sigma\, ds + F_P + F_f + F_M + \int_A f(c)\, dA \\ &+ \int_A k_c |\nabla c|^2\, dA - \lambda_1 \int_A \rho\, dA - \lambda_2 \int_A \rho c\, dA.\end{aligned} \tag{E.14}$$

Expression in (E.14) serves as the general form of energy functional for an open multi-component membrane. If the membrane is isolated or periodic, then the two constants λ_1 and λ_2 are the Lagrange multipliers. If the membrane is connected to a lipid reservoir, the two constants are the "adjusted" chemical potentials defined in (E.13).

Moreover, it can be shown that the membrane's density and composition of lipids can be different from that of the reservoir. On one hand, the membrane and the reservoir have similar density equations as seen in (E.4-E.5); on the other hand, their composition equations (E.6-E.7) are largely different. The first difference is the Laplacian term in equation (E.6) and comes from the penalty on the membrane concentration gradient; this penalty is neglected in the uniform reservoir. The second significant difference are the last two terms of equation (E.6). These two terms comes from the couplings $k_H(c)$ and $H_0(c)$; they allow the membrane composition to be non-uniform and to differ from the reservoir composition. Even if the size of the reservoir is comparable to that of the membrane, the two differences are still important, as the reservoir and the membrane can have different geometry. A direct application of this difference is to explain the lipid/protein sorting phenomena, where the lipid or protein concentration in a pulled tube is different from that of the source vesicle [HTEB10, CJSB11, SMBD12].

Bibliography

[ABH+04] B. Albert, D. Bray, K. Hopkin, A. Johnson, J. Lewis, M. Raff, K. Roberts, and P. Walter. *Essential cell biology*. Garland, 2004.

[AKK92] D. Andelman, T. Kawakatsu, and K. Kawasaki. Equilibrium shape of two-component unilamellar membranes and vesicles. *Europhysics Letters*, 19(1):57–62, 1992.

[BDWJ05] T. Baumgart, S. Das, W. W. Webb, and J. T. Jenkins. Membrane elasticity in giant vesicles with fluid phase coexistence. *Biophys J*, 89(2):1067–1080, 2005.

[BHW03] T. Baumgart, S. T. Hess, and W. W. Webb. Imaging coexisting fluid domains in biomembrane models coupling curvature and line tension. *Nature*, 425(6960):821–824, 2003.

[Boa02] D. Boal. *Mechanics of the Cell*. Cambridge, 2002.

[Bou99] A. A. Boulbitch. Equations of heterophase equilibrium of a biomembrane. *Arch Appl Mech*, 69(2):83–93, 1999.

[BZTM97] R Bar-Ziv, T Tlusty, and E Moses. Critical dynamics in the pearling instability of membranes. *Physical Review Letters*, 79(6):1158–1161, 1997.

[CJSB11] A Callan-Jones, B Sorre, and P Bassereau. Curvature-Driven Lipid Sorting in Biomembranes. *Cold Spring Harbor Perspectives in Biology*, 3(2):a004648–a004648, February 2011.

[DEK+97] HG Dobereiner, E Evans, M Kraus, U Seifert, and M Wortis. Mapping vesicle shapes into the phase diagram: A comparison of experiment and theory. *Physical Review Letters*, 55(4):4458–4474, 1997.

[DLW04] Q. Du, C. Liu, and X.Q. Wang. A phase field approach in the numerical study of the elastic bending energy for vesicle membranes. *Journal of Computational Physics*, 198(2):450–468, 2004.

[DTB08] S. Das, A. Tian, and T. Baumgart. Mechanical stability of micropipet-aspirated giant vesicles with fluid phase coexistence. *J Phys Chem B*, 112(37):11625–11630, 2008.

[ES80] E. A. Evans and R. Skalak. Mechanics and thermodynamics of biomembranes. *CRC Press*, page 254, 1980.

[ES10] C. M. Elliott and B. Stinner. A surface phase field model for two-phase biological membranes. *SIAM J. on Applied Mathematics*, 70(8):2904–2928, 2010.

[Eva74] EA Evans. Bending resistance and chemically induced moments in membrane bilayers. *Biophys J*, 14(12):923–931, 1974.

[FK06] F. Feng and W. S. Klug. Finite element modeling of lipid bilayer membranes. *Journal of Computational Physics*, 220(1):394–408, 2006.

[GGB12] Sefi Givli, Ha Giang, and Kaushik Bhattacharya. Stability of MultiComponent Biological Membranes. *SIAM J. on Applied Mathematics*, 72(2):489, 2012.

[Hel73] W. Helfrich. Elastic properties of lipid bilayers - theory and possible experiments. *Zeitschrift Fur Naturforschung C-A Journal Of Biosciences*, C 28(11-1):693–703, 1973.

[HMO+01] H. Horton, L. Moran, R. Ochs, D. Rawn, and K. Scrimgeour. *Principles of Biochemistry*. Prentice Hall, 2001.

[HTEB10] Michael Heinrich, Aiwei Tian, Cinzia Esposito, and Tobias Baumgart. Dynamic sorting of lipids and proteins in membrane tubes with a moving phase boundary. *PNAS*, 107(16):7208–7213, April 2010.

[Jen77a] J T Jenkins. Static equilibrium configurations of a model red blood cell. *Journal of Mathematical Biology*, 4(2):149–169, May 1977.

[Jen77b] James T Jenkins. The equations of mechanical equilibrium of a model membrane. *SIAM J. on Applied Mathematics*, 32(4):755–764, 1977.

[JL93] F. Julicher and R. Lipowsky. Domain-induced budding of vesicles. *Physical Review Letters*, 70(19):2964–2967, 1993.

[JL96] F Julicher and R Lipowsky. Shape transformations of vesicles with intramembrane domains. *Physical Review Letters*, 53(3):2670–2683, 1996.

[JS94] F Julicher and U Seifert. Shape equations for axisymmetrical vesicles - a clarification. *Phys Rev E*, 49(5):4728–4731, 1994.

[KAKT93] T Kawakatsu, D Andelman, K Kawasaki, and T Taniguchi. Phase-Transitions and Shapes of 2-Component Membranes and Vesicles .1. Strong Segregation Limit. *Journal De Physique Ii*, 3(7):971–997, 1993.

[Lei86] S. Leibler. Curvature instability in membranes. *Journal De Physique*, 47(3):507–516, 1986.

[Lip92] R Lipowsky. Budding of membranes induced by intramembrane domains. *Journal De Physique Ii*, 2(10):1825–1840, 1992.

[LRV09] J. S. Lowengrub, A. Raetz, and A. Voigt. Phase-field modeling of the dynamics of multicomponent vesicles: Spinodal decomposition, coarsening, budding, and fission. *Phys Rev E*, 79(3):031926, 2009.

[MK08] L. Ma and W. S. Klug. Viscous regularization and r-adaptive remeshing for finite element analysis of lipid membrane mechanics. *Journal of Computational Physics*, 227(11):5816–5835, 2008.

[MLK02] L. Miao, M. A. Lomholt, and J. Kleis. Dynamics of shape fluctuations of quasi-spherical vesicles revisited. *The European Physical Journal E*, 9(2):143–160, 2002.

[NO95] H. Naito and M. Okuda. Preferred equilibrium structures of a smectic-a phase grown from an isotropic phase: Origin of focal conic domains. *Phys Rev E*, 52(2):2095–2098, 1995.

[OPJJF97] Sidney Ochs, Rahman Pourmand, Ralph A Jersild Jr, and Richard N Friedman. The origin and nature of beading: A reversible transformation of the shape of nerve fibers. *Progress in Neurobiology*, 52(5):391–426, August 1997.

[Pea59] Carl E Pearson. *Theoretical elasticity.* Harvard Monographs in Applied Science. No. 6. Harvard University Press, Cambridge, Mass., 1959.

[POJ94] R Pourmand, S Ochs, and R A Jersild. The relation of the beading of myelinated nerve fibers to the bands of Fontana. *Neuroscience*, 61(2):373–380, July 1994.

[SBL91] U Seifert, K Berndl, and R Lipowsky. Shape transformations of vesicles: Phase diagram for spontaneous-curvature and bilayer-coupling models. *Phys Rev A*, 44(2):1182–1202, 1991.

[Sei97] U. Seifert. Configurations of fluid membranes and vesicles. *Advances in Physics*, 46(1):13–137, 1997.

[SMBD12] Pankaj Singh, Paritosh Mahata, Tobias Baumgart, and Sovan Lal Das. Curvature sorting of proteins on a cylindrical lipid membrane tether connected to a reservoir. *Phys Rev E*, 85(5):051906, May 2012.

[Sto69] J. J. Stoker. *Differential geometry*. Wiley-Interscience, 1969.

[SvdSvM01] H. Sprong, P. van der Sluijs, and G. van Meer. How proteins move lipids and lipids move proteins. *Nat Rev Mol Cell Bio*, 2(7):504–513, 2001.

[Tan96] T Taniguchi. Shape deformation and phase separation dynamics of two-component vesicles. *Physical Review Letters*, 76(23):4444–4447, 1996.

[TKAK94] Takashi Taniguchi, Kyozi Kawasaki, David Andelman, and Toshihiro Kawakatsu. Phase transitions and shapes of two component membranes and vesicles II: weak segregation limit. *Journal De Physique Ii*, 4(8):1333–1362, 1994.

[VG07] A. Veksler and N. S. Gov. Phase transitions of the coupled membrane-cytoskeleton modify cellular shape. *Biophys J*, 93(11):3798–3810, 2007.

[VK03] S. L. Veatch and S. L. Keller. Separation of liquid phases in giant vesicles of ternary mixtures of phospholipids and cholesterol. *Biophys J*, 85(5):3074–3083, 2003.

[YCN+05] Y. Yin, Y. Q. Chen, D. Ni, H. J. Shi, and Q. S. Fan. Shape equations and curvature bifurcations induced by inhomogeneous rigidities in cell membranes. *J Biomech*, 38(7):1433–1440, 2005.

[Yin05a] Y. Yin. Integral theorems based on a new gradient operator derived from biomembranes (part I): Fundamentals. *Tsinghua Science & Technology*, 10(3):372–375, 2005.

[Yin05b] Y. Yin. Integral theorems based on a new gradient operator derived from biomembranes (part II): Applications. *Tsinghua Science & Technology*, 10(3):376–380, 2005.

[YYC07] J. Yin, Y. Yin, and L. V. Cunjing. General mathematical frame for open or closed biomembranes: Stability theory based on differential operators. *Applied Mathematical Sciences*, 1(29):1439–1463, 2007.

[YYN05] Y. J. Yin, J. Yin, and D. Ni. General mathematical frame for open or closed biomembranes (part I): Equilibrium theory and geometrically constraint equation. *Journal of Mathematical Biology*, 51(4):403–413, 2005.

[YYW07] Y. Yin, J. Yin, and J. Wu. The second gradient operator and integral theorems for tensor fields on curved surfaces. *Applied Mathematical Sciences*, 1(30):1465–1484, 2007.

[ZCH89] O. Y. Zhong-Can and W. Helfrich. Bending energy of vesicle membranes: General expressions for the first, second, and third variation of the shape energy and applications to spheres and cylinders. *Phys Rev A*, 39(10):5280–5288, 1989.

[Zei84] E. Zeidler. *Nonlinear functional analysis and its applications*. Springer-Verlag, 1984.